Experimental Investigation of Solar Powered Steam Sterilizer for Remote Area Health Centers

Samuel Ayana Tadele

A Thesis Submitted to the department of Mechanical Engineering

College of Mechanical, Chemical and Material Engineering

Presented in Partial Fulfilment of the Requirement for the Degree of Masters of Science in Thermal Engineering

Office of Graduate Studies

Adama Science and Technology University

May 2025

Adama, Ethiopia

Experimental Investigation of Solar Powered Steam Sterilizer for Remote Area Health Centers

Samuel Ayana Tadele

Advisor

Dr. Dawit Gudeta

A Thesis Submitted to the department of Mechanical Engineering

College of Mechanical, Chemical and Material Engineering

Presented in Partial Fulfilment of the Requirement for the Degree of Masters of Science in Thermal Engineering

Office of Graduate Studies

Adama Science and Technology University

May 2025

Adama, Ethiopia

DECLARATION

I declare that this Master's Thesis entitled" **Experimental Investigation of Solar Powered Steam Sterilizer for Remote Area Health Centers**" is my own work and has not been submitted to any university for similar purposes. All sources of materials that are used for this thesis have been duly acknowledged through citation.

Samuel Ayana

Name of Student	Signature	Date

RECOMMENDATION OF ADVISORS

I, the advisor of this research thesis, hereby certify that I have closely advised the student while developing this thesis and read the draft thesis entitled "**Experimental Investigation of Solar Powered Steam Sterilizer for Remote Area Health Centers**" prepared under my guidance by Samuel Ayana Tadele. Therefore, I recommend submission of the thesis to the department for further review and evaluation.

Dr. Dawit Gudeta

Major-advisor	Signature	Date

ORIGINALITY DECLARATION

Name of student	Samuel Ayana Tadele
Id. No.	PGR/35846/16
Department	Mechanical Engineering
College	CoMCME
Course Title	M.Sc Thesis
Title of work / Assignment name	Experimental Investigation of Solar Powered Steam Sterilizer for Remote Area Health Centers
Date of submission	22/05/2025

1) I understand what plagiarism is and I am aware of the university's policy in this regard.
2) I declare that this thesis entitled **"Experimental Investigation of Solar-Powered Steam Sterilizer for Remote Area Health Centers"** is my original work and has not been submitted elsewhere for examination or award of a degree or publication. Wherever others' work or my own work has been utilized, it has been duly acknowledged and referenced in compliance with the university's requirements.
3) I have not sought or used the services of any professional agencies to produce this work.
4) I have not permitted, nor will I permit, anyone to plagiarize my work with the intention of presenting it as their own.
5) I am aware that making any false claims regarding this work will lead to disciplinary action in accordance with the university's Anti-Plagiarism Guidelines.

Signature ______________________________

Date 22/05/2025 ______________________________

APPROVAL PAGE

I, the advisor of the thesis entitled "**Experimental Investigation of Solar Powered Steam Sterilizer for Remote Area Health Centers**" and developed by Samuel Ayana Tadele, hereby certify that the recommendation and suggestions made by the board of examiners are appropriately incorporated into the final version of the thesis.

Dr. Dawit Gudeta

Major-advisor	Signature	Date

We, the under signed, members of the Board of Examiners of the thesis by Samuel Ayana Tadele have read and evaluated the thesis entitled "**Experimental Investigation of Solar Powered Steam Sterilizer for Remote Area Health Centers**" and examined the candidate during open defense. This is, therefore, to certify that the thesis is accepted for partial fulfillment of the requirement of the degree of Masters of Science in Thermal Engineering.

Dr.		
Chair Person	Signature	Date
Dr. Melaku Desta		17/06/2025
External Examiner	Signature	Date
Dr. Addisu Bekele		June 18, 2025
Internal Examiner	Signature	Date

Final approval and acceptance of the thesis is contingent upon submission of its final copy to the Office of Postgraduate Studies (OPGS) through the Department Graduate Council (DGC) and College Graduate Committee (SGC).

Department Head	Signature	Date
College Dean	Signature	Date
Office of Postgraduate Studies, Dean	Signature	Date

ACKNOWLEDGMENT

First of all, I want to thank the Almighty God, for being the source of all wisdom and strength and his constant blessings, without his blessing and guidance all this work wouldn't be fruitful.

I appreciate my advisor, Dr. Dawit Gudeta for his assistance. For his continues support and guidance for each footstep for the accomplishment this thesis. Thank you for your kindness, sharing insightful ideas, encouragement through the journey and four your endless penitents.

Moreover, I want to extend my gratitude to my instructors, Dr. Addisu Bekele and Dr. Dejene Kebede. Your lectures led me to develop intellectual understanding and your Exemplary advises are played a great role to look forward towards to pursue more knowledge.

And to my dear parents and friends as well, I want to admire your constant love and motivation towards in work and for having so much patience with me in all stages of undertaking this work. I am deeply grateful to the Holy Virgin Mary, for her boundless blessings and prayer that have guided my journey.

TABLE OF CONTENTS

LIST OF FIGURES

LIST OF TABLES

ACRONYMS

CPC	Compound Parabolic Concentrator
DSG	Direct Steam Generation
EBR	Electron-Beam Radiation
EM	Electromagnetic
ETR	Extraterrestrial Radiation
ETSC	Evacuated Tube Solar Collector
EtO	Ethylene Oxide
FPSC	Flat Plate Solar Collector
HAIs	Healthcare-Associated Infections
HTF	Heat Transfer Fluid
IAM	Incidence Angle Modifier
IR	Infrared
NASA	National Aeronautics and Space Administration
PDC	Parabolic Dish Concentrator
PTC	Parabolic Trough Concentrator
SAF	Synthetic Aromatic Fluid
SSIs	Surgical Site infections
UV	Ultraviolet
WHO	World Health Organization

NOMENCLATURE

C	Specific heat capacity (J/kg. k)
H	Global daily radiation (W/m2)
Hb	Beam Radiation
Hd	Diffuse Radiation
Ho	Extraterrestrial radiation (W/m2)
I	Global hourly radiation (W/m2)
I_{SC}	Solar Constant
Nu	Nusselt number
T_a	Ambient Temperature
T_i	Inlet temperature of HTF (K)
T_m	Mean temperature (K)
Ts	Surface Temperature
T_{sk}	Sky Temperature(K)
h	convective heat-transfer coefficient (W/m2. K)
m	Mass flow rate (kg/s)
τ	Non-dimensional time
ΔP	Pressure drop (N/ m2)
ΔT	Temperature difference (K)
C_P	Specific heat capacity (J/kg. k)

ABSTRACT

Efficient medical equipment sterilization is a major challenge in rural areas of developing countries due to limited access to electricity and modern technologies. In Ethiopia, where 76.84% of the population lives in rural areas (World Bank, 2023). most clinics rely on fossil fuels, which are costly, environmentally harmful, and often difficult to access consistently. To address this challenge, alternative solar-powered steam sterilizer was developed and tested. Designed to meet the average daily demand of rural health centers, it has 10-liter sterilization chamber capable of handling around 5.5 kg of equipment per cycle. The experiment is conducted with different load and weather condition during no-load tests the target temperature and pressure was achieved within 30 minutes, while full-load tests reached 121°C and 2 bar in 52 minutes, with a total sterilization cycle of 1 hour and 20 minutes. Relatively low solar intensity conditions extended the time to reach sterilization temperature to around one hour. The optimum tilt angle of Kobo was determined which resulting monthly radiation gain up to 15%. calculated Solar Radiation result was compared with NASA dataset showed ± 2 % error. A comparative cost-benefit assessment showed that although the initial investment in the solar sterilization system is higher, it offers significant long-term advantages in cost-effectiveness, sustainability, and off-grid accessibility compared to electricity and fossil fuel, these results demonstrate the system's viability.

Keywords: Sterilization, Solar-powered, Rural healthcare, Renewable energy.

CHAPTER ONE

1. INTRODUCTION

1.1. Background of Study

Efficient medical equipment sterilization is a major challenge in rural areas of developing countries due to limited access to electricity and modern technologies. In Ethiopia, where 76.84% of the population lives in rural areas (World Bank, 2023), many are exposed to unhygienic procedures. The main issues contributing to poor sterilization in underdeveloped countries in Africa, particularly in Ethiopian distant health centers, are a lack of stable electricity in rural locations and limited economic resources. This prohibits healthcare facilities from accessing and using necessary sterilization technologies in distant locales, increasing the risk of health care associated illnesses. Due to social and healthcare system shortcomings, which worsen by economic issues. A lack of regulations, guidelines, and qualified workers further elevates the issue (Zubair, 2010).

Medical devices must be disinfected before use in medical procedures such as surgery to prevent the spread of pathogens. Failure to properly sterilize medical instruments significantly increases the risk of healthcare-associated infections (HAIs). This issue is especially critical in developing countries, where inadequate sterilization practices contribute to a higher incidence of HAIs (Panta et al., 2019). These infections can originate from patients, healthcare workers, medical equipment, the healthcare environment, or visitors. Among HAIs, surgical site infections (SSIs) are the most common, particularly in low-resource settings, where they account for 1.2% to 23.6% of surgeries performed between 1995 and 2010. In contrast, the incidence of SSIs in developed countries is much lower, ranging from 1.2% to 5.2% (Nejad et al., 2011).

Most parts of remote health centers are addressing this issue by conventional method by boiling water by using fuel conventional energy resources (fossil fuels) which will be ended up with low sterilization quality and in environmental aspect also it produces emissions to the environment and the inhabitants. Pollutants produced by fossil fuels harm the environment, water, land, and wildlife, endangering public health. But in recent years the developments of researches and innovations on renewable energy like (solar, wind, hydro geothermal) are creating opportunities to focus the energy demand toward these renewable energy sources. Solar energy is particularly critical to this energy shift since it emits no pollutants, uses a limitless resource in the long term, and is widely available (Soto et al., 2022). According to NASA study on earth energy budget of the total solar energy that falls on the Earth, 48% is absorbed at the surface. Although the Earth receives an immense amount of solar energy, its low density and intermittent nature necessitate its capture and concentration through solar collectors to obtain usable solar thermal energy. This thermal energy can be used either directly or stored for later use. To ensure effective system performance, the solar collectors are required to demonstrate high optical efficiency to maximize thermal energy capture. In parallel, the thermal storage subsystems must possess a high storage density, superior heat transfer capability, and long-term structural and functional stability to support continuous and reliable operation (Tian & Zhao, 2013).

Solar energy can be used to disinfect medical tools in rural clinics using either dry heat or steam sterilizers. Research is being conducted on both steam sterilizers and dry heat/hot air oven sterilizers. Steam sterilizers use the solar energy and change temperature water turn it to high temperature steam and pressure to destroy germs such as bacteria, viruses, fungi, and spores found on things placed within the pressure vessel (such as surgical or dental instruments). Whereas heat/hot-air oven is done by only heating the air inside the oven(chamber) it kills all the pathogens and it takes comparatively larger time than steam sterilizer, in this research solar steam sterilizer is gonging to be assessed.

1.2. Statement of the Problem

This study aims to development of a solar-powered steam sterilization system. Its aim is to ensure the effectiveness and safety of medical services in marginalized areas and improve health outcomes in such communities, especially in developing countries like Ethiopia where most health centers are off grid to electricity. Most clinics rely on fossil fuels, which are costly, environmentally harmful, and often difficult to access consistently. Hence, there is necessary for emerging technologies that uses renewable energy such as solar energy, to develop sustainable and economically viable sterilization systems that can operate independent of conventional energy sources. Further, to enhance the safety and effectiveness of sterilization processes in rural health facilities, this research suggests the incorporation of a water distillation system into the solar-powered steam sterilization system.

1.3. Research Questions

- What is the optimum tilt angle for maximizing solar energy capture in Kobo?
- How does the performance of the solar-powered steam sterilizer vary under different weather conditions?

- How does the solar-powered steam sterilizer compare to commercially available steam sterilizers in terms of performance?
- Is the solar-powered steam sterilizer economically viable for use in resource-limited site?

1.4. Objectives

1.4.1. General Objective

The main objective of this thesis is Experimental Investigation of Solar-Powered Steam Sterilizer for Remote Area Health Centers

1.4.2. Specific Objectives

- To determine the optimum tilt angle by performing a solar potential analysis of Kobo.
- To perform of the theoretical analysis of solar-powered steam sterilizer.
- To evaluate the performance of solar-powered steam sterilizer by performing experimental test.
- To evaluate the economic viability of solar-powered steam sterilizer.

1.5. Significant of the Study

The significance of this study is providing a sustainable and reasonably priced way to sterilize medical equipment at remote clinics with limited access to energy sources like electricity lack of recent technological advanced machines. The study shows how vital healthcare procedures can be continued without using fuel. system also use of distilled water, which is generated as a byproduct of the solar-powered process. This research promotes independence on conventional energy for rural communities by incorporating renewable energy into health services.

1.6. Scope and Limitations of Study

The study scopes investigating a performance of solar collector, that specifically generate steam to disinfect reusable medical equipment. This work includes developing suitable machine and investigating experimental results. The study also asses its, cost and benefits analysis. A limitation of the study is the absence of a pyranometer for experimental testing. As a result, the solar radiation data were obtained numerically using the Angström-modified correlation.

1.7. Organization of Thesis

This thesis is organized into seven chapters. Chapter One introduces the study by outlining the background, problem statement, objectives, significance, and scope. Chapter Two presents a literature review that highlights previous work and identifies gaps in the existing knowledge. Chapter Three describes the materials that I used and methods to follow, including experimental procedures and data collection techniques. Chapter Four focuses on the design and analysis of the system, detailing the conceptual framework and engineering calculations. Chapter Five provides a comprehensive explanation of the experimental setup and the configuration of components. Chapter Six presents and discusses the results obtained from the experiments, analyzing their implications in light of the study objectives. Finally, Chapter Seven concludes the research with a summary of key findings and offers recommendations for future work.

CHAPTER TWO

2. LITERATURE REVIEW

2.1. Basics of Solar Energy

Solar energy refers to the total electromagnetic radiation (EM) comes from the Sun that could be captured and converted into usable thermal or electrical energy through appropriate technologies (Kofoworola et al., 2025). Solar energy is a natural energy source that, like other renewable forms, holds significant potential for diverse applications due to its abundance and widespread availability (Bhatia, 2014), it is pure, inexhaustible, and benign to terrestrial life (Tsoutsos et al., 2005). Its harmful short-wavelength ultraviolet (UV) radiation is largely absorbed by the ozone layer—before reaching the troposphere (Şen, 2008). Once solar radiation enters the Earth's atmosphere, a portion of it scattered by atmospheric particles and gases, while the remainder is absorbed by various atmospheric components (Şen, 2008). The scattered portion of solar radiation, known as diffuse radiation, is partially goes back to space, while the rest reaches the Earth's surface as direct radiation (Myers, 2013).

2.1.1. Thermal Radiation and Solar Energy Distribution

The complete electromagnetic (EM) spectrum ranges from very short to very long wavelengths, with thermal radiation lying between these extremes. The wavelength range of thermal radiation is approximately $0.1\ \mu m \leq \lambda \leq 100\ \mu m$

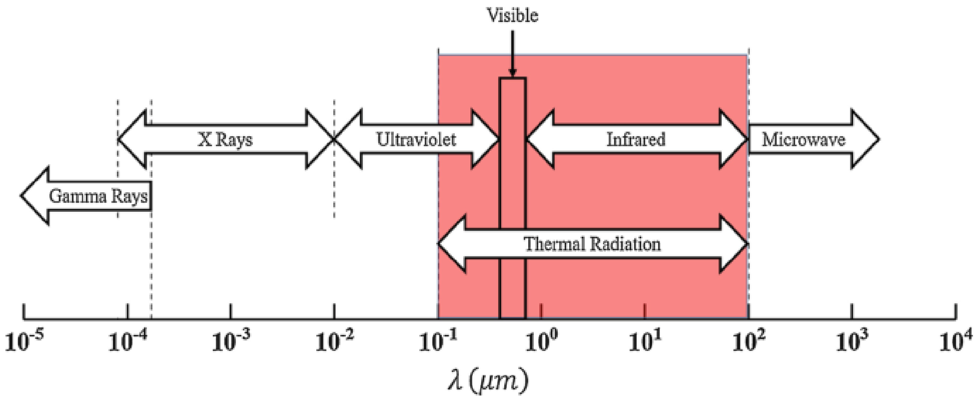

Figure 2.1: Electromagnetic radiation spectrum (Frank P. Incropera,2011)

The Sun, with having surface temperature about 5800 K, emits radiation across a broad spectrum. The distribution of its total emitted energy (σT^4) is as follows:

- 50% in the infrared (IR) region
- 37.5% in the visible spectrum
- 12% in the ultraviolet (UV) region

Since thermal radiation is both a result of and an influence on the thermal state of matter, it plays an important role in heat transfer.

2.1.2. Spectral Distribution of Solar Radiation

A surface radiates heat at various wavelengths at once. In the diagram, the change in strength of radiation as per the color is called its spectral nature(Modest, 2013). The spectrum of the extraterrestrial solar radiation corresponds roughly to that of a 5800 K black body. Most radiation is concentrated in the shorter wavelength region 0.2 μm ≤ λ ≤ 3 μm. The peak occurs at about λmax ≈ 0.50 μm (Wikipedia contributors, 2025).

2.1.3. Impact of Atmosphere on Solar Radiation

The atmosphere of Earth alters the sunlight propagation in terms of its intensity, the nature of the spectrum and the directional distribution due to the absorption and scattering on account of their presence in the atmosphere(Frederick, 2003). The primary gases involved in absorptions are.

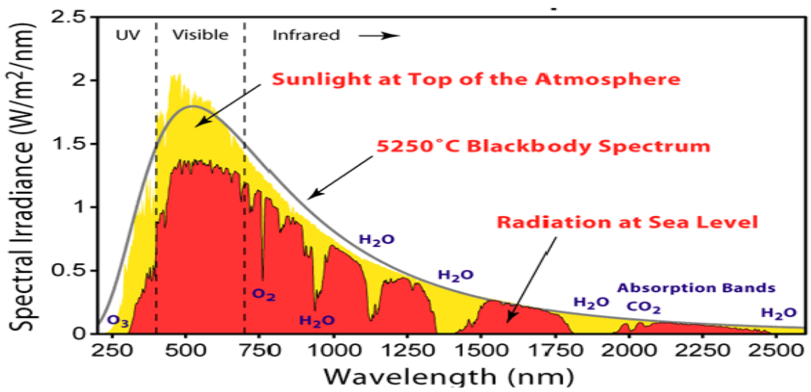

Figure 2.2: Spectral distribution of solar radiation showing atmospheric effects on wavelength composition and total energy received at Earth's surface. (Solar Book, 2011).

- ➢ Ozone absorbs UV radiations strongly which is responsible for Ozone (O3).

- Significant damping for wavelengths less than 0.4 μm
- Total attenuation when the wavelength is less than 0.3 micrometers.
- Oxygen (O2) and Ozone (O3)-It absorbs some light in the visible region.
- Water vapor (H2O) – It has very strong absorption bands in the near infra-red region and also some in far infra-red.
- Carbon dioxide absorbs in infrared- Carbon dioxide or CO2.
- Dust has a short-range continuous wavelength absorption property and so do aerosol

2.2. Solar Energy Conversion

The Solar energy is capable of being transformed into electricity by charging electrons in a solar cell. It can be used to give chemical fuel in natural photosynthesis in plants or artificial photosynthesis in artificial systems, and also give heat in thermal applications (McConnell et al., 2010). Solar energy may be converted into electricity, heat, or both electricity and heat using present-day technology.

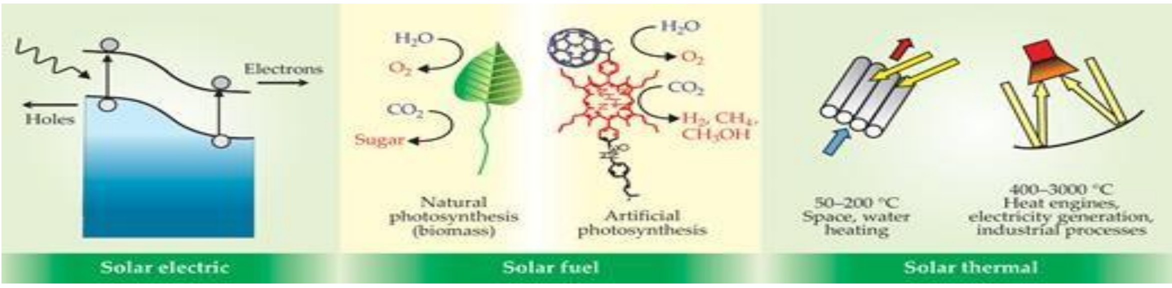

Figure 2.3: Solar Photons Conversion (Crabtree & Lewis, 2007)

2.3. Classifications of Solar Collectors

Solar collectors are devises that solar radiation, that produces thermal energy from solar radiation this thermal energy can be used for run wide range of applications. The main parts of a solar collector are reflector, absorb and the working fluid.(Borode et al., 2019). The categorization of collectors comprehends, as different species, non-concentrating collectors and concentrating collectors. Non-concentrating collectors have the same intercept and focus area, concentrating collectors have a different intercept and focus area (Prasad et al., 2017).

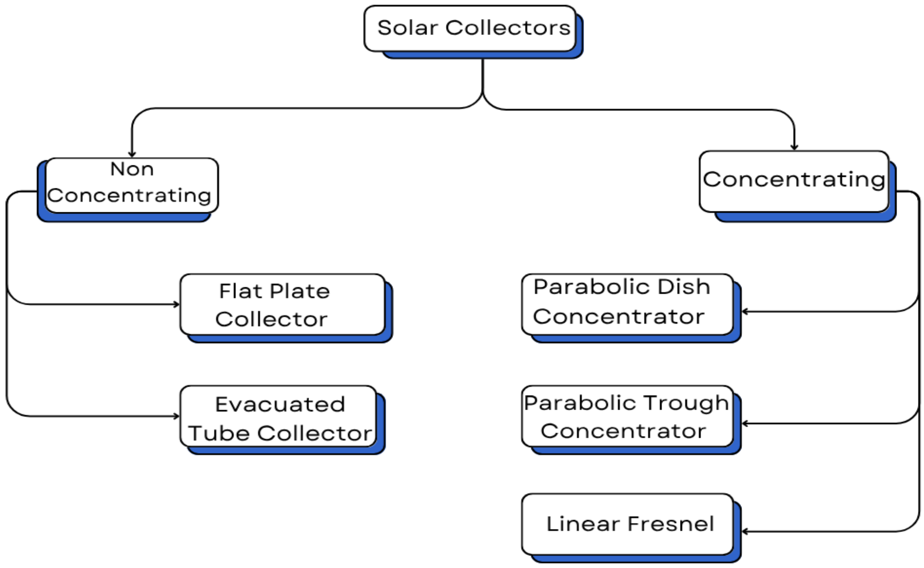

Figure 2.4: Different Types of Solar Collectors Used in Renewable Energy

The first generation of flat-plate solar collectors (FP-SCs) was introduced Early in the 1960s. FPSCs are widely utilized in low-temperature applications, including industrial process heat and building heating. A dark-colored absorber, a transparent glass cover to minimize radiation losses, and insulation to reduce conduction losses are common features of these collectors. There are other alternative designs, like fin-and-tube collectors and sandwich-style collectors. The two primary categories of FPSCs are forced circulation and thermosiphon systems (Sheikholeslami et al., 2021).

Evacuated tube solar collectors (ETSCs) demonstrate comparatively higher efficiency than flat plate collectors at elevated operating temperatures, as the vacuum surrounding the absorber surface minimizes convective heat losses (Aggarwal et al., 2023). Which leads to better heat derivation performance and can be appropriate for cloudy as well as very low-temperature conditions. Apart from that, working fluid is the most important element which should be heated by the collector. It is used in solar domestic water and air heater, medium temperature is used for office, hospital, food industry (Olfian et al., 2020).

A parabolic dish concentrator has 2 important components a reflecting surface (dish) and a optical receiver located at focal point of that changes optical energy to thermal energy (Dincer & Bicer, 2018). Owing to its elevated concentration ratios, the parabolic dish solar concentrator serves a critical function in high-temperature solar thermal applications (S. Abbas et al., 2023). However, the system’s total efficiency is declining due to thermal losses (K. H. Kumar et al., 2022).

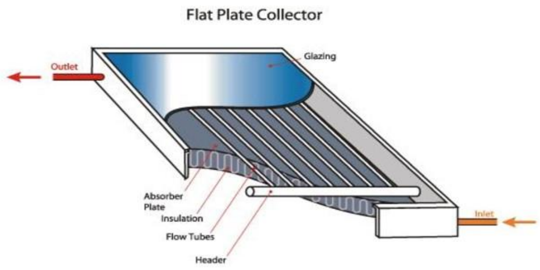

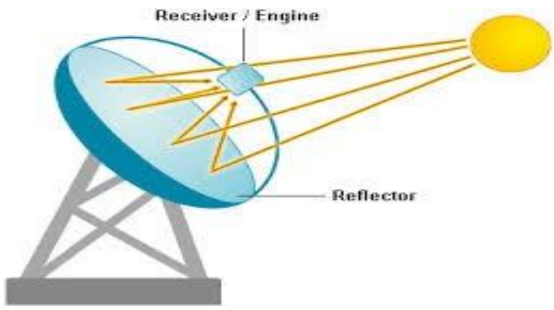

(a) flat plate collector (Kulcu, 2020) (b)parabolicdish collector

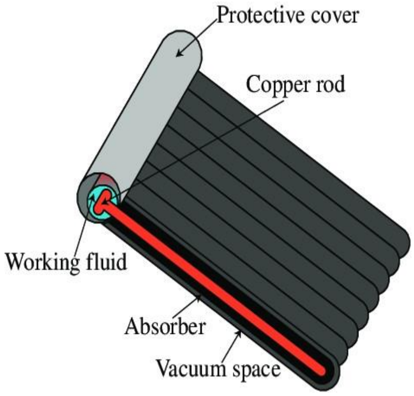

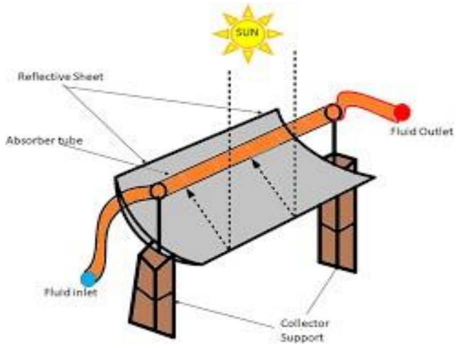

(c) Evacuated-tube (Prabhu et ahwari,2001) (d) parabolic through collector et., 2024)

Figure 2.5: Concentrating and Non-Concentrating Solar Collectors.

2.3.1. Parabolic Trough Concentrator

A solar parabolic trough collector (SPTC) is composed of a curved reflective surface, a receiver tube that carries the heat transfer fluid, and a surrounding transparent enclosure (Malekan et al., 2021a). The receiver is fixed in position at the focal line of the parabolic concentrator (Orosz & Dickes, 2017). The transparent concentric cover insulates the absorber tube, minimizing heat losses and helping to preserve the vacuum environment (Jebasingh & Herbert, 2016). The rigid frame supports he sturdy frame provides structural support for both the parabolic concentrator and the solar tracking system, which is responsible for following the sun’s path (Jebasingh & Herbert, 2016). While the parabolic trough collector is commonly utilized for large-scale power generation, it is also suitable for small-scale applications such as direct steam production (Orosz & Dickes, 2017). Its performance is influenced by several key components, each playing a crucial role in its overall efficiency PTC system comprises Structural support, reflective concentrator, receiver element (Shinde et al., 2022), Heat Transfer Fluid (HTF) (Gharzi et al., 2023) and tracking system.

The trough serves as the primary component of the PTC system, characterized by key geometrical parameters such as rim angle, aperture width, focal length, and overall length. PTC's geometrical characteristics are being optimized through extensive research to make it suitable for a wide range of applications and regions (El Ghazzani & Nait Mensour, 2021). A lower rim angle causes the aperture size and focal length to increase, which complicates and raises the cost of the trough structure. Conversely, a greater rim angle leads to a lower focal length and aperture area. Additionally, it causes the parabolic radius to increase, raising the mirror's price. (Bhargav H. Upadhyay & Ramana, 2022).

.

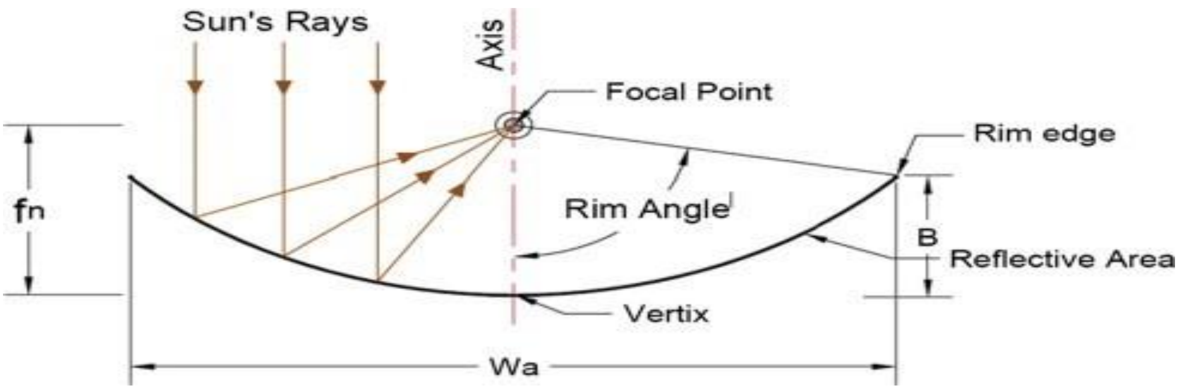

Figure 2.6: Geometrical Parameters of Trough of Parabolic Concentrator (Mokheimer et al., 2014)

The reflector is another crucial component of the PTC system, playing a vital role in concentrating solar radiation onto the receiver. (Ranjan & Prakash, 2019). The primary need for good reflecting materials is their reflective characteristics (Upadhyay, 2020). Silver-coated curved glass mirrors are commonly utilized as reflectors in PTC for commercial applications like as power generating. Researches has been to identify cost-effective alternative materials. Low-cost alternative reflector materials include silver-coated polymer films, aluminum foil, silver-coated PVC sheets, and anodized aluminum panels (Jamali, 2019)

The receiver absorbs the concentrated solar radiation reflected onto it, converts it into usable thermal energy, and transfers the heat to the fluid within the tube (Jianfeng et al., 2010). The receiver material must exhibit high solar absorptance and minimal thermal losses to ensure efficient energy conversion (Mammadov, 2012). To reduce thermal and optical losses at the absorber surface, specialized coatings and thermal insulation are applied (Zhao et al., 2022).

2.4. Sterilization Techniques

Before got through to sterilization techniques in detail it is better to clearly identify the deference between it is cleaning, disinfection and sterilization.

Table 2.1: Level of Decontamination (WHO Definition)

Cleaning	Cleaning is the process of physically removing dirt, dust, and bodily materials in order to effectively disinfect or sterilize and reduce bacteria. This procedure ensures that things are sufficiently prepared for additional processing or use by reducing the chance of contamination, preventing disinfectants from becoming inactive, and limiting the growth of germs.
Disinfection	The process involves reducing or eliminating microorganisms to levels that are considered safe for human health and handling, though it may not necessarily eradicate bacterial spores.
Sterilization	The total eradication or removal of microorganisms, including bacterial spores (Wang & Yu, 2023).

Infections or illnesses associated with medical treatment are typically linked to factors such as injections, surgical procedures, hospital settings, or patient beds. Surgery is the most concerning of these concerns because it involves reusing surgical equipment, which, if improperly sanitized, allow harmful bacteria to spread. As explained above in Table Sterilization is the process of eliminating all living things, including pathogenic and non-pathogenic ones, from medical equipment's surface, whether they are vegetative or single-celled.

Various methods are employed to sterilize medical equipment, including steam sterilization, chemical sterilization, dry heat sterilization, plasma gas sterilization, vaporized hydrogen peroxide sterilization, Health-mark clear top scope sterilization trays, and Health-mark plastic instrument sterilization baskets (Ituna-Yudonago et al., 2021). Here are commonly used sterilizers.

2.4.1. Dry heater sterilization

It is "also known as hot air or oven sterilizers", it uses principle of gravity convection or mechanical convection (Wikipedia contributors, 2023). According to (WHO) The decontamination and reprocessing of medical devices in healthcare facilities are governed by standards, with exposure time and temperature varying according to the specific item being sterilized. Typically, sterilization is performed at 170°C for 60 minutes or 150°C for 150 minutes for critical devices that may be damaged by moisture, pressure, and/or vacuum. This method is rarely used clinically and is suited for sterilizing restricted materials, such as glassware, oils, powders, and moisture-sensitive instruments. It is not widely practiced for sterilizing medical devices (Shyam & Palaniappan, 2023).

2.4.2. Steam sterilization

Steam Sterilization is one of the best and most widely used technique because it has the benefits and advantages of short processing time, low costs, high reliability of sterilization and very small damage to hand-pieces (Ituna-Yudonago et al., 2021), it is frequently used sterilizer for Dental drillers, forceps, scissors, tubes, and other reusable medical supplies (Feurhuber et al., 2017).

Figure 2.7 Medical Equipment That Can Be Sterilized by Steam

Steam sterilization is typically performed with temperatures range from 121°C (250°F) to 134°C (273°F), under pressures of 2.06-2.32 bar, for duration of 10 to 60 minutes, contingent upon the material and the specific organism to be eradicated. A decrease in temperature necessitates an extended exposure duration for effective sterilization. Reusable devices undergo many sterilization cycles, as they are sterilized following each use. In order to preserve performance, safety, and efficacy, materials utilized in such devices must be able to endure the number of cycles required for the device (Mustapha et al., 2021).

2.4.2.1. Physical indicators of Steam Sterilization

Physical indicators are measurable parameters that confirm whether the sterilization process has reached the necessary conditions (such as temperature, pressure, and time) to effectively kill all microorganisms, including spores.

Pressure: Relevant in steam sterilization**,** as increased pressure allows steam to reach higher temperatures necessary for sterilization typical 15–30 psi, measured using gauges or digital sensors.

Temperature: Critical for most sterilization methods, such as steam sterilization at 121°C or 134°C.Measured using: built-in thermometers, thermocouples. K-type thermocouple is one of the most commonly used temperature sensors in industrial applications due to its wide temperature range, reliability, and cost-effectiveness. It is made from Chromel (nickel-chromium) and Alumel (nickel-aluminum) conductors, offering stable performance in both oxidizing and inert environments. With an operating range typically from -200°C to 1260°C, it is well-suited for measuring high-temperature processes like furnaces, engines, and steam systems. Its versatility and durability make it a standard choice in laboratories, manufacturing, and power generation.

Table 2.2: Comparison of Thermocouple Junction Types, Their Characteristics, and Applications

Type	Description	Advantages	Typical Applications
Grounded Junction	Junction welded to sheath	Fast response, good thermal contact	Liquids, gases, pressure vessels
Ungrounded Junction	Junction insulated from sheath	Electrical noise protection	Electrically noisy environments
Exposed Junction	Sensing junction exposed to environment	Very fast response	Air, gases, fast-changing temperatures

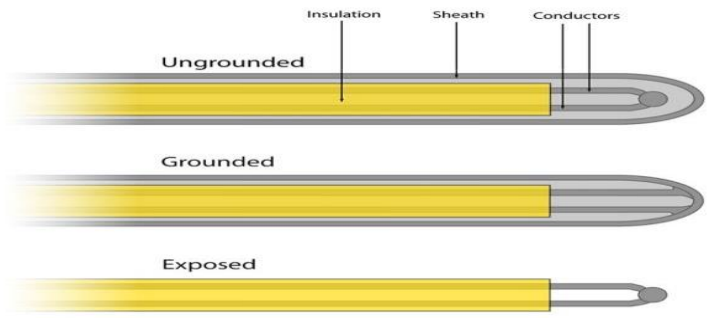

Figure 2.8: Types of Thermocouple Junctions – Grounded, Ungrounded, and Exposed

Table 2.3: Summary of the conditions, mechanisms, advantages, and limitations of common industrial sterilization methods used for medical devices (Tranquillo et al., 2023)

Technique	Mechanisms	Advantages	Limitations
Steam (Autoclave)	Steam sterilization uses high-pressure saturated steam (121°C) for some minutes to denature DNA and inactivate enzyme activity, in effect killing microbes. Routine exposure time is 15 minutes.	Efficient, safe, and rapid, with good penetration. It is cost-effective, easy to monitor, and leaves no toxic residues. Compatible with materials like glass, metals, paper, and certain polymers (e.g., silicones).	High temperatures and moisture can damage thermosensitive polymers, requiring breathable packaging. Some metals may corrode.
Ethylene Oxide (EtO)	EtO gas interferes with cellular metabolism, rendering microbes inactive. It is the most commonly used sterilization method for medical devices.	Suitable for materials sensitive to heat, humidity, and radiation. EtO can penetrate solid materials and is effective on	Requires porous packaging and pretreatment in a warm, humid environment. Post-sterilization diffusion of EtO can

	The typical process duration is 2.5 hours, excluding aeration.	temperature- or humidity-sensitive devices.	take significant time. It is not suitable for biodegradable materials, and residual gas may take up to two weeks to dissipate.
Gamma Radiation	Gamma radiation from isotopes such as cobalt-60 damages microbial DNA, effectively sterilizing materials. The process usually takes less than 24 hours, depending on the dose.	Excellent penetrability, even though metal or foil packaging, and effective on various materials simultaneously. The process is efficient, reliable, and residue free.	Requires specialized containment facilities, and high doses can damage polymers, affecting both functionality and appearance, potentially reducing shelf life.
Electron-Beam Radiation	High-energy electrons from accelerators induce DNA damage in microbes. The typical exposure time ranges from 5 to 7 minutes.	Similar to gamma radiation but with a much shorter exposure time.	Similar to gamma radiation in terms of material damage and potential functional loss.

2.5. Review on Related Works

(Hassan Abbood et al., 2022) Demonstrated a model and design for solar sterilizer that sterilizes at 2.1 bar of pressure and temperature inside an aluminum pressure cylinder set inside an insulated chamber that measured 50 cm in width, 30 cm in height, and 93 cm in depth. Thermal glass, 10 mm thick, covered its front face. The cylinder was fixed using the top face as a frame. To improve heat absorption, matte black paint was applied to the cylinder's exterior. It took 128 minutes to produce steam with the qualities required for sterilization when the model was tested with half a liter of pure water without any surgical instruments. When the water within the cylinder reached 56.1°C, the test began. under climatic settings where the average ambient temperature was 34°C and the average solar radiation intensity was 903 W/m^2. After then, 1.2 kg of instruments were used to test the performance. It took 25.78% longer to reach the sterilizing temperature and pressure when the surgical instruments were present. Additionally, reflecting panels were positioned to direct sun energy toward the cylinder's surface in order to boost the system's thermal enablement. By using this method, the amount of time needed to sterilize steam was reduced by 6.2%. The testing was carried out in various settings and over a number of days.

(Zhao et al., 2020) Developed a stationary solar thermal device and investigated how different design elements affected the device's capacity to produce saturated steam. The gadget effectively transforms solar energy into heat for the production of steam, made possible by an improved transparent aerogel layer. Even in partially foggy and misty conditions, field testing carried out in Mumbai, India, showed successful sterilizing cycles. At 100°C, the device's energy efficiency (47%) was almost double that of earlier models. The thermal concentration method, which provides an inexpensive, passive way to achieve high temperature and pressure without the use of active optical concentrators, is the foundation of the steam generation process.

(Kerr & Scott, 2006) studied on the modification of a large, straightforward, inexpensive panel cooker to significantly lessen dependency on traditional heat sources. Propane is integrated into the hybrid device as a backup in case there is not enough sunlight. The effective design also reduces fuel consumption, even in the absence of sunlight. The key author's background as a surgical nurse informs the concept and operational procedures for real world clinical use. The design, construction, operational principles, and experimental findings for a prototype includes sterilization verification details. Additionally, the device performs exceptionally well for pressure cooking, general cooking, and pressure food preservation, or "canning."

(Li et al., 2018) developed the kinetic benefits of interfacial solar steam generation, and it is shown that this method can provide faster (as little as 8.4 minutes for a complete sterilization cycle) and more energy-efficient (100 J mL-1 for steam reaching 121 °C) sterilization than traditional methods. The sterilizing method is a promising alternative that is especially helpful for off-grid locations. It has been shown to achieve effective sterilization (inactivation of pathogen), surpassing the standards set by the Food and Drug Administration.

(Birhanu & Kahsay, 2018) developed a solar autoclave for use in rural clinics that generates steam in a pressure cooker at 121 °C and 2.06 bar using a parabolic dish collector. By replacing fuel-fueled boiling with this solar-powered technique, rural clinics may now offer sterile medical equipment and infection-free services. Testing verified that within 10 to 30 minutes, the necessary sterilizing temperature of 121 °C and pressure of 2 bar were reached. During the first tests, the relief valve opened automatically at these settings. Furthermore, the temperature rose to 128 °C and the pressure reached 2.6 bar when a little metal strip was applied to the relief valve. With the exception of particularly gloomy days, the sterilizing procedure lasted 40 to 60 minutes.

(Chang et al., 2019) A newly engineered interfacial evaporation system was incorporated into a solar vacuum tube to showcase the generation of superheated steam at ambient pressure and under low-intensity solar radiation. A heat exchanger positioned within the tube further elevates the temperature of the water vapor generated by a high-efficiency, localized-heating evaporator, converting it into superheated steam without the need for pressurization. Under standard solar illumination (one sun), the steam generator exhibited a controllable steam temperature range between 102 °C and 165 °C, achieving a solar-to-steam conversion efficiency of 26% to 49%. Even with an average solar flux of approximately 600 W/m^2, the system reliably produced steam exceeding 121 °C, owing to the interfacial evaporation configuration and minimized thermal losses enabled by the solar vacuum tube. Portable solar steam sterilization, along with other steam-based applications, becomes feasible under ambient solar conditions, as confirmed by successful sterilization results verified using the Geobacillus stearothermophilus biological indicator and Escherichia coli bacteria.

(Khan et al., 2020) conducted an experiment using a pressure cooker as the receiver/absorber in a medical sterilizer system and a paraboloidal dish as the concentrator collector. Solar radiation was directed onto the bottom of the pressure cooker, which was covered in a black substance, by applying aluminum foil to the concentrator to increase reflectance. A pyrheliometer was used to detect solar beam radiation, while thermocouples and pressure gauges were used to track temperature and pressure, respectively. 1.05 kg/cm^2 and 121 °C, the necessary criteria, were met. According to tests conducted at the ICDDRB and BCSIR in Dhaka, Bangladesh, the pressure cooker successfully sterilized the equipment by maintaining these parameters

2.6. Literature Summary and Gap

Current literature presents promising concepts for solar steam sterilizers, yet some gaps remain. the high cost of certain materials makes them inaccessible in developing countries. Non-concentrating collectors, such as flat plate systems, often require extended periods to reach the high temperatures and pressures necessary for effective steam sterilization. Additionally, some designs face issues like construction complexity and shadowing effects in systems using parabolic dish collectors. These limitations underscore the need for a solar sterilizer design that achieves balance of efficiency, simplicity, and affordability, utilizing locally available materials.

CHAPTER THREE

3. MATERIALS AND METHODS

3.1. Location of Experiment and Testing

Despite the testing not being conducted at the remote site, Kobo exhibits slightly higher average sunshine durations across most months compared to Adama, confirming its suitability for solar energy applications. The solar potential analysis was conducted for one of the remote areas, Kobo, which is located 3.5 kilometers from Metehara. The development and initial testing of the solar-powered steam sterilizer system were carried out at the Mechanical Engineering Department of Adama Science and Technology University (ASTU).

3.2. Project Design

This project employed a developmental research design involving the conceptualization, design, fabrication, and laboratory testing of a solar-powered steam sterilizer. The project aimed to create a functional and potentially cost-effective solution for medical instrument sterilization in resource-limited settings. The project comprised the following phases:

- preliminary needs assessment based on literature review,
- Estimation of Solar Potential based on sunshine hours collected from metrology agency,
- design and component selection for the solar steam sterilizer,
- fabrication and assembly of the prototype, and
- Experimental testing of sterilization capabilities.

3.2.1. Estimation of Solar Potential Using Python

The collected sunshine hour data for Kobo town was analyzed using Python programming software (Jupiter notebook). A script was developed to calculate the average daily and monthly sunshine hours. This data was then used, in conjunction with standard solar irradiance models and geographical coordinates of Kobo, to estimate the average solar potential (in $MJ/m^2/day$) throughout the year. The Python libraries used for this analysis included libraries used, e.g., Pandas for data manipulation, NumPy for numerical calculations and Matplotlib to plot and excel is also used for some visualization of data

3.3. Solar-Powered Steam Sterilizer System

This system utilizes solar energy to generate steam directly within the receiver tube for sterilization and incorporates a condenser to distill the water used in the process. The key components are:

- **Solar Collector:** A parabolic trough collector with a reflective surface area of 1.02 square meters, constructed from galvanized stainless-steel sheets supported by a steel frame. The collector is designed to concentrate sunlight onto the receiver pipe. The collector is inclined to facilitate natural convection and steam movement.
- **Receiver Pipe** A black-painted copper pipe (inner diameter: 25 mm, length: 1.4 meters) located at the focal line of the parabolic trough. Water flows through this pipe, where it is directly heated by the concentrated sunlight and converted into steam via natural convection.
- **Sterilization Chamber:** A commercially available 10-liter stainless steel pressure chamber, modified with additional ports for steam inlet and a temperature sensor. It is equipped with its original pressure regulator (set at approximately 15 psi) and safety valve.
- **Condenser:** A heat exchanger designed to cool the steam exiting the sterilization chamber, causing it to condense back into distilled water. This could consist of a coiled copper tube surrounded by water can circulate. The condensed water is collected in a separate container.
- **Insulation:** glass wall insulation is used to minimize heat loss from the steam chamber and the steam transport lines.
- **Piping and Valves:** stainless-steel hose valves are used to connect the receiver pipe (steam generator) to the sterilization chamber and from the sterilization chamber to the condenser.
- **Water Storage:** The distilled water collected from the condenser can also be used to reservoir.

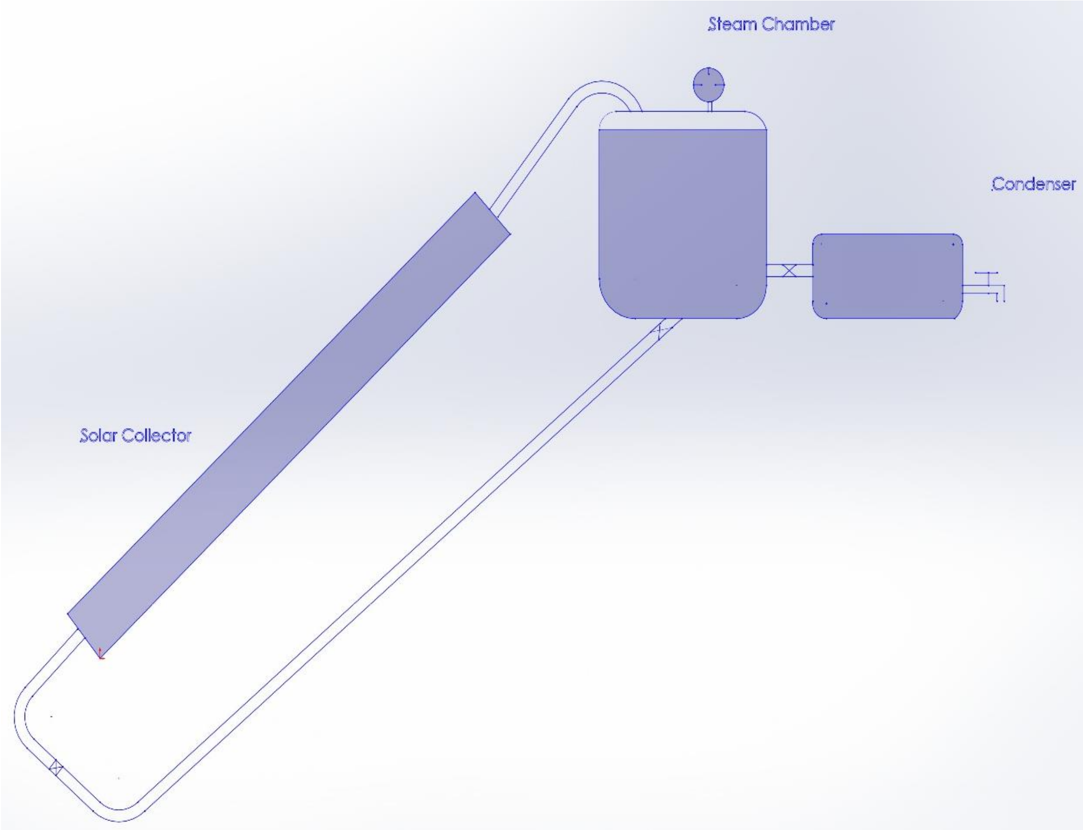

Figure 3.1: Schematic Diagram of Solar Powered Steam Sterilizer

The steam sterilizer, which is integrated with a Parabolic Trough Solar Concentrator (PTC), works by converting concentrated solar energy into high-temperature steam that successfully destroys microorganisms at temperature and pressure. The device has a long, curved reflecting surface that tracks the sun to maximize solar energy capture. This concentrated sunlight is focused on a receiver tube containing water, rapidly raising the temperature. When the water hits 120°C, it vaporizes, producing steam, while the system maintains pressure at 2 bar, increasing sterilizing efficiency. The produced steam is then sent into a sterilizing chamber containing medical tools. High temperature steam denatures proteins and destroys cellular structures, destroying bacteria, viruses, and spores. Typically, the goods are exposed to these conditions for up to 30 minutes to ensure full sterilization. Following the sterilization cycle, steam is vented and pressure gradually reduced, allowing safe access to the sanitized equipment. Following the sterilization cycle, steam is vented and pressure gradually reduced, allowing safe access to the sanitized equipment. Meanwhile, the steam generated during the operation can be channeled to a condenser and used to

the steam passes through the condenser, which is normally composed of copper for high heat transfer durability and corrosion resistance, it cools and condenses back into liquid form, producing distilled water.

CHAPTER FOUR

4. DESIGN AND ANALYSIS

4.1. SOLAR POTENTIAL ANALYSIS

There is a growing need for an accurate map of the energy that is available, even when solar radiation data is not available at many meteorological stations. Solar radiation is a crucial element in many biogeochemical models. The most widely used method for calculating solar radiation is the sunshine duration (Das et al., 2015). Sunshine duration is an extensively measured and used meteorological characteristic. Measuring global solar radiation in developing nations has proved challenging due to inadequate equipment availability or malfunction. Sunshine duration is defined as the number of hours in a day during which direct solar irradiance surpasses a threshold of 120 W/m² (Suehrcke et al., 2013).

Radiation and is used to assess the climate of a location. The duration of sunshine has been used as an alternate method to estimate this metric. Sunshine duration is reliable and easy to utilize across multiple stations. In 1924, Angstrom postulated a link between worldwide solar radiation and hours of bright sunshine (Umoh & Udoh, 2010).

4.1.1. Basic Terms of Solar Analysis

Solar Time: Solar time, which is essential for calculating all solar angles, differs from local clock time due to variations in longitude and the equation of time (Neto et al., 2021). Standard time is adjusted to solar time by incorporating the equation of time, which compensates for the Earth's orbital eccentricity and axial inclination (AL-Rousan et al., 2018). The variation in minutes between solar time and standard time is expressed as (Notton, 2017):

$$\text{Solar Time} - \text{Standard Time} = 4(L_{\text{st}} - L_{\text{loc}}) + E \quad (4.1)$$

Here, L_{st} represents standard meridian of the local time zone, while $\boldsymbol{L_{\text{loc}}}$ denotes the longitude of the specific location, with all longitudes measured in degrees west (0° < L < 360°). The parameter E corresponds to the equation of time, expressed in minutes, and is defined as (Yousef et al., 2023a):

$$E = 9.87\sin(2B) - 7.53\cos(B) - 1.5\sin(B) \quad [\text{min}] \quad (4.2)$$

$$B = \frac{(N-81)360}{365} \quad (4.3)$$

The latitude (**ϕ**) the number of degrees to the north or south measured from the equator ($-90^{\circ} \leq (\phi) \leq 90^{\circ}$). Near the equator the sun is overhead at the noon and receives much radiation than as we move toward the poles.

The latitude and longitude of Kobo are:

- Latitude: 8.9° N
- Longitude: 39.9167° E

Declination Angle (δ): Solar declination refers to the angular distance of the sun's rays relative to the Earth's equatorial plane, with northward declination considered positive (Vician et al., 2017). The rotational axis of the earth to the rotational plane (Ecliptic) of earth around the sun is not exactly perpendicular it is tilted off by nearly 23.45 degree instead it is perpendicular to the equinoctial plane. An equinox occurs when the solar declination is exactly zero. Whereas the North Pole and the south poles are as close as possible to the sun. it is called summer solstice and winter solstice respectively. The value of the declination angle is crucial for determining solar radiation amount that received by various regions of the Earth's surface. It varies between −23.45◦ and 23.45◦, and it is given by (Vician et al., 2017)

$$\delta = 23.45 \sin\left(\frac{360}{365} \times (284 + N)\right) \tag{4.4}$$

where *N* represents the day number of the year.

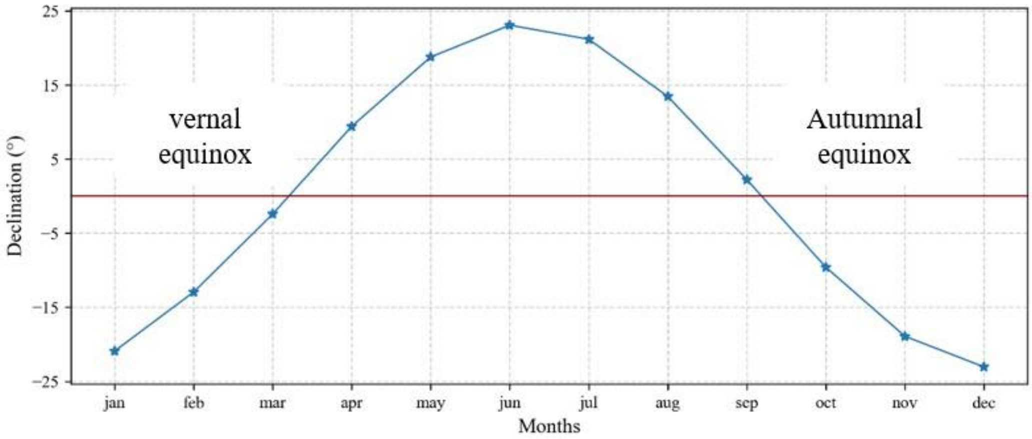

Figure 4.1: Declination angle variations throughout the year.

Declination Angle (δ): Solar declination refers to the angular distance of the sun's rays relative to the Earth's equatorial plane, with northward declination considered positive (Vician et al., 2017). The rotational axis of the earth to the rotational plane (Ecliptic) of earth around the sun is not exactly perpendicular it is tilted off by nearly 23.45 degree instead it is perpendicular to the equinoctial plane. An equinox occurs when the solar declination is exactly zero. Whereas the North Pole and the south poles are as close as possible to the sun. it is called summer solstice and winter solstice respectively. The value of the declination angle is crucial for determining solar radiation amount that received by various regions of the Earth's surface. It varies between -23.45° and 23.45°, and it is given by (Vician et al., 2017)

$$0^\circ \leq \beta \leq 180^\circ \tag{4.5}$$

When $\beta > 90^\circ$, it means the surface is tilted in a downward direction.

Surface Azimuth Angle (γ): The surface azimuth angle (γ) indicates the deviation between the projection of the surface's normal on a horizontal plane and the local meridian (Al-Ghussain & Taylan, 2020), given by:

$$-180^\circ \leq \gamma \leq 180^\circ \tag{4.6}$$

where: zero corresponds to due south, negative values represent east and west is negative and positive respectively.

Hour Angle (*ω*): The hour angle (ω) describes the angular displacement of the sun east or west of the local meridian due to the Earth's rotation at a rate of 15° per hour (Dehghani-Sanij & Bahadori, 2021). It is negative in the morning and positive in the afternoon (Kalogirou, 2012), calculated as:

$$\omega = (ST - 12) \times 15^\circ \tag{4.7}$$

where ST is the local solar time.

Angle of Incidence (θ): The solar incidence angle, θ, is the angle formed between the normal to a surface and the sun's rays, it is given by (Kalogirou, 2009):

$$\cos\theta = \sin\delta\sin\phi\cos\beta - \sin\delta\cos\phi\sin\beta\cos\omega + \cos\delta\cos\phi\cos\beta\cos\omega + \cos\delta\sin\phi\sin\beta\cos\gamma\cos\omega + \cos\delta\sin\beta\sin\gamma\sin\omega \quad (4.8)$$

Zenith Angle (θ_Z): It is the complement of the solar altitude angle (angle between the sun and the Earth's horizon) (Kamran, 2023). The zenith angle is the angle between the vertical and the line to the sun (Martinez-Gracia et al., 2019).

$$\cos\theta_z = \sin\phi\sin\delta + \cos\phi\cos\delta\cos\ \omega \quad (4.9)$$

Solar Altitude Angle (α_S): The solar altitude angle is defined as the angle formed between the horizontal plane and the direct line to the sun It is given by(Ahmad et al., 2013):

$$\alpha = 90° - \theta_z \quad (4.10)$$

Solar Azimuth Angle (γ_s): refers to the angular shift of the sun's beam projection on the horizontal plane, measured from geographic south(Khalil & Shaffie, 2016). It shows the location of the sun in relation to the observer's meridian. An eastward shift is indicated by a negative value, and a westward shift is shown by a positive value. Because it affects how solar collectors are oriented for maximum energy absorption, this parameter is crucial in solar energy applications.

Sunshine Hour (N_S): The total time, in hours, that the Sun moves from sunrise to sunset is determined using the hour angle as follows:

$$\text{Day length} = \frac{2\omega_s}{15} \quad (4.11)$$

where the hour angle at sunset, measured in degrees, is denoted by ω_s. The division by 15 reflects the Earth's rotation rate, indicating that the sun traverses 15 degrees of the sky each hour. This formula is essential for calculating solar energy, as it helps determine the amount of available sunlight for various applications throughout the day. Understanding day length is crucial for optimizing the placement of solar panels and enhancing energy efficiency.
where (ω_s) is sunset hour angle.
For ($\theta_Z = 90°$), calculated as:

$$\omega_s = \cos^{-1}(-\tan\phi \times \tan\delta) \quad (4.12)$$

Thus, the sunshine hour can also be expressed as:

$$N_S = \frac{2}{15}\cos^{-1}(-\tan\phi \times \tan\delta) \tag{4.13}$$

Table 4.1: Monthly mean Adama city sunshine duration

Months	Jan	Feb	Mar	Apr	May	Jun	Jul	Aug	Sep	Oct	Nov	Dec
Average (2012-2017)	8.73	9.25	9.00	8.40	8.23	7.96	6.80	6.86	7.32	8.90	9.38	9.35

Table 4.2: Monthly mean Kobo Town sunshine duration

Months	Jan	Feb	Mar	Apr	May	Jun	Jul	Aug	Sep	Oct	Nov	Dec
Average (2012-2017)	8.9	9.38	9.4	8.45	8.28	8.10	7.01	7.1	7.6	9.16	9.4	9.45

Kobo exhibits almost similar, and in some months even slightly higher, average sunshine durations compared to Adama. Beyond that, it is located in the same geographical region, which confirms the relevance of performing solar potential of Kobo town.

Albedo (ρ) It measures the quantity of reflection of solar radiation after it strikes the a given surface. Its value ranges from 0 for 0 to 1 to 1 (null reflection to complete reflection). The amount of reflected radiation can be found by using the following formula.

$$I_{ref} = \rho I_{sc} \tag{4.14}$$

Where I_{sc} is solar constant.

In our planet clouds have highest albedo effect. Generally brighter surfaces have higher value of albedo than somewhat darker surfaces with this considerations Ice surfaces will have high reflectivity than ground. So, the ground primarily absorbs solar radiation. Here in the table other surfaces albedo are given.

Table 4.3: Albedo Value of Different Surfaces:

Surfaces	Albedo
Fresh snow	0.850-0.950
Dry sand	0.350-0.400
Plain and farmland	0.20-0.30
Tropical forest	~0.13
Ocean	0.04-0.10

Insolation: the term insulation is the amount of Irradiance received over a specific period of time interval and it is measured in KWH/m^2orMJ/m^2. Whereas irradiance is a measure of solar intensity (density) incident on the surface and it is measured by KW/m^2.

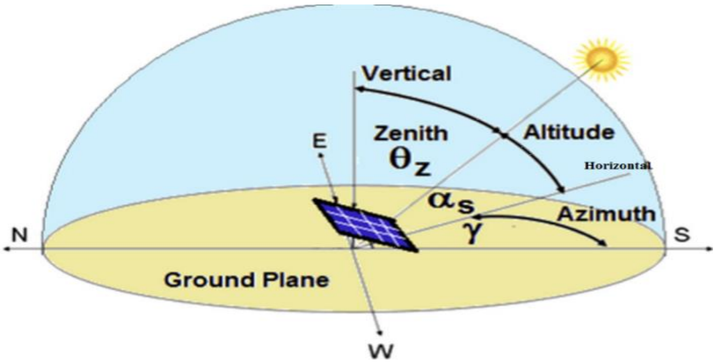

Figure 4.2: Surface azimuth angle, solar azimuth angle, slope, and zenith angle for a tilted surface (Duffie & Beckman, 2013)

Table 4.4: The suggested average number of sunshine days per month of the year (Mousavi Maleki et al., 2017)

Month	n for i^{th} Day of the Month	For the Average Day of the Month		
		Date	n	δ
January	i	17	17	-20.9
February	31+i	16	47	-13.0
March	59+i	16	75	-2.4
April	90+i	15	105	9.4
May	120+i	15	135	18.8
June	151+i	11	162	23.1
July	181+i	17	198	21.2
August	212+i	16	228	13.5

September	243+i	15	258	2.2
October	273+i	15	288	-9.6
November	304+i	14	318	-18.9
December	334+i	10	344	-23.0

4.1.2. Radiation on Horizontal Surface

4.1.2.1. Instantaneous Extraterrestrial Radiation

ER is the solar radiation incident on a horizontal surface above the Earth's atmosphere. It is influenced by factors such as latitude, season, and time of day, and is crucial for determining the net radiation received by a plant surface (Sabzevari & Eslamian, 2022). It may mathematically be defined as:

$$I_o = I_{sc}\left(1 + 0.033cos\left(\frac{360n}{365}\right)\right)(cos\delta cos\phi cos\omega + sin\delta sin\phi) \qquad (4.15)$$

Where, I denotes the extraterrestrial radiation measured in watts per square meter (W/m²). The solar constant Isc is a standardized value of 1367 W/m², representing the amount of solar energy received at an average distance from the sun. Here, n represents the specific day of the year.

4.1.2.2. Extraterrestrial Radiation for an Hour Period

This corresponds to the radiation received between hour angles ω_1 and ω_2 (where ω_2 is the larger). The equation is given by:

$$I_h = \frac{12 * 3600}{\pi} I_{sc}\left(1 + 0.033\, cos\frac{360n}{365}\right)$$
$$\left[cos\,\phi\, cos\,\delta\,(sin\,\omega_2 - sin\,\omega_1) + \frac{\pi(\omega_2 - \omega_1)}{180} sin\,\phi\, sin\,\delta\right] \qquad (4.16)$$

where: I_{sc} is solar constant, ω_2 and ω_1 are max and min hour angles,ϕ is latitude angle,
δ is declination angle,

4.1.2.3. Daily Extraterrestrial Radiation

denoted as H_o (in J/m^2/day), is calculated by integrating the aforementioned equation over the interval from sunrise to sunset.

If I_{sc} is measured in watts per square meter, then Ho will be expressed in joules per square meter per day. The formula for H_o is given by:

$$H_o = \frac{24*3600}{\pi} I' \left(cos\, \phi\, cos\, \delta\, sin\, \omega_s + \frac{\pi\omega_s}{180} sin\, \phi\, sin\, \delta\right) \quad (4.17)$$

where:

- I' is modified solar constant,
- ω_s is sunset hour angles.

4.1.2.4. Monthly Mean Daily Terrestrial Global Radiation

When estimating monthly average daily solar radiation on a horizontal surface, the most straightforward approach is the equation given by well-known Angstrom. The first empirical connection that estimated global solar radiation using sunshine hours was put forth by Angstrom.

$$\frac{\overline{H}}{\overline{H_o}} = a + b\left(\frac{\overline{n_s}}{\overline{N_s}}\right) \quad (4.18)$$

$$a = -0.11 + 0.2350 \cos \phi + 0.3230 \left(\frac{\overline{n_s}}{\overline{N_s}}\right) \quad (4.19)$$

$$b = 1.449 - 0.53300 \cos \phi - 0.694 \left(\frac{\overline{n_s}}{\overline{N_s}}\right) \quad (4.20)$$

where:

- $\overline{n_s}$ is monthly Mean daily sunshine hour.
- $\overline{N_s}$ is the monthly mean of the maximum possible daily hours of bright sunshine.

The extraterrestrial radiation$\overline{H_o}$ can be obtained by the Klein relationship:

$$\overline{H_o} = \frac{24\times3600\times I_{sc}}{\pi}\left(1 + 0.0330 \cos\left(\frac{360.0n}{365}\right)\right)\left(\cos\phi \cos\delta \cos\omega_s + \frac{\pi\times\omega_s}{180}\sin\phi \sin\delta\right)$$

(4.21)

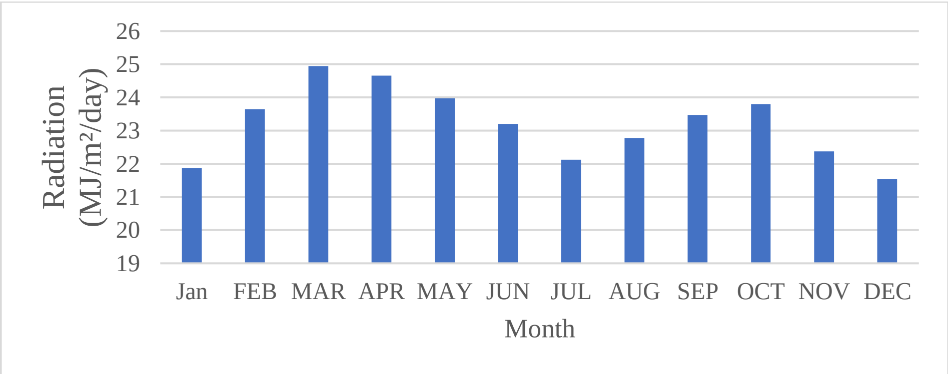

Figure 4.3: Monthly Average Daily radiation

4.1.2.5. Terrestrial Monthly mean Daily Diffuse Radiation

The monthly mean diffuse radiation on a horizontal surface can be estimated using the monthly average global radiation data along with the recorded number of bright sunshine hours (Ulgen & Hepbasli, 2009).

$$\frac{\overline{H_d}}{\overline{H}} = 0.931 - 0.814\left(\frac{\overline{n_s}}{\overline{N_s}}\right) \quad (4.22)$$

Where:

- $\overline{H}$ is monthly average daily global radiation,
- $\overline{H_d}$ is monthly average daily diffuse radiation.

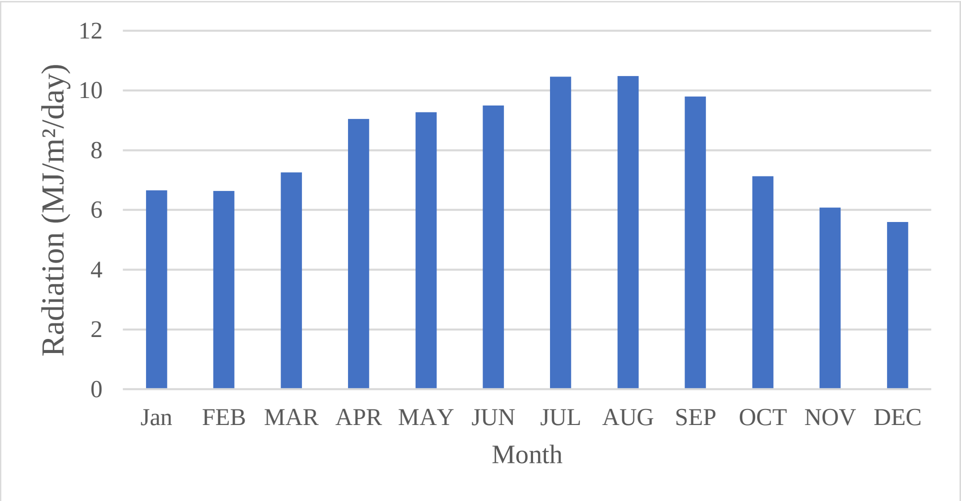

Figure 4.4: Monthly Average Daily Diffuse Radiation on a Horizontal Surface

The monthly mean daily beam radiation can be found based on modified angstrom equation as follows:

$$\overline{H_b} = \overline{H} - \overline{H_d} \quad (4.23)$$

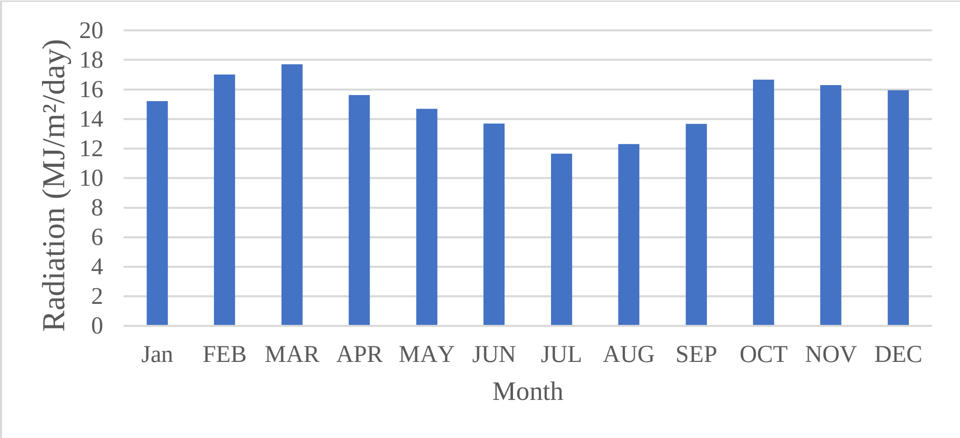

Figure 4.5:Monthly Average Daily Beam Radiation on a Horizontal Surface

4.1.2.6. Monthly Average Hourly Global Radiation on a Horizontal Surface

$\bar{I}$ is the average amount of total solar radiation received per hour on a unit horizontal surface during each month, typically expressed in megajoules per square meter per hour (MJ/m²/h).

$$\frac{\bar{I}}{H} = \frac{\pi}{24}(a + b\cos\varpi)\frac{(\cos\varpi - \cos\varpi_s)}{\left(\sin\varpi_s - \frac{\pi}{180}\varpi_s\cos\varpi_s\right)} \tag{4.24}$$

Where:

- $a = \ 0.4090 + 0.50160\sin(\varpi_s - 60)$,
- $b \ = 0.66090 - 0.47670\sin(\varpi_s - 60)$,

4.1.2.7. Monthly Mean Hourly Diffuse Radiation on a Horizontal Surface

$\overline{I_d}$ is the average amount of solar radiation per hour that is scattered by the atmosphere and received on a unit horizontal surface during each month, excluding the direct beam radiation.

$$\frac{\overline{I_d}}{\overline{H_d}} = \frac{\pi}{24}\frac{(\cos\varpi - \cos\varpi_s)}{\left(\sin\varpi_s - \frac{\pi}{180}\varpi_s\cos\varpi_s\right)} \tag{4.25}$$

4.1.2.8. Monthly Mean Hourly Beam Radiation on a Horizontal Surface

Beam Radiation or direct radiation is solar radiation that comes in a direct line from the sun to the Earth's surface without any diffusion or scattering of the atmosphere. It is extremely concentrated and directional and can cause sharp shadows. Beam radiation is strongest when the sun is clear and unobstructed and the sky is cloudless, and therefore it is an essential component in solar power concentration systems and solar energy estimates.

$$\overline{I_b} = \bar{I} - \overline{I_d} \tag{4.26}$$

Where:

- $\overline{I}$ is monthly average hourly global radiation,
- $\overline{I_d}$ is monthly average hourly diffuse radiation.

4.1.3. Radiation on Tilted Surface

4.1.3.1. Total Hourly Irradiance on a Tilted Surface

Radiation on tilted surfaces denotes the quantity of solar energy striking a surface that is inclined at an angle from the horizontal rather than being horizontally aligned. This inclination facilitates improved alignment with solar radiation, potentially enhancing the quantity of energy absorbed by solar collectors. Consequently, system designers require solar radiation data for tilted surfaces; however, most accessible data pertains either to normal incidence or horizontal surfaces.

The total hourly irradiance on a tilted surface I_T is given by (Venkatachalam, 2019):

$$I_T = I_b R_b + I_d \left(\frac{1+\cos\beta}{2}\right) + (I_b + I_d)\rho \left(\frac{1-\cos\beta}{2}\right) \quad (4.27)$$

Where:

- I_T total hourly radiation of a tilted surface (W/m²) ,
- I_b is hourly beam radiation (W/m²),
- I_d is hourly diffuse radiation (W/m²),
- R_b is ratio of $\frac{\cos\theta}{\cos\theta_z}$,
- β is Surface slope angle,
- ρ is Ground albedo (reflectivity), ρ = 0.2 for bare earth, ρ = 0.7 for snow.

The geometric factor R_b , the ratio of beam radiation on the tilted surface to that on a horizontal surface at any time, is given by:

$$R_b = \frac{I_{bT}}{I_{bH}} = \frac{I_b \cos\theta}{I_b \cos\theta_z} = \frac{\cos\theta}{\cos\theta_z} \quad (4.28)$$

$$\cos\theta = \sin\delta\sin\phi\cos\beta - \sin\delta\cos\phi\sin\beta\cos\omega + \cos\delta\cos\phi\cos\beta\cos\omega + \cos\delta\sin\phi\sin\beta\cos\gamma\cos\omega + \cos\delta\sin\beta\sin\gamma\sin\omega \quad (4.29)$$

$$\cos\theta_z = \sin\phi\sin\delta + \cos\phi\cos\delta\cos\omega \quad (4.30)$$

4.1.3.2. Daily Total Radiation on a Tilted Surface

The daily total radiation on a tilted surface is given by (Venkatachalam, 2019):

$$H_T = H_b R_b + H_d\left(\frac{1+\cos\beta}{2}\right) + (H_b + H_d)\rho\left(\frac{1-\cos\beta}{2}\right) \tag{4.31}$$

$$R_b = \frac{\cos(\phi-\beta)\cos\delta\sin\omega_s' + \frac{\pi}{180}\omega_s'\sin(\phi-\beta)\sin\delta}{\cos\phi\cos\delta\sin\omega_s + \frac{\pi}{180}\omega_s\sin\phi\sin\delta} \tag{4.32}$$

$$\omega_s' = min[cos^{-}(-tan\,\phi\, tan\,\delta)\; or\; cos^{-}(-tan(\phi-\beta)\, tan\,\delta)] \tag{4.33}$$

Where:

- H_T is total daily solar radiation incident on an inclined surface,
- H_b is daily direct (beam) solar radiation received on a flat horizontal surface,
- H_d is daily scattered (diffuse) solar radiation falling on a horizontal surface.

4.1.4. Hourly Variation of Temperature

One of the main inputs to model and design a parabolic trough solar collector is the ambient temperature. Such high-quality data for most sites in Ethiopia is not easily accessible. A mathematical model that is based on using the daily lowest and highest temperature values, to estimate the hourly change of outdoor temperature. Consequently, a practical approach involves modeling the daily temperature fluctuations using a sinusoidal function (Shumeta, 2021). This simplification allows for a reasonable estimation of the ambient temperature, denoted as T(t), at any given time, t, throughout the day.

$$T(t) = T_{max} - (T_{max} - T_{min})\left(1 - \sin\left(\frac{\pi(t-6)}{12}\right)\right) \tag{4.34}$$

Where: $T(t)$ - Ambient temperature at time t (in hours), T_{max} - Mean daily highest temperatureT_{min} - Mean daily lowest temperature

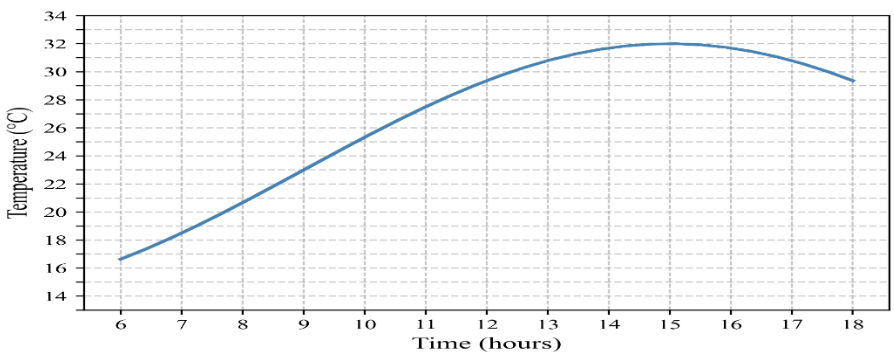

Figure 4.6: Variation of Temperature Throughout the Daytime (Sunrise to Sunset)

4.2. Water in Steam Sterilization Systems

4.2.1. Thermodynamic Properties of Water

Water absorbs sensible heat until it reaches its boiling point. At this stage, latent heat facilitates the phase transition from liquid to vapor. As long as liquid water remains, the steam temperature remains equal to that of the water. Saturated steam forms when liquid water and its vapor coexist in thermal equilibrium (C¸engel & Boles, 2019).

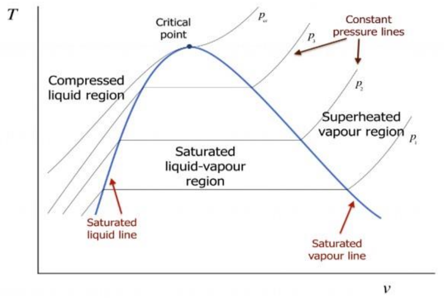

Figure 4.7: A T-v diagram showing the compressed liquid, saturation, and superheated vapor regions (Moran et al., 2018)

Saturated steam provides rapid and uniform heating through latent heat transfer, enables temperature control via pressure regulation, and has a high heat transfer coefficient. Industries commonly utilize saturated steam for heating, cooking, and drying, whereas superheated steam is primarily used in turbines.

Different types of steam exhibit varying energy transfer capacities, measured by the heat transfer coefficient (*U*), which quantifies the watts transferred per unit surface area per degree of temperature difference. A higher coefficient indicates greater heat transfer efficiency. Once all the liquid water has vaporized, any additional heat increases the steam temperature. Steam that is heated beyond the saturation point is referred to as superheated steam. Superheated steam transfers only sensible heat in an exchanger and must first cool before heating another substance. When in contact with a surface, it releases energy as it cools. However, due to its insulating properties—like all gases—superheated steam farther from the surface does not readily transfer heat.

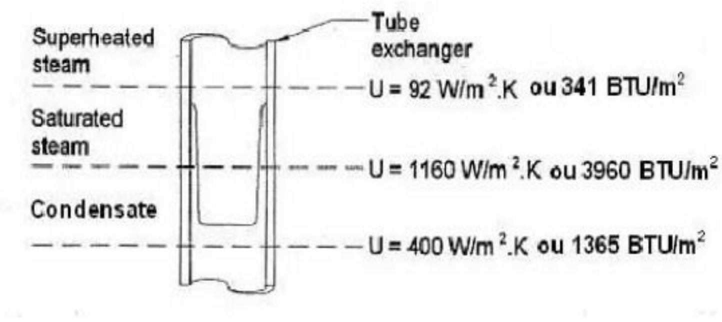

Figure 4.8: Heat Transfer Capacity (U) for Water at Different State

To raise the water's boiling point to 121°C in a vessel, pressure must be applied. Stated differently, the boiling point of water will rise in response to an increase in pressure. The water will evaporate due to the chamber's heat, increasing the pressure. Following the After the water has evaporated, either saturated or superheated steam can be utilized to disinfect the equipment. Despite having more energy and being hotter than saturated steam, superheated steam transfers heat poorly due to its low heat transfer capacity. Due to its superior capability for energy exchange, saturated steam is preferred.

4.2.2. Water Quality for Sterilization

Water quality has an even greater effect on steam autoclaves in isolated locations with limited availability to treated or filtered water. Numerous rural medical facilities depend on groundwater from lakes, rivers, or wells, which can have high concentrations of dissolved minerals including iron, calcium, and magnesium. In autoclaves, where steam must pass via small pipes and valves to reach the sterilizing chamber, this scaling effect is especially troublesome (Panta et al., 2021). Furthermore, the existence of mineral deposits may result in unequal heating and steam dispersion, which could leave medical equipment not fully sterilized. Medical devices' efficacy and lifespan may be risked if they are exposed to hard water residues for an extended period of time because this can cause corrosion, pitting, and surface degradation.

When it comes to reprocessing medical devices, water is crucial. During the reprocessing cycle, water is mostly utilized for the steam sterilization and cleaning procedures. While water is used primarily to generate steam during moist-heat sterilization processes, it can also be used to maintain the moisture content of used medical devices, rinse organic solids from medical devices, prepare cleaning solutions (such as detergents), and rinse the decontaminated device one last time. Depending on these procedures, different water quality standards are needed.

The three most essential aspects of water quality are pH, TDS, and hardness the pH scale indicates acidity (pH < 7), alkalinity (pH > 7), or neutrality (pH = 7). TDS (Total Dissolved Solids) measures the total concentration of all dissolved solids Hardness is determined by the concentration of calcium (Ca^{2+}) and magnesium (Mg^{2+}) ions Other chemical contaminants also affect the quality of water meaning the presence of ionic solid increase the conductivity of water.

4.3. Estimation of Thermal load for Sterilization

To design an efficient solar-powered steam sterilizer, we must consider three main factors: the thermal energy required to heat the water, the energy needed to heat the load (such as instruments or glassware), and heat losses due to insulation and design. For this scenario, we took a water volume of 1 liter (1 kg), a load mass of 5.5 kg (typical for small medical tools or media bottles), and a load material of stainless steel or glass. The process starts at an initial temperature (T_1) of 25°C and reaches a sterilization temperature (T_2) of 121°C, creating a temperature difference (ΔT).

The total energy demand depends on the specific heat capacities of both water and the load material, along with their respective masses. Minimizing heat loss through proper insulation and an optimized steam sterilizer design is crucial for energy efficiency. By accurately calculating these requirements, we can develop a solar-powered system that reliably generates sufficient steam for sterilization while maximizing renewable energy use. This ensures effective sterilization performance in off-grid or resource-limited settings.

In order to determine the energy required to heat water, the following equation can be applied:

The total heat is the sum of the heat required for heating and vaporization:

$$Q_t = Q_w + Q_v \tag{4.35}$$

Where Q_t is the total heat require Q_v the heat required to vaporize Q_w the heat required to heat water.

Calculate Energy for Water to rise the temperature

$$Q_w = m_w \times Cp_w \times \Delta T \tag{4.36}$$

For effective sterilization of medical equipment by the solar steam sterilizer, the steam temperature must be increased from room temperature (25°C) to 121°C. values from

(C¸engel & Boles, 2019 and applying Equation, the required energy transfer can be calculated once the water mass is known. Since the boiler utilizes 1 liter of water, which is equivalent to approximately 1 kilogram at room temperature.

The heat required to raise stainless steel and glass equipment to 121°C depends on its mass, specific heat capacity, and temperature increase. The amount of heat needed is determined by:

$$Q_l = m_s \times Cp_s \times \Delta T + m_g \times Cp_g \times \Delta T \tag{4.37}$$

$$Q_l = (4.5\, kg \times 0.5 \times +1\, kg \times 0.8) \times 96$$

Where Q_l = Thermal energy to heat the load (J), m_s = Mass of stainless-steel instruments (kg), Cp_s = Specific heat of stainless steel (~500 J/kg·K), m_g = Mass of glassware (kg), Cp_g = Specific heat of glass (~840 J/kg·K)

Total Thermal Energy

$$Q_{total} = Q_w + Q_{lS} + Q_{lg} + Q_v \tag{4.38}$$

$$Q_v = 0.1\, kg \times 2257\, kJ/kg = 225.7\, kJ \tag{4.39}$$

$$Q_{total} = 401.3 + 192 + 115.2 + 225.7 = 934.2kJ(\approx 0.26kWh)$$

Where Q_{lS} the heat for steel Q_{lg} heat for glass

The energy required to heat the water in the autoclave can be determined using the equation provided above. Once this energy is transferred to the water in the boiler, the pressure increases, enabling the water to reach 121°C.

4.4. Sizing of PTC Solar Collector

In this section involves the calculation of the appropriate PTC geometry are calculated that are required to meet a specified thermal energy demand, so that the system will be capable of delivering sufficient energy for the intended application at a given solar radiation and efficiency.

4.4.1. Geometry of parabolic trough collector

is a solar thermal energy collector whose reflective surface is parabolically shaped so that sunlight is focused onto a receiver tube along the parabola's focal line. This tube, also known as an absorber, contains a heat transfer fluid, the temperature of which is increased by solar radiation that has been concentrated. Here important geometries are sized

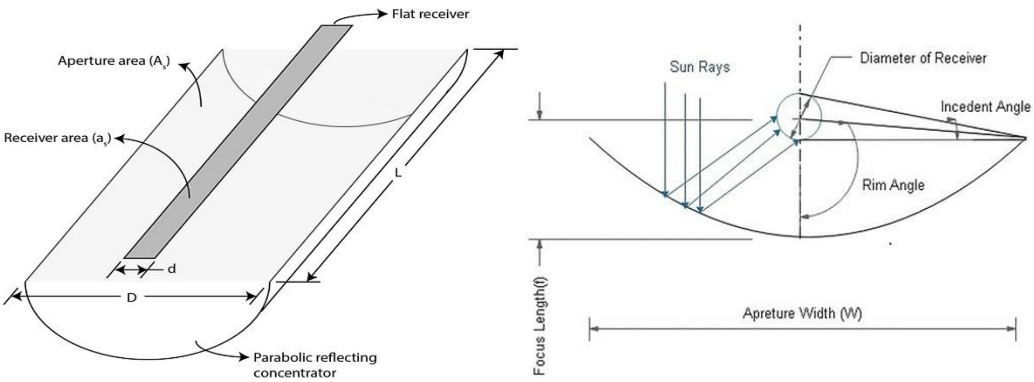

Figure 4.9: Geometry of parabolic trough collector (Al-Rabeeah et al., 2023)

The geometrical profile of the PTC is defined by the following parabolic equation in Cartesian coordinates *x* and *y* (Duffie & Beckman, 2013).

$$x^2 = 4yf \tag{4.40}$$

Reflector Aperture Area: Most solar concentrators function with a thermal efficiency generally ranging from 40% to 60%, though this can vary depending on factors such as solar flux intensity and the flow rate of the heat transfer fluid (Wadate & Dharmadhikari, 2019a).

The thermal efficiency η_{th} of the PTC system measures the effectiveness of converting available solar energy Q_s into useful thermal energy Q_u. It is expressed as:

$$\eta_{th} = \frac{Q_u}{Q_s} \tag{4.41}$$

where: $Q_s = I_b A_{ap}$, Q_u =useful energy, I_b - beam radiation, and A_{ap} - aperture area of the parabolic trough reflector. The aperture area is determined by multiplying the aperture width by the collector length.

$$A_{ap} = w_a \cdot l \tag{4.42}$$

Where w_a, l are aperture area width and length of the trough respectively.

The useful thermal energy Q_u is determined by the mass flow rate of the fluid $\dot{m}$ and the temperature difference between the inlet T_{in} and outlet T_{out} temperatures, as given by the equation (Abed & Afgan, 2020):

$$Q_u = \dot{m}C_p(T_{out} - T_{in}) \tag{4.43}$$

Focal length: is the critical distance from the vertex of its parabolic surface to the focal line where sunlight is concentrated onto the receiver tube. This parameter significantly influences the collector's concentration ratio and overall efficiency. Smaller PTCs for research or educational purposes may have focal lengths ranging from 0.1 to 0.3 meters (Upadhyay et al., 2021).

The parameter the parameter *f* represents the focal line, indicating the position of the solar receiver (Abed & Afgan, 2020). It is determined by the following formula:

$$f = \frac{w_a}{4\tan\left(\frac{\phi_r}{2}\right)} \tag{4.44}$$

Where

- w_a = is width of aperture
- ϕ_r = is rim angle

Rim Angle (ϕ_r): is defined as the angle between the optical axis of the reflector and the line that connects its focal point to the outer edge of the collector. It is a key geometric parameter and typically lies between 70° and 110° to ensure effective solar energy concentration and optimal system performance (Wadate & Dharmadhikari, 2019b). The rim angle determines the shape of the parabolic trough; an optimal value is required, as both excessively small and large rim angles are undesirable. A small rim angle leads to a narrow parabolic trough, which increases solar radiation incidence but also heightens heat loss through convection and radiation. The rim angle ϕ_r is calculated as a function of the aperture width and focal length. The rim angle ϕ_r is a critical geometric parameter that influences the number of solar rays concentrated by the parabolic trough, the concentration ratio, and the heat flux distribution on the receiver tube (Sup et al., 2015). This parameter is governed by the focal line distance and the collector aperture width (*W*). It is computed using the as follows (Akbarzadeh& Valipour, 2018):

$$\phi_r = \arctan\left[\frac{8\,(f/W)}{\sqrt{16\,(f/W)^2 - 1}}\right] = \sin^{-1}\left(\frac{W}{2r_r}\right) \tag{4.45}$$

The rim radius is obtained when ϕ =ϕ_r (Yilmaz & Mwesigye, 2018):

$$r_r = \frac{2f}{1+\cos\phi_r} \tag{4.46}$$

Where:

- r_r is rim radius,

- f is focal length,
- ϕ_r is rim angle.

Concentration Ratio: An optical concentration ratio is known as flux concentration ratio or intensity concentration ratio. It is defined as ratio average energy flux on the absorber to the aperture of the concentrator (Letcher, 2022). The total aperture area of a solar collector refers to the surface area through which solar radiation is captured. It is calculated using (Bellos and Tzivanidis, 2019a):

$$A_a = wa \cdot l \tag{4.47}$$

The outer surface area of the receiver tube is calculated using the formula for the lateral surface area of a cylinder (Malekan et al., 2021b):

$$A_{ro} = \pi \cdot D_o \cdot l \tag{4.48}$$

The unit area radiative energy input to the receiver surface is a function of concentration ratio, where the concentration ratio is the ratio of the collector aperture area to the absorber surface are (Malekan et al., 2021b):

$$C_R = \frac{A_a}{A_r} \tag{4.49}$$

$$C_R = \frac{w \cdot l}{\pi \cdot D_{sa} \cdot l} = \frac{w}{\pi \cdot D_{sa}} \tag{4.50}$$

The total curved surface area of parabolic trough is calculated as follows:

$$A_s = \left(\frac{W_a}{2} \sqrt{1 + \frac{W^2}{16f^2}} + 2f \ln\left(\frac{W_a}{4f} + \sqrt{1 + \frac{{W_a}^2}{16f^2}} \right) \right) \times 1 \tag{4.51}$$

4.4.2. Sun Tracking System

Due to the fact that PTCs operate with direct beam radiation, solar tracking systems are required. In order to optimize the collector’s one-axis rotation, a solar tracking system positions the collector in relation to the sun (Tagle-Salazar et al., 2020). A parabolic trough’s tracking is seen in the following figure. The rotating axis is typically parallel to or slightly below the parabolic trough’s vertex line.

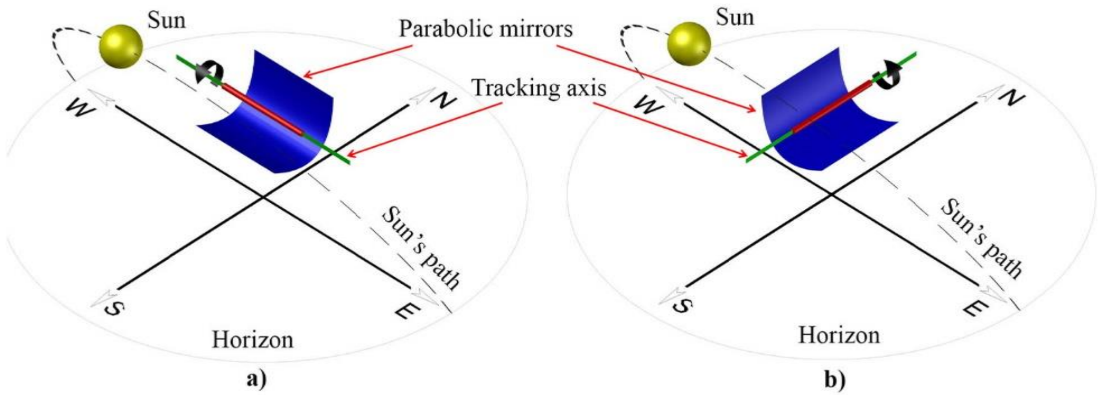

Figure 4.10: Sun Tracking System (Tagle-Salazar et al., 2020)

which allow the trough to follow the sun's movement from east to west throughout the day. This type of tracking ensures that the sunlight is consistently focused on the receiver tube, maximizing the thermal energy collected.

4.4.3. Incidence Angle Modifier

It is a factor used to account for the reduction in a solar collector's efficiency when sunlight strikes the collector surface at an angle other than perpendicular (normal incidence). When solar radiation hits a collector at an angle, a portion of the energy is reflected instead of being absorbed. The IAM adjusts the collector performance to reflect this angular dependence. A regression model of the measured data yields the following expression (Duffie & Beckman, 2013):

$$K = \cos(\theta) - B\,(\theta) - C\,\theta^2 \tag{4.52}$$

where: K ranges from 0 to 1, θ is the solar incident, B is the coefficient for the linear term, and "C is the coefficient for the nonlinear term". Test results for the SEGS LS-2 SCA provide an incident angle modifier expression as reported by (C¸engel & Boles, 2007). The reduction in the incidence angle modifier becomes more pronounced as the angle of incidence increases (M. Abbas et al., 2019).

$$K = \cos\theta - 0.0003512\theta - 0.0003137\theta^2 \tag{4.53}$$

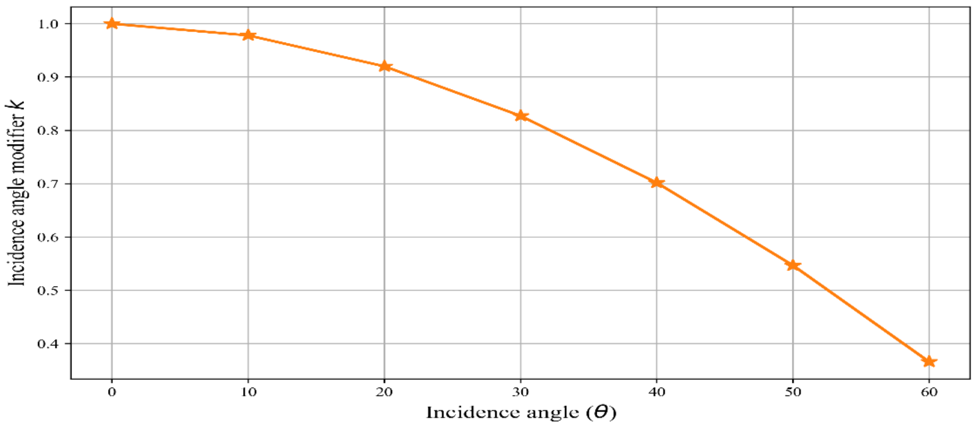

Figure 4.11: Variation of incidence angle modifier (k) with respect to the incidence angle (θ).

4.4.4. End Losses

At normal incidence, the reflected solar radiation from the concentrator fully illuminates the heat receiver. However, as the incident angle increases, regions near the ends of the receiver cease to be illuminated resulting in what are known as end losses. These losses depend on the focal length of the collector, the collector's length, and the incident angle. The equation for end losses is expressed as:

$$E_L = 1 - \frac{f \tan(\theta)}{L_{\text{SCA}}} \tag{4.54}$$

Where:

- f *is* focal length,
- θ *is* angle of solar incidence,
- L_{SCA} is total length of PTC.

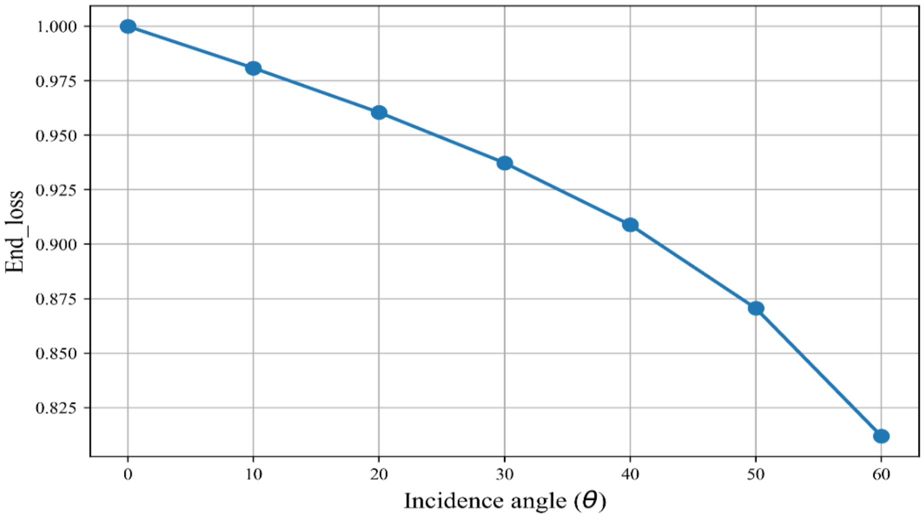

Figure 4.12: Effect of End losses with incident angle of solar radiation.

4.4.5. The Optical Efficiency of PTC

The optical efficiency of PTC represents the fraction of incident solar radiation that is effectively captured and directed toward the receiver. It influences the overall efficiency of the system, influencing the amount of thermal energy available for conversion.

Several factors affect the optical efficiency, including reflectivity of surface, the absorptivity and emissivity of the receiver tube, the geometric concentration ratio, and optical losses such as shading, end losses, and tracking errors. High-quality reflective materials and precise alignment of the parabolic trough are essential to maximize efficiency and reduce energy losses.

Mathematically, the optical efficiency can be expressed as:

$$\eta_o = \rho\tau\alpha\gamma \qquad (4.55)$$

Where:

- ρ = Reflectivity of the surface,
- τ = Transmittivity of the glass cover (if present),
- α = Absorptivity of the receiver,
- γ = Intercept factor.

By optimizing these parameters, the optical efficiency for a PTC can be improved, leading to better energy capture and enhanced thermal performance in solar energy applications.

4.4.6. Thermal Analysis of PTC

In this heat transfer model one dimensional heat transfer is considered and mainly it focuses on the receiver tube because it is where optical energy is converted to thermal energy and it is exposed to the environment and to the HTF

4.4.7. Heat Transfer Methods and Losses on Receiver Tube

I. Q_{conve} inside the tube

II. Q_{cond} across tube wall

It is calculated by assuming the receiver temperature is uniform across the circumference of the tube and considering all properties at steady state of mean temperature of inlet and outlet given by the Fourier's low of conduction.

$$q = \frac{T_i - T_o}{R} \tag{4.56}$$

$$R = \frac{\ln\frac{r_o}{r_i}}{2\pi kl} \tag{4.57}$$

III. Heat transfer between receiver tube and the atmosphere.

Q_{conv} and Q_{rad} are the two ways that heat is transferred between the receiver tube and the surroundings. As the receiver tube loses heat to the surrounding air, convection heat transfer occurs. At the same time, the temperature differential between the sky and the receiver tube causes radiative heat transfer. The overall heat loss to atmosphere is given by:

$$Q_{loss} = A_o\, h_{c(r-a)}\,(T_r - T_a) + A_o \varepsilon\sigma\left(T_r^4 - T_{sky}^4\right) \tag{4.58}$$

$$\mathrm{U_l} = h_{c(r-a)} + h_{r(r-a)} \tag{4.59}$$

$$h_{r(r-a)} = \varepsilon\sigma\left(T_r^2 + T_{sky}^2\right)(T_r + T_s) \tag{4.60}$$

$$R_r = \frac{1}{h_r A} \tag{4.61}$$

$$Q_r = \frac{(T_r - T_s)}{R_r} \tag{4.62}$$

a. Convection heat loss to atmosphere

$$Q_{c(r-a)} = A_o\, h_{c(r-a)}\, (T_r - T_a) \tag{4.63}$$

The heat transfer coefficient due to convection between the receiver tube and surrounding air is evaluated. $h_{c(r-a)}$ is given by the following correlation (Bellos, 2018).

$$h_{c(r-a)} = 4.\, V_{wi}^{0.58} D_o^{-0.48} \tag{4.64}$$

Where:

- A_o = Outer surface area of the pipe (receiver),
- $Q_{c(r-a)}$= Convective heat loss from receiver to ambient,
- $h_{c(r-a)}$ = Convective heat transfer coefficient at average temperature,
- T_r= Temperature of the receiver (Kelvin),
- T_a= Ambient temperature (Kelvin),
- K_a =Thermal conductance of air at average temperature.

Nu number in the absence of wind it is treated as natural convection over the horizontal cylinder and the formula is given by (C¸engel, 2018) for $Ra_D \leq 10^{12}$.

$$Nu = \left\{0.6 + \frac{0.387 \cdot Ra_D^{1/6}}{\left[1+\left(\frac{0.559}{Pr}\right)^{9/16}\right]^{8/27}}\right\}^2 \tag{4.65}$$

$$Ra_D = \frac{g\beta(T_s - T_a)d_o}{\alpha \cdot \nu} \tag{4.66}$$

Where:

- $\overline{Nu}_{do}$ =The average Nusselt number calculated using the outer diameter of the absorber,
- Ra_D: Rayleigh number, a dimensionless quantity that describes the flow regime (natural convection),
- g: gravity ($9.81 m/s^2$),
- β: Thermal expansion coefficient of the fluid (in units of 1/K),
- α: Thermal diffusivity of the fluid,
- ν: Kinematic viscosity

All fluid properties at the mean temperature.

b. Radiation heat loss to atmosphere

Heat losses from receiver tube to the ambient air is also need to be considered .and it is affected by its temperature gradient and the optical and thermal characteristic of the receiver tube and it is given by:

$$q_{rad} = \sigma\pi\varepsilon dl\left(T_r^4 - T_{sky}^4\right) \quad \textit{(4.67)}$$

$$T_{sky}^4 = 0.0552T_a^{1.5} \quad \textit{(4.68)}$$

Where:

- σ is Stefan Boltzmann constant $5.67 * 10 - 8\ \frac{W}{m^2k^4}$,
- ε is emissivity of the tube,
- l is length of tube,
- d is outer diameter of the tube.

The highest attainable heat gain in a solar collector occurs when the whole absorber remains at the inlet temperature of the working fluid. The heat removal factor quantifies the ratio of the actual heat extracted to this maximum potential, resembling the efficiency measure used in conventional heat exchangers (Yousef et al., 2023b), and it is calculated as:

$$F_R = mC_p \frac{A_0U_1}{1-\exp\left(\frac{-A_0F'U_1}{mC_p}\right)} \quad (4.69)$$

Where cp is the fluid specific heat, m is the collector flow rate F' is collector efficiency factor, defined as the ratio of heat transfer coefficient from the receiver surface to the ambient air and the Overall heat transfer coefficient and given as follows (Yousef et al., 2023b).

$$F' = \frac{\frac{1}{U_l}}{\left(\frac{1}{U_1}+\frac{D_0}{h_fD_i}\right)+\left(\frac{D_0}{2k}\ln\left(\frac{D_0}{D_i}\right)\right)} \quad (4.70)$$

From energy balance the for PTC Experimental and theoretical useful heat gain Q_u and Q_u respectively is given by.

$$Q_u = mc_p(T_o - T_i) \quad (4.71)$$

$$Q_{th} = F_RA_a\left[S - U_l\frac{(T_{fin}-T_{amb})}{C}\right] \quad (4.72)$$

$$S = \eta_oI_b \quad (4.73)$$

Where, A_a is aperture area C = concentration ratio, I_b is radiation intensity $\left(\frac{W}{m^2}\right)$

And its efficiency is calculated as follows

The actual efficiency (η_{expe}) given by (Yassen, 2012):

$$\eta_{expe} = \frac{Q_u}{I_b A_a} \tag{4.74}$$

The theoretical thermal efficiency is given as:

$$\eta_{th} = \frac{Q_{th}}{I_b A_a} \tag{4.75}$$

The local concentration ratio over the circumference of the receiver tube is given by.

$$C_{loc} = \frac{q(\theta)}{I_b A_{ap}} \tag{4.76}$$

Where $q(\theta)$ is local solar intensity $I_b$is direct irradiance and A_{ap} is aperture area of the trough. Integrating the local flux over the circumferential area of the receiver tube and dividing it to the amount of direct rate of energy reaches on the aperture area gives an optical efficiency of the PTC.

$$\eta_o = \frac{\int q(\theta)}{I_b A_{ap}} = \frac{q_{aver} A_r}{I_b A_{ap}} \tag{4.77}$$

Where, q_{aver} is the mean heat flux on the receiver tube. The extent of which heat flux intensity across the circumferential area deviation from the mean heat flux is assigned by uniformity of heat flux (U). The uniformity of heat flux over the circumference of the receiver tube is given by

$$U = \left(1 - \frac{\sigma_q}{q_{aver}}\right) * 100\% \tag{4.78}$$

Where σ_q is standard deviation of heat density over the circumference of the receiver tube. And if U is 100% meaning that heat is uniformly dispersed over the surface of the receiver.

This equation is critical in determining the efficiency of the heat transfer process within the solar power plant, ensuring that heat losses are minimized for optimal system performance.

Table 4.5: Some important Parameters of PTC Design

Parameter	Symbol	Value
PTC Aperture Width	w_a	0.60 m
PTC Length	l	1.6 m
PTC Aperture area	A_{ap}	1.015 m^2

PTC focal length	f	0.21 m
PTC rim angle	φr	83.88°
Concentration ratio of the PTC	C	25
Receiver outer diameter	d_{ro}	0.024 m
Receiver inner diameter	d_{ri}	0.022 m
Useful heat gain	Q_u	519 W
Total heat loss	Q_l	222 W
Maximum thermal power	Q_{sc}	741 W

4.5. Thin Walled Pressure Vessel

Codes such as the ASME Boiler and Pressure Vessel Code (BPVC) regulate the safe operation, maintenance, design, and installation of pressure vessels, which are vessels utilized for holding gases or fluids under pressures that are not equal to atmosphere. Cracked or broken vessels are more likely to rupture or leak, creating health and safety risks (Langer, et al., 2009).

The element under consideration is stressed with both faces respectively parallel and perpendicular to the axis of the tank to examine an internally pressure-loaded thin-walled circular tank. The side faces are loaded with the normal stresses σl and σt. Due to the symmetry of the vessel and loading, shear stresses are absent, making σ_t and σ_l principal stresses. σ_t, known as the circumferential or hoop stress, and σ_2, referred to as the longitudinal or axial stress, are determined using static equilibrium equations. In a thin-walled cylinder, the radial stress is considered negligible due to the small wall thickness relative to the radius. This implies that the radial stress, acting inwards or outwards, is minimal and can generally be ignored in calculations. Consequently, the primary stresses in the cylinder are the hoop (circumferential) stress and the longitudinal stress. The following assumptions are applied to derive the expressions for these stresses (Bansal, 2012):

- Plane sections remain unchanged.
- The ratio $\frac{r}{t} \geq 10$, where t is constant and uniform.
- The material exhibits linear-elastic behavior and is isotropic and homogeneous.
- The stress distribution is uniform across the wall thickness.
- Fluid weight negligible.

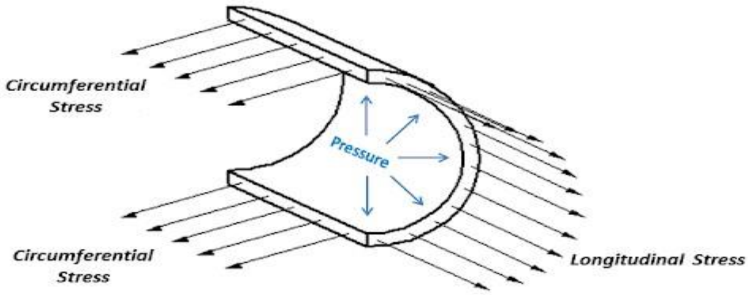

Figure 4.13: Hoop Stress and Longitudinal Stress in a Thin Cylinder under Pressurehin Cylinder under Pressure

The circumferential (hoop) stress in a pressurized cylinder is given by the equation (Bansal, 2012):

$$\sigma_t = \frac{p \cdot r}{t} \tag{4.79}$$

where:

- σ_θ circumferential stress,
- p is the internal pressure 2 bar,
- r inner radius of cylinder 20 cm,
- t wall thickness of cylinder 2 mm.

The longitudinal stress in a cylindrical pressure vessel is given by:

$$\sigma_t = \frac{p \cdot r}{2t} \tag{4.80}$$

$$\tau_{\max} = \frac{\sigma_t - \sigma_l}{2} = \frac{pr}{2t} \tag{4.81}$$

The maximum out-of-plane shear stresses occur on planes that are rotated 45° about the x and y axes, respectively:

$$\tau_{\max,x} = \frac{\sigma_t}{2} = \frac{pr}{2t} \quad \text{and } \tau_{\max,y} = \frac{\sigma_l}{2} = \frac{Pr}{4t} \tag{4.82}$$

Therefore, the maximum absolute shear stress is:

$$\tau_{\max} = \frac{pr}{2t} \tag{4.83}$$

This occurs on a plane rotated by 45° about the x-axis.

When the ratio $\frac{r}{t}$ is very large (thin-walled assumption), the term $\frac{P}{2}$ can be disregarded, and the resulting equations remain the same as those at the outer surface (Ibrahim et al., 2015).

4.6. Sizing of Condenser

In this study, a shell and tube type water condenser were used. It consists of a tank filled with water and a copper tube attached to it. When steam passes through the copper tube, it heats the water and converts it to liquid form, producing desalinated water. This sort of condenser is affordable and suitable.

the amount of heat required to remove to condense equals to heat in by cold water and it is given by:

$$Q = mh_{fg} \tag{4.84}$$

The relationship between the log mean temperature difference, total surface area, and the overall heat transfer coefficient (U) can be used to calculate the actual heat transfer.

$$Q = UA\Delta T_{\mathrm{lm}} \tag{4.85}$$

By using the following equation (U)can be found from h_i and h_o

$$\frac{1}{U} = \frac{A_o}{A_i h_i} + \frac{A_o \ln\left(\frac{d_o}{d_i}\right)}{2\pi k L_c} + \frac{1}{h_o} \tag{4.86}$$

Overall Heat Transfer Coefficient (U) For steam-water shell-and-tube Typical U = 500–1500 W/m²·K The area of the tube is the surface area that is exposed to the heat exchanging $A = \pi D\ L$, L is tube length.

The Reynold number of the tube of the condenser is given by

$$Re = \frac{\rho u D_h}{\mu} \tag{4.87}$$

$$u = \sqrt{\frac{2(p_o - p_a)}{\rho}} \tag{4.88}$$

where:

- ρ is the density,
- u is the velocity,
- D_e is the equivalent diameter,
- μ is the dynamic viscosity.

The ratio of conductive to convective heat transfer in a fluid flow is known as the Nusselt number. It can be expressed using the following empirical correlation turbulent and laminar flow respectively:

$$Nu = 0.023Re^{0.8}Pr^{0.5} \quad \text{and} \quad Nu = 1.86\left(\frac{D_h Re Pr}{L}\right)^{0.333}, \quad Re < 2300 \tag{4.89}$$

The coefficient of convective heat transfer is given by the following equation

$$h_i = \frac{Nu \cdot k}{D_h} \tag{4.90}$$

$$LMTD = \frac{(\Delta T_1 - \Delta T_2)}{ln(\Delta T_1 - \Delta T_2)}$$

Where ΔT_1 = Temperature difference at one end of the condenser (hot side), ΔT_2 = Temperature difference at the other end (cold side).

$$A = \frac{Q}{U\Delta T_{\mathrm{lm}}} \tag{4.91}$$

A=0.024 m², 4 tubes × 6 mm diameter .318 m length required to successfully condense. Because of their superior thermal conductivity, which facilitates effective heat exchange between the steam and cold water, copper tubes are frequently chosen. And its resistance to corrosion and capacity to tolerate high pressures. The condenser can be made to run more effectively and guarantee that the system maintains the appropriate temperatures by carefully examining variables including tube diameter, length, and configuration.

4.7. Material Selection

4.7.1. Reflective Material Selection Comparison

Reflective materials are used to redirect and concentrate sunlight in solar energy systems, improving their efficiency. These materials vary in properties like reflectance, durability, and cost, which affect their suitability for different applications. Common types include metals, glass mirrors, and specialized films. Choosing the right reflective material is crucial to optimize energy capture and system performance.

Table 4.6: Selection Matrix for Reflective Materials in Solar Thermal Systems

Reflective Material Selection	Type	Cost	Reflectance	Efficiency	Durability
Reflective Aluminum Sheet	Metal	Low	High (0.85–0.95)	High	High
Glass Mirror	Glass	Medium	High (0.85–0.90)	High	Medium
Silver-Coated Glass	Glass	High	Very High (0.95)	Very High	Medium–High
Polished Stainless Steel	Metal	Medium	Medium (0.60–0.70)	Low–Medium	Very High

Based on the evaluation, glass mirror was selected due to its high reflectance, efficiency, and availability. Although it is fragile compared to some alternatives, it offers a good balance of performance and cost.

4.7.1.1. Receiver Tube

The selection of an appropriate receiver tube material is critical for efficient heat transfer and long-term operation of solar thermal systems. Various materials were evaluated based on their thermal conductivity, corrosion resistance, temperature resistance, and cost. The table below summarizes the comparison.

Table 4.7: Comparative Evaluation of Receiver Tube Materials for Solar Thermal Systems

Material	Thermal Conductivity	Corrosion Resistance	Cost
Copper	Very High	Moderate	High
Aluminum	High	Low	Medium
Stainless Steel	Moderate	High	Medium
Carbon Steel	Moderate	Low	Low
Nickel Alloys	High	Very High	Very High

Copper was selected as the receiver tube material because of its exceptional thermal conductivity, which facilitates efficient heat transfer in solar thermal systems. Although it is relatively costly and has moderate corrosion resistance, its thermal performance outweighs these drawbacks in applications where maximizing heat absorption is essential.

4.7.2. Material Selection for Steam Chamber

The steam chamber is a key component in a solar-powered sterilizer, requiring a material that can withstand high temperature and pressure (121°C and 1.5–2 bar), resist corrosion from steam, and maintain hygiene. Material selection was based on performance, durability, cost, and suitability for rural medical use.

Table 4.8: Comparative Evaluation of Materials for Steam Chamber Construction

Material	Pressure & Temperature Suitability	Corrosion Resistance	Cost	Overall Suitability
Stainless Steel 316	Excellent	Excellent	Moderate to High	Highly Recommended
Aluminum 6061-T6	Fair (low-pressure)	Fair	Low to Moderate	Limited Use
Copper / Brass	Fair	Fair	High	Not Ideal
Carbon Steel	Excellent (but prone to rust)	Poor	Low	Not Recommended

Stainless steel, especially Grade 316, is the most suitable material due to its excellent resistance to heat, pressure, and corrosion, along with good hygienic properties. It ensures reliable and safe operation, making it ideal for steam sterilization in off-grid settings.

4.8. Experimental Setup and Procedure

4.8.1. Introduction

This chapter details the of the experimental setup, which includes building a parabolic trough solar collector, a steam sterilizer, and a condenser. It also shows the design of the entire system as visualized in SolidWorks ® 2023. Finally, it describes the physical setup and the instruments used for measurements.

4.8.2. Fabrication and Assembly

The components of the solar-powered steam sterilizer were fabricated and assembled in the engineering workshop. This involved constructing the parabolic trough, connecting the receiver pipe to the steam generator, installing insulation, and integrating the steam transfer lines to the sterilization chamber.

4.8.2.1. Parabolic Trough Solar Collector with Reflector

The construction of this parabolic trough solar collector involves a reflective surface composed of numerous 2 cm wide mirror strips meticulously arranged to fit the 1.4 meter by 0.7 m galvanized steel sheet. This segmented mirror design allows for precise shaping and adherence to the parabolic curve. The galvanized steel sheet, now serving as a substrate for the mirror strips, is then positioned to rest on top of likely a series of supporting ribs or a specifically designed structure – integrated into the angle iron frame. This provides the necessary contour and support to maintain the intended parabolic form of the reflective assembly.

Figure 4.14: Construction of PTC and Reflective Mirror

4.8.2.2. Sterilization Chamber and Condenser

The sterilization chamber is a 10-liter cylindrical vessel made from high-grade stainless steel (SS316), designed to withstand high temperatures and pressures commonly used in medical sterilization. It is equipped with an integrated pressure gauge for real-time monitoring of internal pressure. It includes a steam inlet for external boiler connection, a manual drain valve for condensate removal, and a perforated stainless-steel tray inside to hold instruments while allowing even steam distribution. This compact, durable unit is ideal for use in remote clinics and small healthcare facilities

4.8.3. Experimental Procedure

4.8.3.1. Water Filling and Initial State weight Measure:

- Using the graduated cylinder, a measured a liter of water will be poured into the receiver pipe. Ensure the system is initially at ambient temperature and atmospheric pressure.
- Digital weight balance**:** a device used to measure the mass or weight of an object before the test.

4.8.3.2. Solar Collector Positioning:

- The parabolic trough solar collector will be placed outdoors in an open area with unobstructed access to sunlight.
- The collector will be manually oriented to track the sun's movement throughout the testing period to maximize solar energy capture. The inclination of the collector will be set as per the design to facilitate natural convection and steam movement within the receiver pipe.

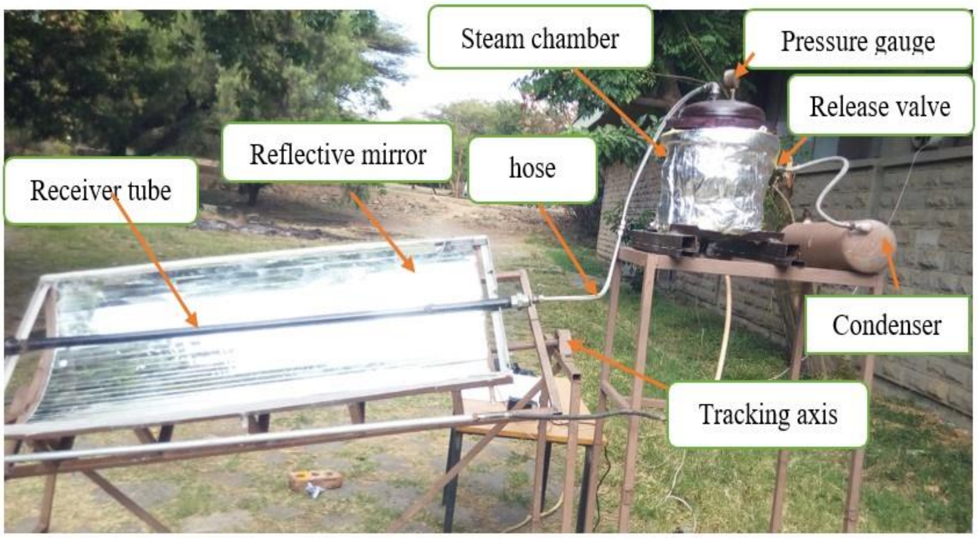

Figure 4.15: setup of the developed steam sterilizer.

4.8.4. Experimental Testing

- The steam generator was filled with a measured volume of water 1 litters.
- The solar collector was positioned to maximize solar energy capture (or the solar simulator was activated).
- Temperature and pressure data were recorded at every 2 minutes from the thermocouples and pressure transducer.
- The time taken to reach the target steam sterilization temperature 121°C and pressure 15 psi in the sterilization chamber was recorded.

4.8.4.1. Data Recording

- Manual readings of the pressure gauge on the sterilization chamber will be recorded at the same 2-minute intervals, with the temperature data logging.
- The stopwatch will be started when the solar collector is positioned under sunlight.
- The time taken to reach the target sterilization temperature (121°C) and pressure (15 psi) inside the sterilization chamber will be noted.
- The duration of the different phases of the experiment (e.g., heating phase, sterilization holding time, cooling phase) will be recorded using the stopwatch.
- The volume (using the graduated cylinder) or mass (using the digital weight balance) of the distilled water collected in the condenser over the duration of the experiment will be measured and recorded.

- Receiver pipe temperature measurement**:** A K-type thermocouple will be securely attached to the outer surface of the receiver pipe at a representative point along its length to monitor the temperature of the pipe, which will correlate with the heating of the water inside.
- Sterilization chamber temperature measurement**:** Another K-type thermocouple will be inserted into the sterilization chamber through one of the modified ports. The tip of the thermocouple will be positioned within the chamber to measure the temperature of the steam surrounding the area where instruments would be placed.
- Ambient air temperature measurement. It is measured by thermometer

Figure 4.16: Measuring instrument Pressure gauge, thermometer,Thermocouple

4.8.5. Safety Measures:

- Ensure the pressure relief valve on the steam generator and the pressure regulator and safety valve on the sterilization chamber are functioning correctly and are not obstructed.
- The experimental area should be clear of flammable materials.
- Personnel involved in the experiment should wear appropriate personal protective equipment (PPE).
- Sterilization chamber pressure measurement**:** The pressure gauge will be securely mounted onto one of the modified ports of the sterilization chamber. Ensure the gauge is clearly visible for manual readings.

CHAPTER FIVE

5. RESULT AND DISCUSSION

5.1. Solar Radiation Result

The Meteorology data and NASA (Surface Meteorology and Solar Energy) data were used to collect the solar radiation data for Kobo used in this study. The measurements used in the study are ground-based measurements coming from the Eastern and Central Oromia Meteorological Service Center Meteorology Agency that are specific to the city. NASA satellite data was used for checking and adding to local data, which enhanced the time cover and reliability of total solar radiation.

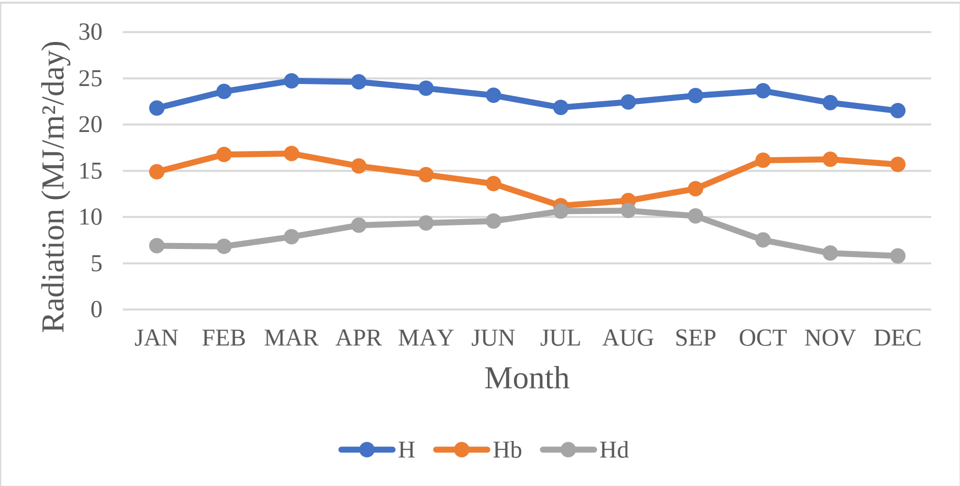

Figure 5.1: Monthly mean Radiation on a Horizontal Surface

The monthly solar radiation data indicate seasonal variations in global (H), diffuse (Hd), and beam (Hb) radiation. Peak diffuse radiation occurs during the rainy months (June to August), reducing the beam component due to increased cloud cover. In contrast, the dry months (January to March and October to December) exhibit higher beam radiation, making them more favorable for direct solar energy applications.

5.1.1. Validation of Calculated Radiation with NASA Data

The comparison of calculated monthly mean global daily radiation values using an internationally available dataset becomes increasingly important when locally measured data is not available. by comparing against trustworthy data like NASA POWER. We can cheek reliability of values.

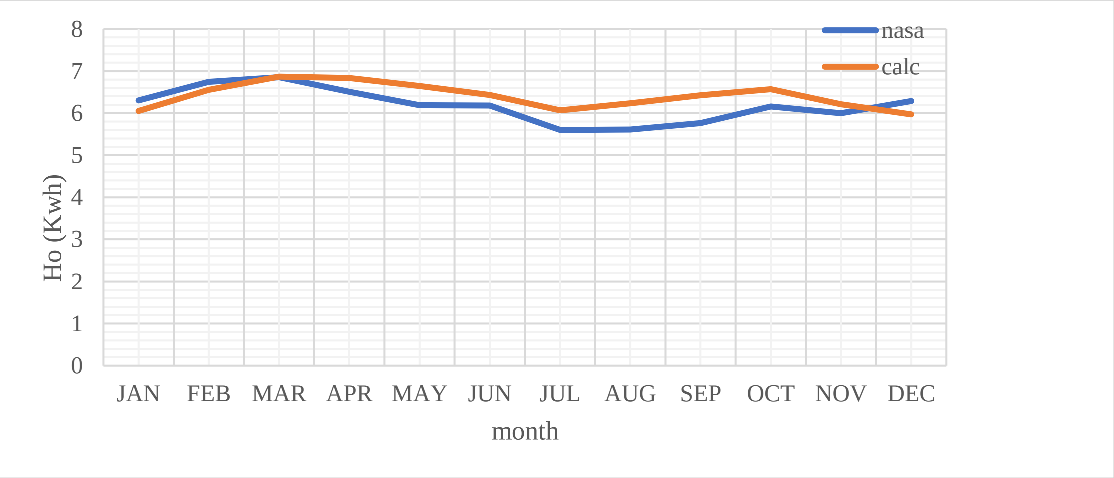

Figure 5.2: Comparison of Calculated Radiation with NASAs dataset

The comparison graph demonstrates a very strong similarity between the calculated daily Global radiation values and the internationally validated NASA POWER dataset, with close agreement in both magnitude and temporal trends. The good correspondence verifies that solar geometry equations, orbital assumptions, and calculation procedures employed are accurate and reliable. Minor deviations, likely due to variations in atmospheric correction models or time-step resolutions, do not detract from the general agreement. This is use full in solar energy applications, climate modeling, and agricultural planning.

5.1.2. Instantaneous Solar Radiation on Horizontal Surfaces

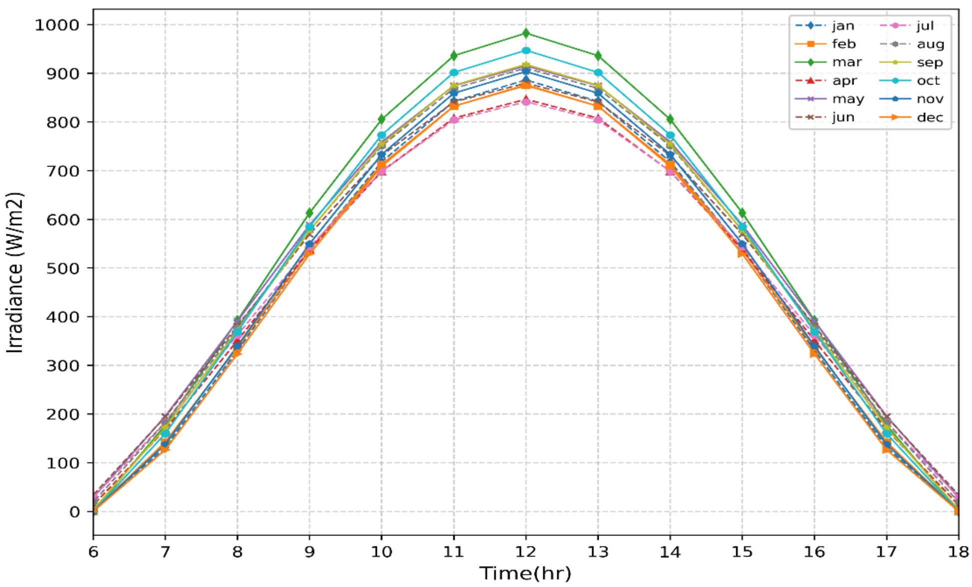

Figure 5.3: Instantaneous Mean Hourly Global Radiation on horizontal surface

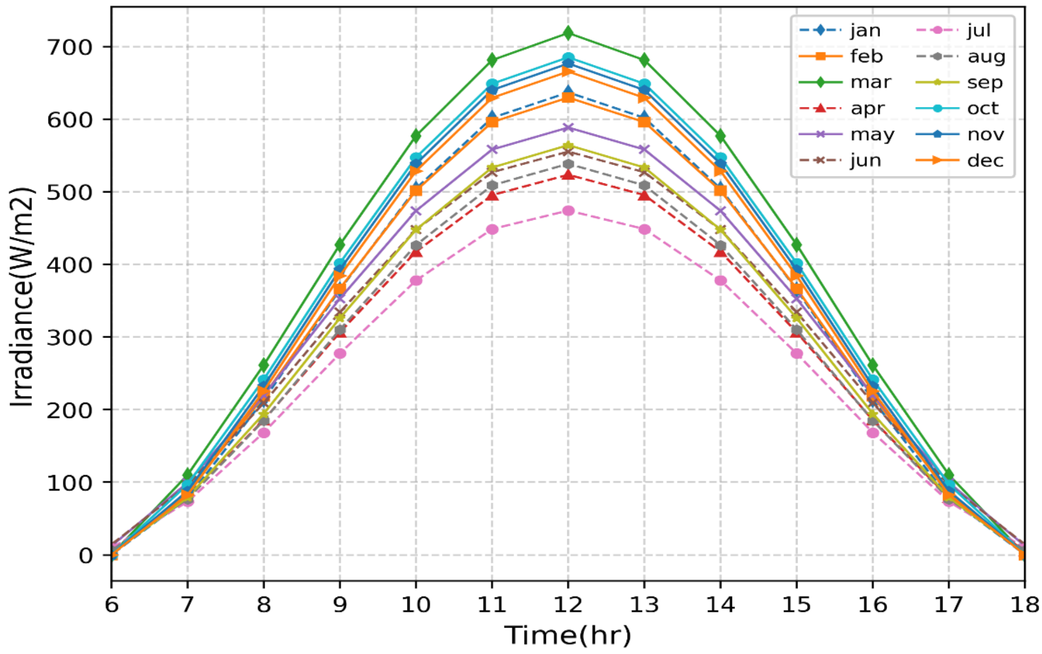

Figure 5.4: Instantaneous Mean Hourly Beam Radiation on horizontal surface

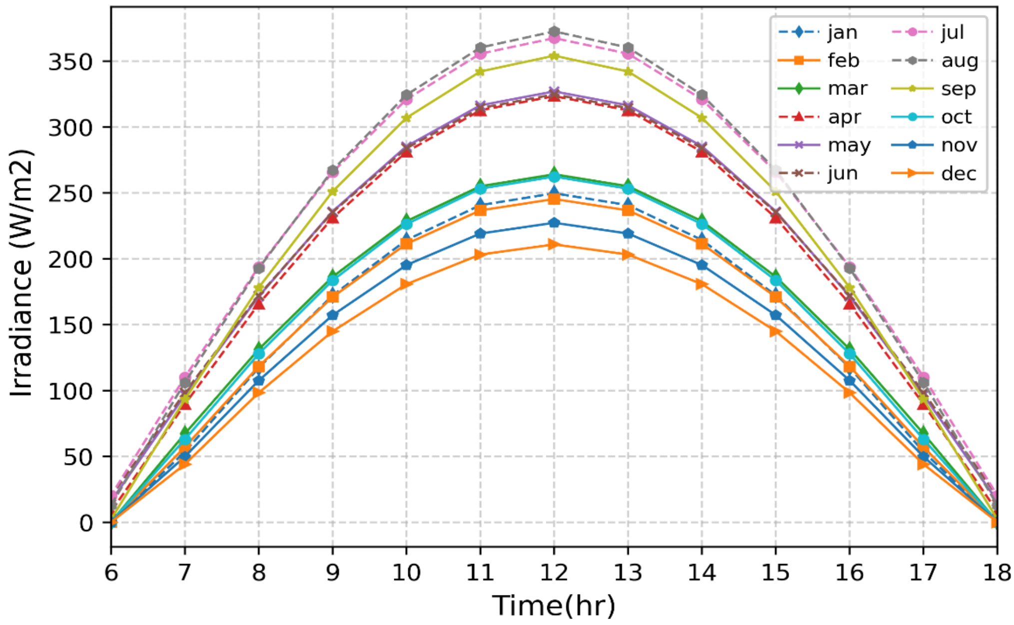

Figure 5.5: Instantaneous Mean Hourly Diffuse Radiation on horizontal surface

The data in the chart illustrates the monthly variation of global H, beam Hb, and diffuse (Hd) solar radiation. Global radiation H peaks in March and April, indicating high overall solar availability during these months. Beam radiation Hb is highest in the dry season (January to March), but it drops notably during the rainy season (July to September), likely due to increased cloud cover. Conversely, diffuse radiation Hd increases from May through August, peaking in July and August, which aligns with higher atmospheric scattering and cloudiness.

The lowest values of all components occur in December, suggesting minimal solar energy potential during that month. This seasonal variation highlights the importance of adjusting solar energy system design and usage according to local climatic patterns.

5.2. Seasonal Solar Radiation Results

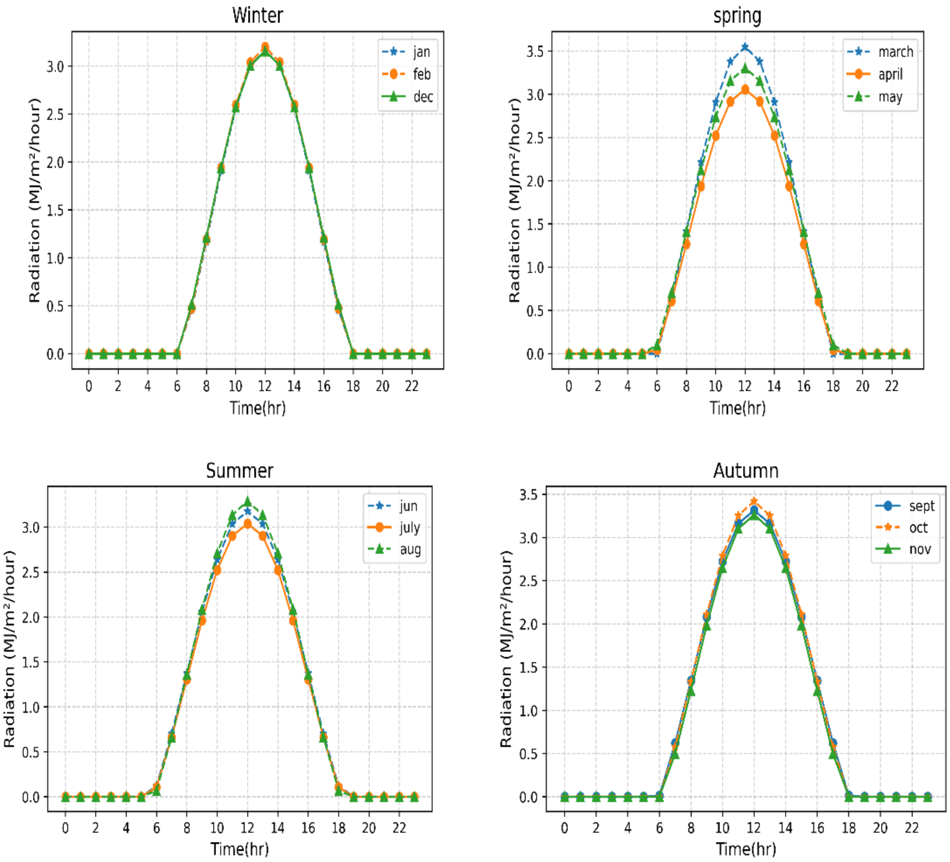

Figure 5.6: Monthly mean Hourly Global Radiation on Different Seasons

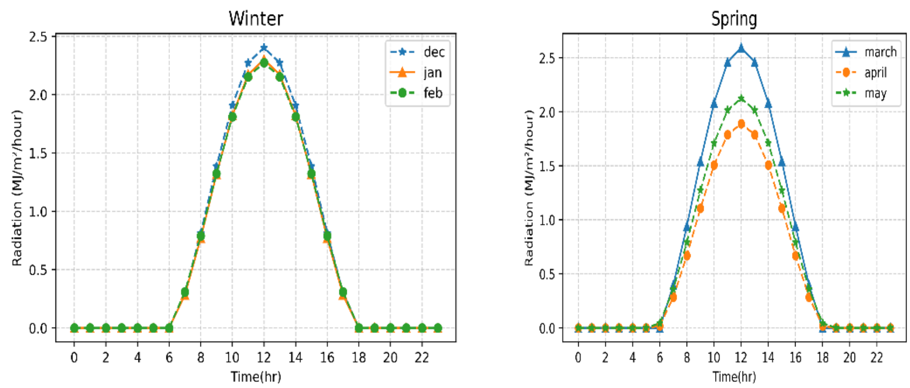

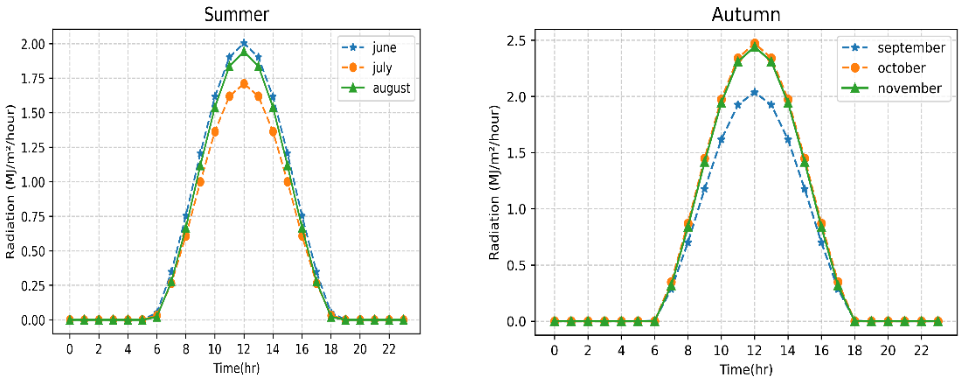

Figure 5.7: Monthly mean Hourly Beam Radiation on Different Seasons

5.2.1. Collector Tilt Angle

Adopting a fixed tilt angle for solar collectors, while offering a static and potentially simplified installation, represents a compromise that deviates from the monthly optimum required for maximal energy harvesting. Empirical evidence from studies conducted in comparable latitudes underscores the benefits of dynamic tilt angle adjustments. Research consistently demonstrates that aligning the collector tilt with the seasonal variations in solar declination yields a notable enhancement in energy collection compared to installations employing a static, annually optimized tilt.

The Heatmap illustrates the correlation between the optimum tilt angle for solar collectors each month and its corresponding solar radiation intensity, represented by color.

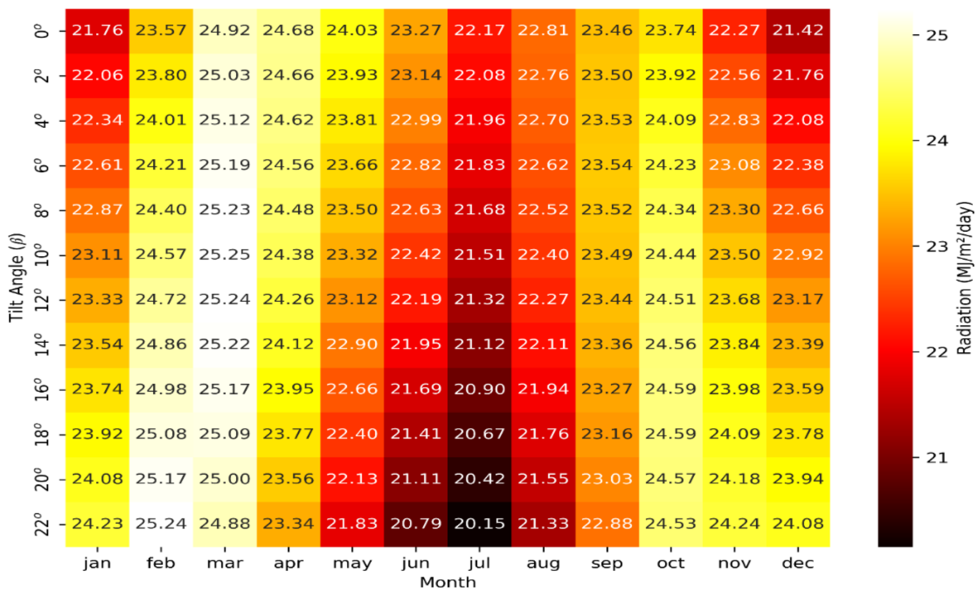

Figure 5.8: Heatmap for monthly solar radiation variation at different tilt angles

The color intensity effectively highlights periods of peak solar energy availability, typically around mid-year. This relationship confirms that adjusting the tilt angle seasonally maximizes energy capture, with the strongest radiation intensities aligning with near-optimal tilt angles during high-sun months. The clear trend supports the use of dynamic tilt adjustments to enhance solar collector efficiency.

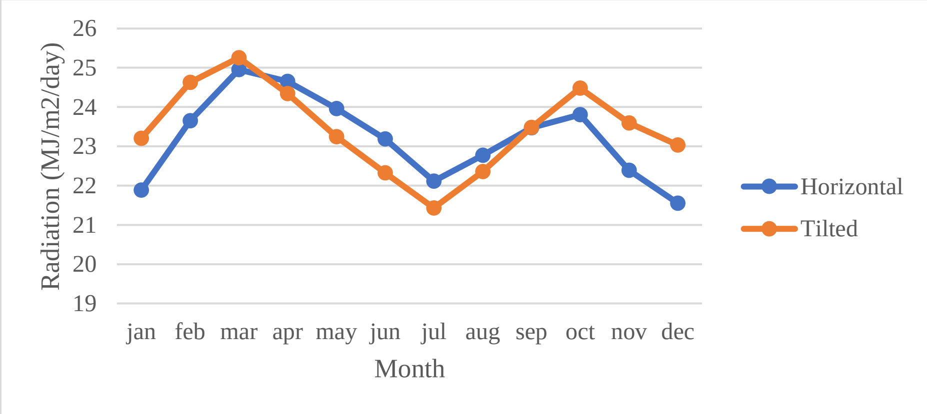

Figure 5.9: Comparison of monthly (ETR) between horizontal and tilted surfaces

Table 5.1: Monthly Optimum Tilt Angles for Kobo

Month	Jan	Feb	Mar	Apr	May	Jun	Jul	Aug	Sep	Oct	Nov	Dec
Best Tilt	22°	22°	6°	0°	0°	0°	0°	0°	6°	18°	20°	22°

Although the best tilt angle varies throughout the year, analysis shows that a fixed tilt angle of approximately 20° provides a close approximation to the seasonal optimums. This angle captures a substantial portion of available solar radiation, especially during mid-year when solar intensity peaks. The color intensity pattern confirms that a 20° tilt aligns well with high-radiation months and offers a practical balance between simplicity and performance.

5.3. Expermuntal result on sterilization

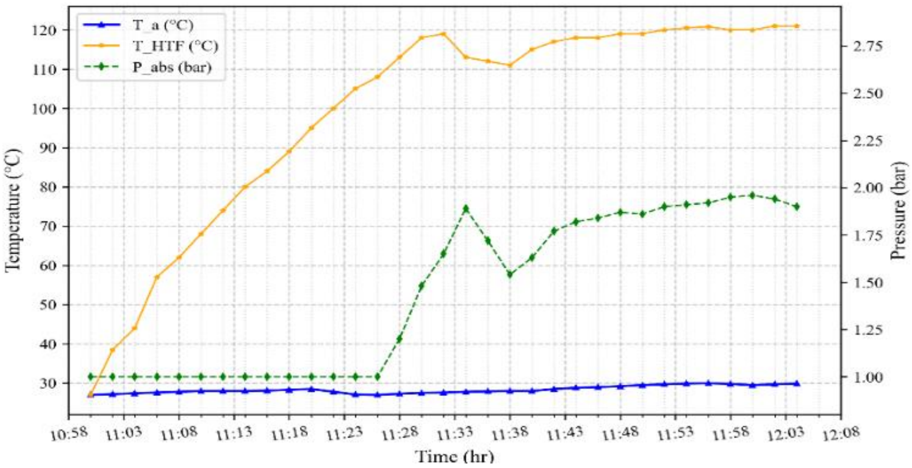

Figure 5.10: Experimental result on ambient and steam Temperature and Pressure at no load under clear sky

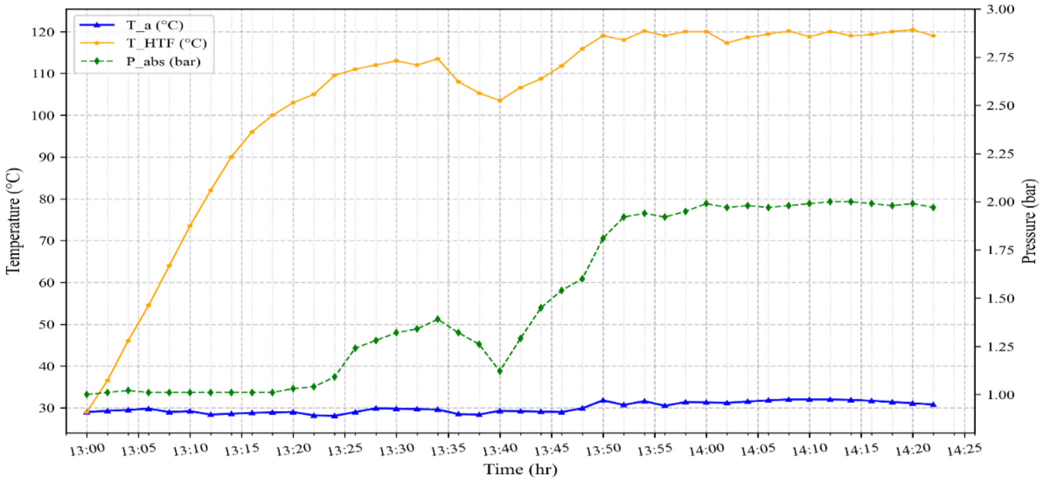

Figure 5.11: Experimental result on ambient and steam Temperature and Pressure at full load under clear sky

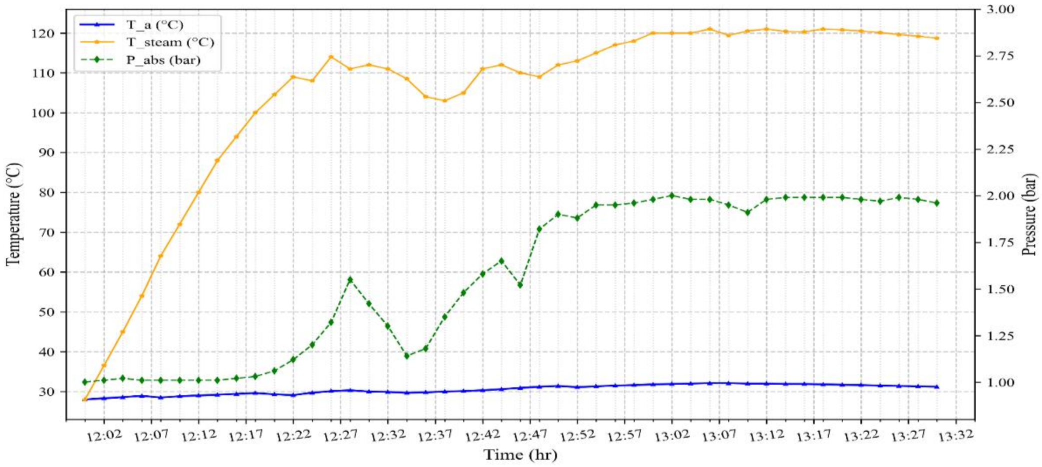

Figure 5.12: Experimental result on ambient and steam Temperature and Pressure at full load relatively low solar intensity

A series of experimental evaluations were carried out to assess the performance of the developed solar steam sterilizer under both no-load and full-load conditions. These tests aimed to determine the time required to achieve and maintain standard steam sterilization conditions—specifically, a temperature of 121°C and a pressure range of 1.5–2 bar—under varying environmental settings.

Under no-load conditions and clear sky scenarios, the sterilizer demonstrated rapid thermal response. For instance, during a test conducted at 11:00 AM with an ambient temperature of approximately 29°C and high solar irradiance, the chamber temperature reached 121°C within 30 minutes. A temporary drop in temperature and pressure was observed when the air-release valve was opened, but the system quickly recovered and successfully maintained sterilization conditions for the required 30 minutes. Pressure was effectively regulated by the relief valve, which activated as the pressure approached 2 bar.

Full-load evaluations were performed under different environmental conditions to simulate real-use scenarios. In one representative test conducted at 1:00 PM with an ambient temperature of 31°C, the chamber reached 121°C in approximately 52 minutes, and the full sterilization cycle lasted around 1 hour and 20 minutes. These findings highlight the system's increased thermal demand under load, which results in extended heat-up times.

Another test was conducted during the afternoon under partially cloudy skies, with an ambient temperature of around 27°C and reduced solar irradiance. Despite less favorable conditions, the sterilizer reached the target temperature and pressure within about 1 hour, followed by a 35-minute sterilization phase. This demonstrated the system's capability to operate under fluctuating solar input, though with a slightly delayed performance.

These experimental results clearly show that system performance is affected by both the thermal load and ambient environmental conditions. Under full-load and low-irradiance conditions, the time required to reach saturation increased due to higher thermal inertia and thermal losses—primarily through convection and radiation. Nevertheless, across all test scenarios, the system consistently achieved and sustained the required sterilization parameters, confirming its reliability and effectiveness for use in off-grid healthcare environments.

5.4. Result on Water Distillation

The condensed water collected from the distillation system was tested from 1 litter of and gave a measured conductivity level of 5 μS/cm and pH 6.8. These findings indicate that the water is high purity water containing only traces of dissolved ionic substance. The low conductivity is a confirmation that purification by the distillation has been effective in removing existing salts and other impurities present in untreated water. The acidic pH is to be expected and is caused by the presence of absorbed atmospheric carbon dioxide, which exists as a weak carbonic acid within the water. The quality of water from the system is satisfactory for applications requiring clean, low-conductivity water, for medical sterilization.

Table 5.2: Summary of Parameters on the Distilled Water

Parameter	Before Distillation (Raw Water)	After Distillation (Condensate)	Recommended
Conductivity (μS/cm)	450	5	< 50
pH	7.5	6.8	6.5-8
TDS	600	80	50-200

5.5. Economic Analysis

To ascertain a project's viability, effectiveness, and overall impact, economic analysis involves assessing both its financial and non-financial components. Through a periodical evaluation of costs, benefits, and risks, it aids in decision-making.

Basic solar energy equipment purchases are a significant component of solar process economics. Costs for supporting structures for collectors and other modifications required by the solar equipment should also be mentioned. The cost of the solar steam sterilizer's primary parts, including the condenser, steam chamber, and parabolic solar collector, adds up to the total cost. These components come with prices for labor, materials, and construction. Therefore, understanding these particular costs is necessary for the project's economic analysis.

5.5.1. Initial Investment Costs

Initial investment costs refer to the total expenses incurred at the beginning of a project or business venture before it becomes operational. These costs typically include expenses for equipment, infrastructure, installation, research and development, permits, and any necessary upfront materials. In the context of a solar-powered steam sterilization system, the initial investment costs would cover the procurement of the parabolic trough, metal tube heat absorber, pressure vessel, reflective materials, insulation costs. These components come with prices for labor and construction. Therefore, understanding these particular costs and Proper evaluation of these costs is essential for determining the project's feasibility and long-term economic viability.

5.5.2. Cost Breakdown

Table 5.3: Cost Break Down of the System

Item	Unit	Quantity	Cost (ETB)
Material cost and Construction cost			
Galvanized Sheet metal	36" × 96" × 2mm	1	3000
Couper tube	¾ inch (d) × 1.6 length	1.5 m	1000
Copper tube	¼ inch (9 mm), L		1000
Mirror	1.4 (m)×0.7 (m)		2000
Metal bar(frame) steel	4cm×3mm×8m	1	7000
Gate valve	½ inch (d)	3 PCs	1050
Hose	½ inch (d)	4	1200
Electrode	3.2mm x 350mm (MMA, E6013)	1 Pack	400
Grinding disk	4-inch (100 mm)	2 PCs	400
Elbow	1/2 inch	1 PCs	100
Nipples	½ inch	6 PCs	300
Reducer	1 to ½ inch	2 PCs	200
Bearing	¾ inch	2 PCs	500
Pressure Gauge	0-30 psi (0-2 bar)	1 PCs	2850
Labor	-------	----	4000
Total			25000 (ETB)

5.5.3. Economic Feasibility and Cost Analysis

Initial investment cost or the up-front cost is $I_{cost} = 25000$

Monthly benefit from Fuel can be calculated as follows

The calculation determines the monthly fuel cost for a device operating two times a day. It begins by calculating the energy required per cycle in both kWh and kJ, using the given power of 520 watts.

$$E_k = \frac{E_r}{\eta_{\text{burner}}} \tag{6.1}$$

Where η_{b} = efficiency of traditional burner E_r is energy required E_k fuel energy. Mass of Fuel required is found Energy of Fuel and Calorific Value of Fuel.

$$m_k = \frac{E_k}{CV_k} \tag{6.2}$$

Where, CV_k is calorific value of fuel. Then, using the calorific value of fuel (43,000 kJ/kg) and the burner efficiency of 45% (Sharma et al., 2009), it finds the mass of fuel needed per cycle. This is scaled up to daily and monthly consumption in kilograms, then converted to liters using fuel's density (0.8 kg/liter). Finally, the total monthly cost is calculated by multiplying the total liters of fuel used per month by the price of fuel (120 Birr/liter), resulting cost of 480 Birr.

Annual revenue is calculated simply by multiplying the monthly benefit with the numbers of month

$$AR \;=\; 12 * 480.07 \tag{6.3}$$

$$= 5700 \;\; birr$$

Annual operating and maintenance cost (AM) is 9 percent of monthly income: This represents the projected yearly expenses for essential replacements (e.g., mirror tubes, hoses) necessary for the solar steam sterilizer's continued operation, estimated at 9% of its monthly income.

$$AM \;=\; AR * 0.09 \tag{6.4}$$

$$= \;\; 518.4 \, birr$$

Net annual revenue: This refers to the total income generated by the solar steam sterilizer over one year, after deducting any directly related operational costs (excluding major maintenance already accounted for separately). In a non-revenue-generating context, this could represent the annual value generated through cost savings compared to alternative sterilization methods.

$$(NAR) = AR - AM \tag{6.5}$$

$$NAR = 5181.6 \;\; birr$$

Payback period (n): This is the calculated timeframe required to recover the initial investment in the solar steam sterilizer system through the income generated by its use or the accumulated savings realized from employing it instead of other sterilization methods.

$$n = \frac{I_{cost}}{NAR} \tag{6.6}$$

$$n = 6\, year$$

Calculating net present value: This involves determining the present-day value of all anticipated future cash flows—both inflows (revenue or savings) and outflows (initial investment and operational costs)—associated with the solar steam sterilizer project, discounted at a specified rate of return, to assess its overall economic viability.

$$NPV = -I_{cost} + NAR(P/A, i, n) \tag{6.7}$$

Where i rate of return 0.1 $(P/A, 10\%, n) = P = \frac{((1+i)^N - 1)}{(i*(1+i)^N)}$

Analysis of electric utility cost

To begin calculating the monthly electricity cost, we first determine the energy consumed per operation by multiplying the power consumption (1 kW) by the operating time per session (0.75 hours), resulting in 0.75 kWh per session. Estimated service charge 53.57 Birr per month.

Energy consumption per session:

$$Power\ = 1\, kW \times 0.75\, hours = 0.75\, kWh/operation \tag{6.8}$$

Daily energy consumption: Energy per session× $operation$ per day

$$P_{daily} = 0.75\, kWh/s \times 2\, operation/d = 1.5\, kWh/d \tag{6.9}$$

Monthly energy consumption (assuming 30 days):

$$P_{monthly} = 1.5\, kWh/d \times 30\, d/m = 45\, kWh\, /m \tag{6.10}$$

Total monthly energy cost:

$$C_{monthly} = 45\, kWh \times 4\, Birr/kWh = 180\, Birr/m \tag{6.11}$$

Estimated total monthly payment (including service charge=53.57 Birr):

$$C_{total} = C_{monthly} + S_{charge} = 233.57\, Birr/month \tag{6.12}$$

Let the solar system consuming 1 kW of power and operating for 45 minutes (0.75 hours) twice daily in Ethiopia, where electricity costs 4 Birr per kWh, would have a daily energy consumption of 1.5 kWh (1 kW x 0.75 hours/session x 2 $operation$). Over a 30-day month, this equates to 45 kWh of energy used. The estimated total monthly electricity payment for this system would be around 233.57 Birr. This cost is without including the coast of sterilizing machine in terms of only the amount of birr saved only electrical utility payment.

5.6. Financial Benefits

- Reduced Fuel Costs: If clinics previously relied on fuel-based sterilization (e.g., autoclaves using diesel or gas), the transition to solar power eliminates fuel expenses.
- Extended Equipment Lifespan: The use of solar-powered steam sterilization may reduce wear and tear on equipment compared to traditional methods, decreasing maintenance and replacement costs.

5.7. Non-Financial Benefits

- Improved Healthcare Access: Reliable sterilization enhances infection control, reducing disease transmission and improving patient outcomes in rural clinics.
- Environmental Impact: The system reduces carbon emissions by replacing fossil-fuel-based sterilization methods.
- Sustainability and Independence: Rural clinics become less dependent on grid electricity and external fuel supplies, ensuring continuous sterilization even in remote areas.

Large capital investment and low running costs are the common characteristics of solar energy schemes. A balancing act between certain one-time investment and future operating expenses, calculated, is thus the underlying problem of economics. Besides the monetary value, social and environmental benefits, i.e., improved health care access to remote health centers and reduced dependence on existing sources of energy are additional values to the project.

CHAPTER SIX
6. CONCLUSION AND RECOMMENDATION

6.1. Conclusion

This study assessed the performance of a solar-powered steam sterilization and water distillation system designed for rural healthcare applications. Beyond that the solar radiation potential for Kobo (Metehara) was evaluated using data from Eastern and Central Oromia Meteorological Service Center and validated with NASA POWER datasets, which showed a strong correlation and confirmed the reliability of the solar geometry calculations. Peak global radiation occurred in March, while diffuse radiation was highest in July and August due to increased cloud cover. Optimal tilt analysis indicated that a fixed 20° tilt outperformed, providing monthly radiation gains of up to 15%, particularly during the winter season.

Experimental results from the solar steam sterilizer demonstrated its functionality under varying load and weather conditions. Under no-load conditions, the system achieved the sterilization threshold of 121°C and 2 bar in 30 minutes. In full-load tests, this took 52–60 minutes depending on solar irradiance, with the sterilization process lasting about 80–95 minutes. Even under cloudy conditions, with an ambient temperature of 27°C, the system-maintained sterilization temperatures after one hour of heating, proving its reliability in less ideal weather. For water distillation, 300 milliliters of condensate showed high purity, with a conductivity of 5 μS/cm, pH of 6.8, and TDS reduced from 600 to 80 ppm—meeting WHO standards for medical-grade distilled water.

Economic analysis indicates that the system achieves monthly savings of 480 ETB through reduced fuel consumption. After accounting for an annual maintenance cost equivalent to 9% of these savings, the payback period is approximately six years. These results underscore the technical feasibility, energy efficiency, and cost-effectiveness of the solar thermal system for medical sterilization and water purification in off-grid rural clinics, offering a sustainable and alternative technologies.

6.2. Recommendations

In order to enhance the usability and efficiency of the solar-powered steam sterilizing system, the following are proposed:

- Training of health workers in system use and maintenance guarantees long-term sustainability.
- Promoting governmental and NGO support will ensure that the system is established in poor regions.
- An automated tracking system can increase the collection of solar energy.
- Comparison studies in varying geographical locations can confirm its effectiveness in different locations.
- Scaling up the design to accommodate larger sterilization loads is suitable for larger clinics.
- Integration of thermal energy storage will facilitate sterilizing during off-peak sunshine periods.

These recommendations, if implemented, will enhance the efficiency, scalability, and efficacy of the system and offer a sustainable and workable alternative in rural health.

REFERENCES

Abbas, M., Sapit, A. B., Balla, H., & Mohammed Hayder, A. (2019). Investigation on performance of parabolic trough collector (PTC) with smooth receil at different mass flow rates. Journal of Advanced Research in Dynamical and Control Systems, 11, 41–54.

Abbas, S., Yuan, Y., Hassan, A., Zhou, J., Ahmed, A., Yang, L., & Bisengimana, E. (2023). Effect of the concentration ratio on the thermal performance of a conical cavity tube receiver for a solar parabolic dish concentrator system. Applied Thermal Engineering,227,120403. https://doi.org/10.1016/J.APPLTHERMALENG.2023.120403

Abed, N., & Afgan, I. (2020). An extensive review of various technologies for enhancing the thermal and optical performances of parabolic trough collectors. *International Journal of Energy Research*, *44*(7), 5117–5164. https://doi.org/https://doi.org/10.1002/er.5271

Ahmad, S., Shafie, S., Ab Kadir, M. Z. A., & Ahmad, N. S. (2013). On the effectiveness of time and date-based sun positioning solar collector in tropical climate: A case study in Northern Peninsular Malaysia. Renewable and Sustainable Energy Reviews, 28, 635–642. https://doi.org/10.1016/J.RSER.2013.07.044

Aggarwal, S., Kumar, R., Lee, D., Kumar, S., & Singh, T. (2023). A comprehensive review of techniques for increasing the efficiency of evacuated tube solar collectors. *Heliyon*, *9*(4), e15185. https://doi.org/10.1016/J.HELIYON.2023.E15185

Akbarzadeh, S., & Valipour, M. S. (2018). Heat transfer enhancement in parabolic trough collectors: A comprehensive review. *Renewable and Sustainable Energy Reviews*, *92*, 198–218. https://doi.org/https://doi.org/10.1016/j.rser.2018.04.093

Al-Ghussain, L., & Taylan, O. (2020). Comparison of objective functions on the sizing of hybrid PV and wind energy systems with and without energy storage systems. Hybrid Energy System Models, 239–277. https://doi.org/10.1016/B978-0-12-821403-9.00004-4

Ab Kadir, M. Z. A., & Rafeeu, Y. (2010). A review on factors for maximizing solar fraction under wet climate environment in Malaysia. Renewable and Sustainable Energy Reviews, 14(8), 2243–2248. https://doi.org/10.1016/j.rser.2010.04.009

AL-Rousan, N., Isa, N. A. M., & Desa, M. K. M. (2018). Advances in solar photovoltaic tracking systems: A review. Renewable and Sustainable Energy Reviews, 82, 2548–2569. https://doi.org/10.1016/j.rser.2017.09.077

Al-Rabeeah, A. Y., Seres, I., & Farkas, I. (2023). Experimental investigation of improved parabolic trough solar collector thermal efficiency using novel receiver geometry design. *International Journal of Thermofluids*, *18*, 100344. https://doi.org/https: //doi.org/10.1016/j.ijft.2023.100344

AL-Rousan, N., Isa, N. A. M., & Desa, M. K. M. (2018). Advances in solar photovoltaic tracking systems: A review. Renewable and Sustainable Energy Reviews, 82, 2548–2569.https://doi.org/10.1016/j.rser.2017.09.077

Bahadori, M. N. (1976). Design of a solar autoclave. *Solar Energy*, *18*(6), 489–496. https: //doi.org/https://doi.org/10.1016/0038-092X (76)90068-2

Bansal, R. (2012). *Strength of materials*. Laxmi Publications. https://vipulzblog.wordpress. com

Bellos, E., & Tzivanidis, C. (2019). Alternative designs of parabolic trough solar collectors. *Progress in Energy and Combustion Science*, *71*, 81–117. https://doi.org/https: //doi.org/10.1016/j.pecs.2018.11.001

Bhatia, S. C. (2014). Solar radiations. *Advanced Renewable Energy Systems*, 32–67. https://doi.org/10.1016/B978-1-78242-269-3.50002-4

Bhargav H. Upadhyay, A. J. P., & Ramana, P. V. (2022). A detailed review on solar parabolic trough collector. *International Journal of Ambient Energy*, *43*(1), 176–196. https: //doi.org/10.1080/01430750.2019.1636869

Birhanu, H. A., & Kahsay, M. B. (2018). Solar autoclave for rural clinics. *Int J Adv Res Eng Technol*, *9*, 293–309.

Borode, A., Ahmed, N., & Olubambi, P. (2019). A review of solar collectors using carbon-based nanofluids. Journal of Cleaner Production, 241. https://doi.org/10.1016/j.jclepro.2019.118311

C¸engel, Y. A., & Boles, M. A. (2007). *Thermodynamics: An engineering approach* (6th). McGraw-Hill Education.

C¸engel, Y. A., & Boles, M. A. (2019). *Thermodynamics: An engineering approach* (9th). McGraw-Hill.

Chang, C., Tao, P., Xu, J., Fu, B., Song, C., Wu, J., Shang, W., & Deng, T. (2019). Highefficiency superheated steam generation for portable sterilization under ambient pressure and low solar flux [doi: 10.1021/acsami.9b04535]. *ACS Applied Materials & Interfaces, 11*(20), 18466–18474. https://doi.org/10.1021/acsami.9b04535

Crabtree, G. W., & Lewis, N. S. (2007). Solar energy conversion. *Physics Today, 60*(3), 37–42. https://doi.org/10.1063/1.2718755

Das, A., Park, J.-k., & Park, J.-h. (2015). Estimation of available global solar radiation using sunshine duration over south Korea. *Journal of Atmospheric and Solar-Terrestrial Physics, 134*, 22–29. https://doi.org/https://doi.org/10.1016/j.jastp.2015.09.001

Dehghani-Sanij, A., & Bahadori, M. N. (2021). Natural production of ice. Ice-Houses, 57–88. https://doi.org/10.1016/B978-0-12-822275-1.00007-2

Dincer, I., & Bicer, Y. (2018). Solar Thermochemical Energy Conversion. Comprehensive Energy Systems: Volumes 1-5, 4, V4-895-V4-946. https://doi.org/10.1016/B978-0-12-809597-3.00440-5

Duffie, J. A., & Beckman, W. A. (2013). *Solar engineering of thermal processes* (4th). Wiley.

El Ghazzani, B., & Nait Mensour, O. (2021). Shape Optimization of A Parabolic Trough Collector, Geometrical Considerations. International Journal of Engineering Research And, V10. https://doi.org/10.17577/IJERTV10IS010001

Feurhuber, M., Cattide, A., Magno, M., Miranda, M., Prieler, R., & Hochenauer, C. (2017). Prediction of the fluid flow, heat transfer, and inactivation of microorganisms at medical devices in modern steam sterilizers using computational fluid dynamics. Applied Thermal Engineering, 127, 1391–1403. https://doi.org/10.1016/j.applthermaleng.2017.08.085

Foster, R., Ghassemi, M., & Cota, A. (2009). Solar energy: Renewable energy and the environment (1st). CRC Press. https://doi.org/10.1201/9781420075670

Frederick, J. E. (2003). OZONE | Ozone as a UV Filter. Encyclopedia of Atmospheric Sciences, 1621–1627. https://doi.org/10.1016/B0-12-227090-8/00296-7

Gharzi, M., Kermani, A. M., & Tash Shamsabadi, H. (2023). Experimental investigation of

A parabolic trough collector-thermoelectric generator (PTC-TEG) hybrid solar system with a pressurized heat transfer fluid. Renewable Energy, 202, 270–279 https://doi.org/10.1016/J.RENENE.2022.11.110

Hassan Abbood, M., Rashid, F., & Jassim, M. (2022). Design and construction solar steam sterilizer. *International Journal of Nonlinear Analysis and Applications*, *13*(1), 2535– 2547. https://doi.org/10.22075/ijnaa.2022.5955

Ibrahim, A., Ryu, Y., & Saidpour, M. (2015). Stress analysis of thin-walled pressure vessels Mechanical Engineering, 5(1), 1–10. https://doi.org/10.4236/mme.2015. 51001.

Ituna-Yudonago, J.-F., Galindo-Luna, Y.-R., Garc´ıa-Valladares, O., y Brown, R. B., Shankar, R., & Ibarra-Bahena, J. (2021). Review of solar-thermal collectors powered autoclave for the sterilization of medical equipment. *Alexandria Engineering Journal*, *60*(6), 5401–5417. https://doi.org/https://doi.org/10.1016/j.aej.2021.04.007

Jamali, H. (2019). Investigation and review of mirrors reflectance in parabolic trough solar collectors (ptscs). *Energy Reports*, *5*, 145–158. https://doi.org/https://doi.org/10. 1016/j.egyr.2019.01.006

Jebasingh, V., & Herbert, G. J. (2016). A review of solar parabolic trough collector. *Renewable and Sustainable Energy Reviews*, *54*, 1085–1091. https://doi.org/https://doi.org/10.1016/j.rser.2015.10.043

Jianfeng, L., Jing, D., & Jianping, Y. (2010). Heat transfer performance of an external receiver pipe under unilateral concentrated solar radiation. Solar Energy, 84(11),1879–1887. https://doi.org/10.1016/J.SOLENER.2009.11.015

Kalogirou, S. A. (2009). Environmental Characteristics. *Solar Energy Engineering*, 49–762. https://doi.org/10.1016/B978-0-12-374501-9.00002-9

Kalogirou, S. A. (2012). 3.01 - Solar Thermal Systems: Components and Applications Introduction. Comprehensive Renewable Energy, 1–25. https://doi.org/10.1016/B978-0-08-087872-0.00301-2

Kamran, M. (2023). Planning and modeling of solar energy systems. *Fundamentals of Smart Grid Systems*, 219–270. https://doi.org/10.1016/B978-0-323-99560-3.00004-1

Kerr, M. B. P., & Scott, J. (2006). Use of the solar panel cooker for medical pressure steam sterilization. *Kerr-Cole Sustainable Living Center. Taylor, AZ*, 6.

Khalil, S. A., & Shaffie, A. M. (2016). Evaluation of transposition models of solar Irradiance Over Egypt. Renewable and Sustainable Energy Reviews, 66, 105–119. https://doi.org/10.1016/j.rser.2016.06.066Khan, K., Rasel, S. R., Zian Reza, S., Saime, M.,

Alam, N., Abu Salek, M., & Hasan, M. (2020). Solar medical sterilizer using pressure cooker for rural off-grid areas. Energy Systems, Drives and Automations: Proceedings of ESDA 2019, 277–288.

Kirk-Othmer Encyclopedia of Chemical Technology. (2007). Reference Reviews, 21(2), 49–50. https://doi.org/10.1108/09504120710728879

Kulcu, R. (2020). Determining the effects of insulation materials used in solar water heaters on efficiency in afyon city. *Proceedings of the International Conference on Renewable Energy Applications*.

Kumar, K. H., Daabo, A. M., Karmakar, M. K., & Hirani, H. (2022). Solar parabolic dish collector for concentrated solar thermal systems: A review and recommendations. *Environmental Science and Pollution Research*, *29*(22), 32335–32367. https://doi.org/10.1007/s11356-022-18586-4

Kumar, L., Hasanuzzaman, M., & Rahim, N. (2019). Global advancement of solar thermal energy technologies for industrial process heat and its future prospects: A review. *Energy Conversion and Management*, *195*, 885–908. https://doi.org/https://doi.org/10.1016/j.enconman.2019.05.081

Kofoworola, A., Ezekiel, A., Joshua, A., Oluwapelumi, O., Oyeshola, H., & Azeez, O. (2025). Solar Tracking Device for Photovoltaic Solar Energy System: A Review. *OALib*, *12*, 1–25. https://doi.org/10.4236/oalib.1113070

Langer, B., William, Nickell, R., William, E., Cooper, P., Asada, Y., Bernstein, M., Karasawa, T., Nickerson, D., Ahl, T., Canonico, D., Deardorff, A., Deboo, G., Gorman, J., Graber, H., Hechmer, J., Hunt, S., Kajimura, Y., Kuo, P., . . . Kenneth, R. (2009). Companion Guide to the ASME Boiler and Pressure Vessel Code, Volume 3, Third edition. In ASME Press eBooks. https://doi.org/10.1115/1.802717

Letcher, T. M. (Ed.). (2022). Comprehensive Renewable Energy (2nd ed.). Elsevier. https://www.sciencedirect.com/referencework/9780128197349/comprehensive-renewable-energy

Li, J., Du, M., Lv, G., Zhou, L., Li, X., Bertoluzzi, L., Liu, C., Zhu, S., & Zhu, J. (2018). Interfacial solar steam generation enables fast-responsive, energy-efficient, and lowcost off-grid sterilization. Advanced Materials, 30(49), 1805159. https://doi.org/ https://doi.org/10.1002/adma.201805159

Malekan, M., Khosravi, A., & Assad, M. E. H. (2021). Parabolic trough solar collectors. Design and Performance Optimization of Renewable Energy Systems, 85–100. https://doi.org/10.1016/B978-0-12-821602-6.00007-9

Mammadov, F. (2012). Study of Selective Surface of Solar Heat Receiver. *International of Energy Engineering*, *2*(4), 138–144. https://doi.org/10.5923/j.ijee.20120204.05

Martinez-Gracia, A., Arauzo, I., & Uche, J. (2019). Solar energy availability. Solar Hydrogen Production: Processes, Systems and Technologies, 113–149. https://doi.org/10.1016/B978-0-12-814853-2.00005-9

McConnell, I., Li, G., & Brudvig, G. W. (2010). Energy Conversion in Natural and Artificial Photosynthesis. *Chemistry & Biology*, *17*(5), 434–447. https://doi.org/10.1016/J.CHEMBIOL.2010.05.005

Modest, M. F. (2013). Fundamentals of Thermal Radiation. *Radiative Heat Transfer*, 1–30. https://doi.org/10.1016/B978-0-12-386944-9.50001-7

Mokheimer, E. M., Dabwan, Y. N., Habib, M. A., Said, S. A., & Al-Sulaiman, F. A. (2014). Techno-economic performance analysis of parabolic trough collector in dhahran, Saudi arabia. *Energy Conversion and Management*, *86*, 622–633. https://doi.org/ https://doi.org/10.1016/j.enconman.2014.06.023

Moran, M. J., Shapiro, H. N., Boettner, D. D., & Bailey, M. B. (2018). *Fundamentals of engineering thermodynamics* (9th). Wiley.

Mousavi Maleki, S. A., Hizam, H., & Gomes, C. (2017). Estimation of Hourly, Daily and Monthly Global Solar Radiation on Inclined Surfaces: Models Re-Visited. *Energies*, *10*. https://doi.org/10.3390/en10010134

Mustapha, M. T., Uzun Ozsahin, D., Uzun, B., & Ozsahin, I. (2021). Chapter 13 - application of fuzzy topsis in the sterilization of medical devices. In I. Ozsahin, D. U. Ozsahin, & B. Uzun (Eds.), *Applications of multi-criteria decision-making theories in healthcare and biomedical engineering* (pp. 197–216). Academic Press. https://doi.org/10.1016/B978-0-12-824086-1.00013-X

Myers, D. R. (2013). Solar Radiation: Practical Modeling for Renewable Energy Applications. CRC Press, Taylor & Francis Group.

Neto, R. V. P., de Souza, L. G. M., de Lima, J. C., de Souza, L. G. V. M., & Mendes, E. V. (2021). Theoretical-experimental study of a box-type solar oven made from disused recyclable elements. *Solar Energy*, *230*, 732–746. https://doi.org/10.1016/J.SOLENER.2021.10.024

Nejad, S. B., Allegranzi, B., Syed, S. B., Ellis, B., & Pittet, D. (2011). Health-care-associated infection in africa: A systematic review. *Bulletin of the World Health Organization*, *89*(10), 757–765.

Notton, G. (2017). Solar Radiation for Energy Applications. Encyclopedia of Sustainable Technologies, 339–356. https://doi.org/10.1016/B978-0-12-409548-9.10130-7

Olfian, H., Ajarostaghi, S. S. M., & Ebrahimnataj, M. (2020). Development on evacuated tube solar collectors: A review of the last decade results of using nanofluids. *Solar Energy*, *211*, 265–282. https://doi.org/https://doi.org/10.1016/j.solener.2020.09.056

Orosz, M., & Dickes, R. (2017). Solar thermal powered Organic Rankine Cycles. *Organic Rankine Cycle (ORC) Power Systems: Technologies and Applications*, 569–612. https://doi.org/10.1016/B978-0-08-100510-1.00016-8

Palacios, A., Amaya, D., & Ramos, O. (2021). Solar tracking control of a parabolic trough collector by traditional pid, fuzzy sets and particle swarm optimization algorithm. *International Review of Automatic Control (IREACO)*, *14*(3). https://doi.org/10. 15866/ireaco.v14i3.19267

Panta, G., Richardson, A. K., & Shaw, I. C. (2019). Effectiveness of autoclaving in sterilizing reusable medical devices in healthcare facilities. *The Journal of Infection in Developing Countries*, *13*(10), 858–864.

Prabhu, B., Vengadesan, E., Senthil, S., & Arunkumar, T. (2024). Comprehensive energy and enviro-economic performance analysis of a flat plate solar water heater with a modified absorber. *Thermal Science and Engineering Progress*, *54*, 102848. https: //doi.org/https://doi.org/10.1016/j.tsep.2024.102848

Prasad, G. C., Reddy, K., & Sundararajan, T. (2017). Optimization of solar linear Fresnel reflector system with secondary concentrator for uniform flux distribution over absorber tube. *Solar Energy*, *150*, 1–12. https://doi.org/10.1016/j.solener.2017.04.026

Ranjan, A., & Prakash, E. V. (2019). Performance Optimization of Solar PTC System Using Two Different Receiver Tube Materials. *International Journal of Engineering Research & Technology (IJERT)*, *8*(11).

Sabzevari, Y., & Eslamian, S. (2022). Reference evapotranspiration in water requirement: Theory, concepts, and methods of estimation. Handbook of HydroInformatics: Volume II: Advanced Machine Learning Techniques, 269–289. https://doi.org/10.1016/B978-0-12-821961-4.00005-1

Şen, Z. (2008). Solar Energy Fundamentals and Modeling Techniques: Atmosphere, Environment, Climate Change and Renewable Energy. Springer-Verlag London Limited. https://doi.org/10.1007/978-1-84800-134-3Shinde, T. U., Dalvi, V. H.,

Patil, R. G., Mathpati, C. S., Panse, S. V., & Joshi, J. B. (2022). Thermal performance analysis of novel receiver for parabolic trough solar collector. *Energy*, *254*, 124343. https://doi.org/10.1016/J.ENERGY.2022.124343

Sheikholeslami, M., Farshad, S. A., Ebrahimpour, Z., & Said, Z. (2021). Recent progress on flat plate solar collectors and photovoltaic systems in the presence of nanofluid: A review. *Journal of Cleaner Production*, *293*, 126119. https://doi.org/https://doi.org/10.1016/j.jclepro.2021.126119

Shumeta, A. (2021). Air heater transient analysis – amanuel shumeta. https://www.academia.edu/69208201/Air_heater_transient_analysis_Amanuel_shumeta

Shyam, R., & Palaniappan, A. (2023). Effect of sterilization techniques on biomaterial inks' properties and 3D bioprinting parameters. Bioprinting, 33. https://doi.org/10.1016/j.bprint.2023.e00294

Soto, E. A., Hernandez-Guzman, A., Vizcarrondo-Ortega, A., McNealey, A., & Bosman, L. B. (2022). Solar energy implementation for health-care facilities in developing and underdeveloped countries: Overview, opportunities, and challenges. *Energies*, *15*(22). https://doi.org/10.3390/en15228602

Suehrcke, H., Bowden, R. S., & Hollands, K. G. T. (2013). Relationship between sunshine duration and solar radiation. Solar Energy, 92, 160 171.https://doi.org/10.1016/J.SOLENER.2013.02.026

Sup, B. A., Zainudin, M. F., Ali, T. Z. S., Bakar, R. A., & Ming, G. L. (2015). Effect of rim angle to the flux distribution diameter in solar parabolic dish collector [2nd International Conference on Sustainable Energy Engineering and Application (ICSEEA)2014 Sustainable Energy for Green Mobility]. *Energy Procedia*, *68*, 45–52. https: //doi.org/https://doi.org/10.1016/j.egypro.2015.03.231

Sharma, M., Mishra, S., & Acharjee, P. (2009, December). Thermal efficiency study of conventional kerosene pressure stoves equipped with porous radiant inserts. *International Energy Journal*, *10*, 247–254.

Tian, Y., & Zhao, C. Y. (2013). A review of solar collectors and thermal energy storage in solar thermal applications. *Applied Energy*, *104*, 538– https://doi.org/10.1016/J.APENERGY.2012.11.051

Tsoutsos, T., Frantzeskaki, N., & Gekas, V. (2005). Environmental impacts from the solar energy technologies. *Energy Policy*, *33*(3), 289–296. https://doi.org/10.1016/S0301-4215(03)00241-6

Tranquillo, J., Goldberg, J., & Allen, R. (2023). Chapter 8 - detailed design. In J. Tranquillo, J. Goldberg, & R. Allen (Eds.), *Biomedical engineering design* (pp. 235–285). Academic Press. https://doi.org/https://doi.org/10.1016/B978-0-12-816444-0.00008-0

Ulgen, K., & Hepbasli, A. (2009). Diffuse solar radiation estimation models for Turkey's big cities. *Energy Conversion and Management - ENERG CONV MANAGE*, *50*, 149–156. https://doi.org/10.1016/j.enconman.2008.08.013

Umoh, M. D., & Udoh, S. O. (2010). Estimation of global solar radiation from sunshine hours for warri, nigeria. *Global Journal of Environmental Sciences*, *9*(1&2), 51–56. http://www.globaljournalseries.com

Upadhyay, B. H. (2020). Design Optimization and Performance Analysis of Solar Parabolic Trough Collector. Gujarat Technological University. Upadhyay, B. H., Patel, A. J., Sadasivuni, K. K., Mistry, J. M., Ramana, P. V., Panchal, H.,

Ponnamma, D., & Essa, F. A. (2021). Design, development and techno economic analysis of novel parabolic trough collector for low-temperature water heating applications. *Case Studies in Thermal Engineering*, *26*, 100978. https://doi.org/10.1016/J.CSITE.2021.100978

Venkatachalam, C. (2019). Dataset of solar energy potential assessment for Adama city (Ethiopia). *Data in Brief*, *24*, 103879. https://doi.org/10.1016/J.DIB.2019.103879

Vician, P., Palacka, M., Durcansky, P., & Jnadacka, J. (2017). Determination of Optimal Position of Solar Trough Collector. *Procedia Engineering*, *192*, 941–946. https://doi.org/10.1016/j.proeng.2017.06.162

Wadate, P. R., & Dharmadhikari, H. M. (2019a). A Review of Thermal Performance of Solar Concentrator – The Future Needs. *International Journal of Engineering Science*, *12*(3). https://doi.org/10.36224/ijes.120303

Wang, L., & Yu, J. (2023). Principles of photocatalysis. *Interface Science and Technology*, *35*, 1–52. https://doi.org/10.1016/B978-0-443-18786-5.00002-0

Wikipedia contributors. (2023). Dry heat sterilization — Wikipedia, the free encyclopedia [[Online; accessed 15-October-2024]]. https://en.wikipedia.org/w/index.php?title=Dry heat sterilization%20%5C&%20oldid=1152803722

Yılmaz, ˙I. H., & Mwesigye, A. (2018). Modeling, simulation and performance analysis of parabolic trough solar collectors: A comprehensive review. *Applied Energy*, *225*, 135–174. https://doi.org/https://doi.org/10.1016/j.apenergy.2018.05.014

Yousef, B. A. A., Radwan, A., Olabi, A. G., & Abdelkareem, M. A. (2023a). Sun composition, solar angles, and estimation of solar radiation. *Renewable Energy - Volume 1: Solar, Wind, and Hydropower Definitions, Developments, Applications, Case Studies, and Modelling and Simulation*, *1*, 3–22. https://doi.org/10.1016/B978-0-323-99568-9.00023-6

Zhao, L., Bhatia, B., Zhang, L., Strobach, E., Leroy, A., Yadav, M. K., Yang, S., Cooper, T. A., Weinstein, L. A., Modi, A., Kedare, S. B., Chen, G., & Wang, E. N. (2020). A passive high-temperature high-pressure solar steam generator for medical sterilization [doi: 10.1016/j.joule.2020.10.007]. *Joule*, *4*(12), 2733–2745. https://doi.org/10. 1016/j.joule.2020.10.007

Zubair, A. (2010). Biomedical instruments: Safety, quality control, maintenance, prospects & benefits of african technology. *African journal of medicine and medical sciences*, *39*, 35–40.

Zhao, K., Jin, H., Gai, Z., & Hong, H. (2022). A thermal efficiency-enhancing strategy of parabolic trough collector systems by cascadingly applying multiple solar selective-absorbing coatings. *Applied Energy*, *309*, 118508. https://doi.org/10.1016/J.APENERGY.2021.118508

APPENDIX

Appendix A

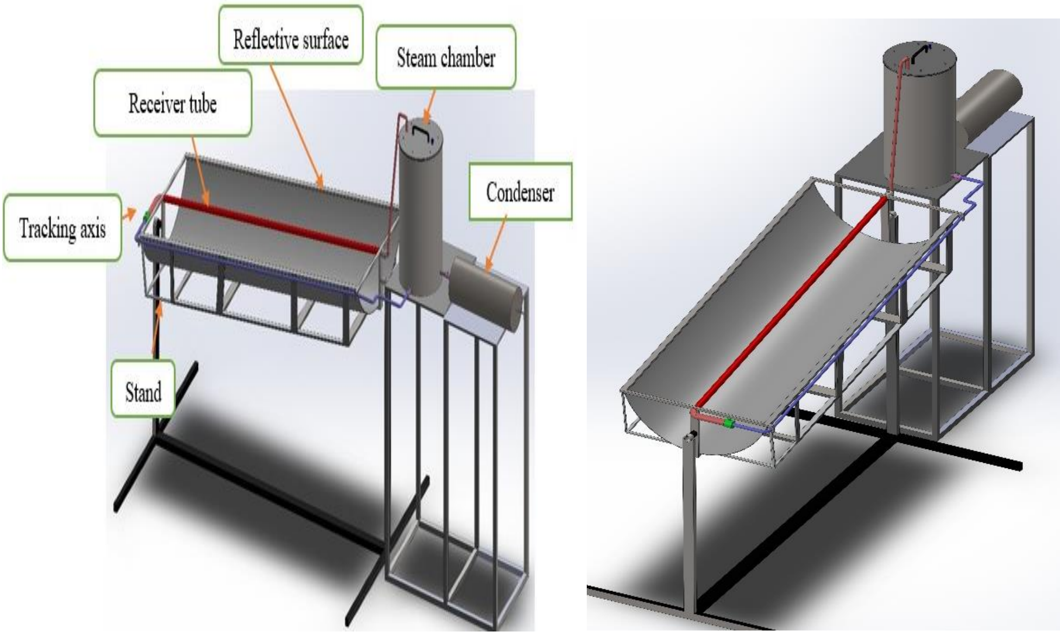

Figure A. 1. Solid work Design of the system

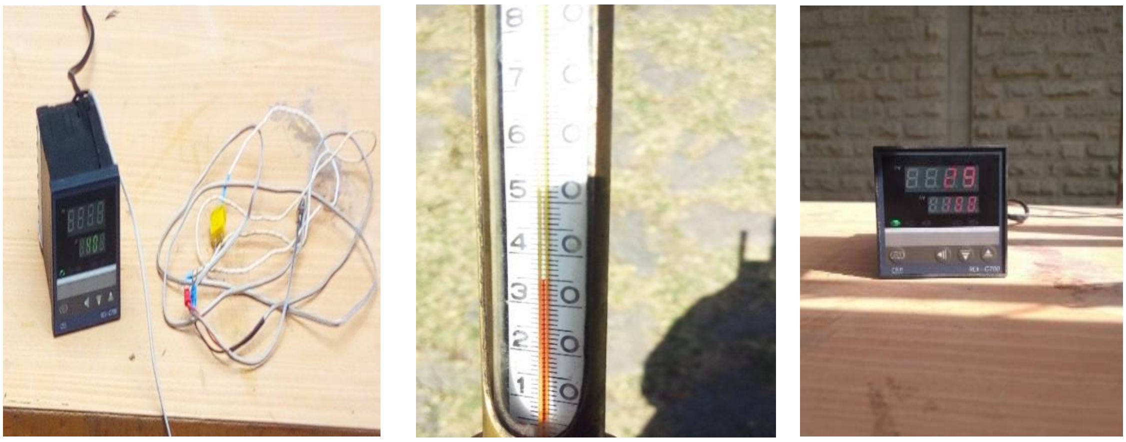

Figure A. 2. Experimental Setup Readings and Measuring Instruments of Temperature during the test

Table A. 1. Monthly Average Daily Extraterrestrial Insolation on a Horizontal Surface (Foster et al., 2009)

Latitd	Jan	Feb	Mar	Apr	May	Jun	Jul	Aug	Sep	Oct	Nov	Dec
-45	42.78	37.35	29.23	20.34	13.59	10.65	12.00	17.55	25.94	34.79	41.50	44.37
-40	43.07	38.48	31.33	23.14	16.65	13.72	15.07	20.48	28.35	36.26	42.00	44.38
-35	43.12	39.36	33.20	25.78	19.65	16.81	18.12	23.29	30.54	37.48	42.26	44.16
-30	42.92	39.97	34.81	28.24	22.56	19.86	21.12	25.96	32.50	38.43	42.26	43.71
-25	42.46	40.30	36.17	30.50	25.36	22.84	24.02	28.46	34.21	39.11	42.00	42.99
-20	41.73	40.35	37.25	32.54	28.01	25.72	26.79	30.77	35.67	39.49	41.46	42.02
-15	40.73	40.11	38.04	34.35	30.48	28.46	29.41	32.86	36.85	39.59	40.64	40.80
-10	39.47	39.59	38.55	35.90	32.76	31.03	31.85	34.72	37.76	39.40	39.56	39.31
-5	37.95	38.78	38.77	37.19	34.82	33.43	34.09	36.33	38.38	38.92	38.21	37.58
0	36.18	37.69	38.70	38.20	36.65	35.61	36.12	37.69	38.71	38.16	36.60	35.61
5	34.18	36.33	38.33	38.94	38.24	37.58	37.91	38.77	38.75	37.11	34.75	33.42
10	31.95	34.72	37.67	39.38	39.57	39.31	39.46	39.58	38.50	35.79	32.66	31.03
15	29.53	32.85	36.73	39.54	40.63	40.79	40.74	40.10	37.95	34.21	30.37	28.45
20	26.93	30.76	35.51	39.40	41.42	42.02	41.77	40.34	37.11	32.38	27.88	25.71
25	24.17	28.45	34.02	38.98	41.93	42.99	42.52	40.29	36.00	30.31	25.22	22.83
30	21.28	25.95	32.28	38.27	42.17	43.70	43.01	39.95	34.61	28.03	22.41	19.85
35	18.29	23.28	30.29	37.29	42.14	44.15	43.24	39.34	32.96	25.55	19.49	16.80

40	15.24	20.46	28.07	36.04	41.85	44.37	43.22	38.46	31.07	22.89	16.48	13.71
45	12.17	17.52	25.65	34.53	41.32	44.36	42.96	37.33	28.94	20.08	13.42	10.64

Table A. 2. Summary of Solar Geometry and Radiation Parameters

	Months	Rep_Day	Date	ns	δ	ωs	$\omega' s$	ωs_min	N	ns/N	Isc	$\bar{H}o$	a	b	H	Hd	Hb	index(k)	Hk
0	jan	17	17	8.73	-20.917	86.710	103.232	86.710	11.561	0.755	1410.193	32.655	0.366	0.398	21.772	6.887	14.884	0.667	4.135
1	feb	16	47	9.25	-12.955	88.020	95.591	88.020	11.736	0.788	1410.193	35.069	0.377	0.375	23.583	6.826	16.757	0.672	4.655
2	mar	16	75	9.00	-2.418	89.637	90.533	89.637	11.952	0.753	1410.193	37.111	0.366	0.399	24.728	7.864	16.864	0.666	4.684
3	apr	15	105	8.40	9.415	91.427	89.903	89.903	12.190	0.689	1410.193	37.828	0.345	0.444	24.615	9.110	15.505	0.651	4.307
4	may	15	135	8.23	18.792	92.929	93.017	92.929	12.391	0.664	1410.193	37.208	0.337	0.461	23.929	9.340	14.589	0.643	4.052
5	jun	11	162	7.96	23.086	93.670	95.686	93.670	12.489	0.637	1410.193	36.542	0.328	0.480	23.165	9.549	13.616	0.634	3.782
6	jul	17	198	6.80	21.184	93.336	94.394	93.336	12.445	0.546	1410.193	36.688	0.299	0.543	21.845	10.621	11.223	0.595	3.118
7	aug	16	228	6.86	13.455	92.059	90.828	90.828	12.275	0.559	1410.193	37.328	0.303	0.534	22.448	10.687	11.761	0.601	3.267
8	sep	15	258	7.32	2.217	90.333	89.697	89.697	12.044	0.608	1410.193	37.159	0.319	0.500	23.137	10.095	13.043	0.623	3.623
9	oct	15	288	8.90	-9.599	88.545	93.453	88.545	11.806	0.754	1410.193	35.489	0.366	0.399	23.653	7.506	16.146	0.666	4.485
10	nov	14	318	9.38	-18.912	87.051	100.907	87.051	11.607	0.808	1410.193	33.113	0.383	0.361	22.358	6.108	16.251	0.675	4.514
11	dec	10	344	9.35	-23.050	86.337	106.072	86.337	11.512	0.812	1410.193	31.799	0.385	0.358	21.487	5.798	15.688	0.676	4.358

Appendix B

Table A. 3. No Load Test Results April 30

Time	T_amb	T_steam	P_abs	Time	T_amb	T_steam	P_abs
13:00	29.1	29	1	11:00	27.0	27.0	1.0
13:02	29.4	35	1	11:02	27.2	38.5	1.0
13:04	28	44	1	11:04	27.4	44.0	1.0
13:06	29.2	59	1	11:06	27.6	57.0	1.0
13:08	29.5	62	1	11:08	27.8	62.0	1.0
13:10	29.8	68	1	11:10	28.0	68.0	1.0
13:12	29	74	1	11:12	28.0	74.0	1.0
13:14	29.3	83	1	11:14	28.0	80.0	1.0
13:16	29.5	86	1	11:16	28.1	84.0	1.0
13:18	30.8	89	1	11:18	28.3	89.0	1.0

13:20	30	97	1	11:20	28.5	95.0	1.0
13:22	30.2	100	1	11:22	27.8	100.0	1.0
13:24	29.5	106	1.2	11:24	27.1	105.0	1.0
13:26	29.7	109	1.55	11:26	27.0	108.0	1.0
13:28	28.9	115	1.72	11:28	27.3	113.0	1.2
13:30	29.9	119	1.95	11:30	27.5	118.0	1.48
13:32	29.5	109	1.72	11:32	27.6	119.0	1.65
13:34	30.2	117	1.82	11:34	27.8	113.0	1.89
13:36	31.9	118	1.91	11:36	27.9	112.0	1.72
13:38	31.7	119	1.93	11:38	28.0	111.0	1.54
13:40	31.5	116	1.91	11:40	28.0	115.0	1.63
13:42	31.3	118	1.94	11:42	28.5	117.0	1.77
13:44	31	119	1.97	11:44	28.8	118.0	1.82
13:46	32.7	120	1.97	11:46	29.0	118.0	1.84
13:48	32.5	121	1.98	11:48	29.2	119.0	1.87
13:50	32.3	119	1.96	11:50	29.5	119.0	1.86
13:52	33	120	1.98	11:52	29.7	120.0	1.9
13:54	32.7	118	1.97	11:54	29.9	120.5	1.91
13:56	32.5	119	2	11:56	30.0	120.8	1.92
13:58	33.3	120	1.98	11:58	29.8	120.0	1.95
14:00	33.1	121	1.99	12:00	29.5	120.0	1.96
14:02	32.9	120	1.97	12:02	29.7	121.0	1.94
14:04	33	120	2	12:04	29.9	121.0	1.9

Table A. 4. Full Load Test Results may 1

Time	T_amb	T_steam	P_abs	Time	T_amb	T_steam	P_abs
12:00	29.0	29.0	1.0	14:00	29	29	1
12:02	29.3	38.5	1.01	14:02	29.3	37.5	1.0
12:04	29.5	47.0	1.02	14:04	29.6	46	1.0
12:06	29.8	56.5	1.01	14:06	29.9	55	1.0
12:08	29.0	66.0	1.01	14:08	29.5	65	1.0
12:10	29.2	75.5	1.01	14:10	29.8	73	1.0
12:12	28.4	84.0	1.01	14:12	30	81	1.0
12:14	28.6	92.0	1.01	14:14	30.2	89	1.0
12:16	28.8	98.0	1.01	14:16	30.4	95	1.0

12:18	28.9	102.0	1.01	14:18	30.6	101	1.0
12:20	29.0	105.0	1.03	14:20	30.3	105.5	1.0
12:22	28.2	107.0	1.04	14:22	30.1	110	1.12
12:24	28.1	111.5	1.09	14:24	30.7	109	1.2
12:26	29.0	113.0	1.24	14:26	31.1	115	1.32
12:28	29.9	114.0	1.28	14:28	31.3	112	1.37
12:30	29.8	115.0	1.32	14:30	31	113	1.42
12:32	29.7	114.0	1.34	14:32	30.9	112	1.3
12:34	29.6	115.5	1.39	14:34	30.7	109.5	1.14
12:36	28.5	110.0	1.32	14:36	30.8	110	1.18
12:38	28.4	107.3	1.1	14:38	31	112	1.35
12:40	29.3	105.5	1.12	14:40	31.1	116	1.48
12:42	29.2	108.6	1.29	14:42	31.3	117	1.58
12:44	29.1	110.7	1.45	14:44	31.6	119	1.65
12:46	29.0	113.8	1.54	14:46	31.9	118.5	1.52
12:48	29.9	117.9	1.6	14:48	32.2	122	1.82
12:50	31.8	116.0	1.7	14:50	32.4	121.5	1.9
12:52	30.7	120.0	1.8	14:52	32.1	122.5	1.88
12:54	31.6	119.1	1.94	14:54	32.3	121.3	1.95
12:56	30.5	120.1	1.92	14:56	32.5	122	1.99
12:58	31.4	121.2	2.01	14:58	32.6	122.8	1.96
13:00	31.3	120.2	1.96	15:00	32.8	121	1.98
13:02	31.2	117.3	1.95	15:02	32.9	121.2	1.96
13:04	31.5	118.6	1.96	15:04	33	121	1.96
13:06	31.8	119.4	1.97	15:06	33.1	122.2	1.98
13:08	32.0	120.1	1.98	15:08	33.1	120.4	1.95
13:10	32.0	120.8	1.99	15:10	33	121.5	1.91
13:12	32.0	121.0	2.0	15:12	33	122	1.95
13:14	31.9	120.7	2.0	15:14	32.9	121.4	1.99
13:16	31.7	120.3	1.99	15:16	32.9	121.3	1.98

13:18	31.4	120.0	1.98	15:18	32.8	122	1.96
13:20	31.1	119.4	1.97	15:20	32.7	121.8	1.99
13:22	30.8	119.0	1.96	15:22	32.6	121.5	1.98

Table A. 5. Full Load Test Results may 2

Time	T_amb	T_steam	P_abs	Time	T_amb	T_steam	P_abs
11:00	27	27	1	13:00	28	28	1
11:02	27.3	35.5	1.0	13:02	28.3	36.5	1.0
11:04	27.6	44	1.0	13:04	28.6	45	1.0
11:06	27.9	53	1.0	13:06	28.9	54	1.0
11:08	27.5	63	1.0	13:08	28.5	64	1.0
11:10	27.8	71	1.0	13:10	28.8	72	1.0
11:12	28	79	1.0	13:12	29	80	1.0
11:14	28.2	87	1.0	13:14	29.2	88	1.0
11:16	28.4	93	1.0	13:16	29.4	94	1.0
11:18	28.6	99	1.0	13:18	29.6	100	1.03
11:20	28.3	103.5	1.0	13:20	29.3	104.5	1.06
11:22	28.1	108	1.08	13:22	29.1	109	1.12
11:24	28.7	107	1.2	13:24	29.7	108	1.2
11:26	29.1	113	1.32	13:26	30.1	114	1.32
11:28	29.3	110	1.37	13:28	30.3	111	1.37
11:30	29	111	1.42	13:30	30	112	1.42
11:32	28.9	110	1.3	13:32	29.9	111	1.3
11:34	28.7	107.5	1.14	13:34	29.7	108.5	1.14
11:36	28.8	108	1.18	13:36	29.8	109	1.18
11:38	29	110	1.35	13:38	30	111	1.35
11:40	29.1	114	1.48	13:40	30.1	115	1.48
11:42	29.3	115	1.58	13:42	30.3	116	1.58
11:44	29.6	117	1.65	13:44	30.6	118	1.65
11:46	29.9	116.5	1.52	13:46	30.9	117.5	1.52

11:48	30.2	120	1.82	13:48	31.2	121	1.82
11:50	30.4	119.5	1.9	13:50	31.4	120.5	1.9
11:52	30.1	120.5	1.88	13:52	31.1	121.5	1.88
11:54	30.3	119.3	1.95	13:54	31.3	120.3	1.95
11:56	30.5	120	1.99	13:56	31.5	121	1.99
11:58	30.6	120.8	1.96	13:58	31.6	121.8	1.96
12:00	30.8	119	1.98	14:00	31.8	120	1.98
12:02	30.9	119.2	1.96	14:02	31.9	120.2	1.96
12:04	31	119	1.96	14:04	32	120	1.96
12:06	31.1	120.2	1.98	14:06	32.1	121.2	1.98
12:08	31.1	118.4	1.95	14:08	32.1	119.4	1.95
12:10	31	119.5	1.91	14:10	32	120.5	1.91
12:12	31	120	1.95	14:12	32	121	1.95
12:14	30.9	119.4	1.99	14:14	31.9	120.4	1.99
12:16	30.9	119.3	1.98	14:16	31.9	120.3	1.98
12:18	30.8	120	1.96	14:18	31.8	121	1.96
12:20	30.7	119.8	1.99	14:20	31.7	120.8	1.99
12:22	30.6	119.5	1.98	14:22	31.6	120.5	1.98
12:24	30.5	119.1	1.97	14:24	31.5	120.1	1.97
12:26	30.4	118.6	1.96	14:26	31.4	119.6	1.96
12:28	30.3	118.2	1.95	14:28	31.3	119.2	1.95
12:30	30.2	117.7	1.94	14:30	31.2	118.7	1.94

Appendix C

Thermocouple calibration

The thermocouple that is used to measure the temperature of the system has to be calibrated with the standard temperature measuring device that is found in thermal Engineering laboratory in order to find the deviation from the standard and the to correct the measurement during the time of data collection of the result.

Figure C. 1. Thermocouple Calibration with The Standard

Table C. 1. Calibration of Thermocouple (Tm_2) Against Standard Temperature Sensor (Ts)

Time (min)	Ts (°C)	Tm_2 (°C)	Absolute Error (°C)	Relative Error (%)
1	27.5	27.4	0.1	0.36%
3	38.0	37.8	0.2	0.53%
5	55.4	55.2	0.2	0.36%
7	60.5	60.3	0.2	0.33%
9	69.0	68.7	0.3	0.43%
11	75.8	75.6	0.2	0.26%
13	88.9	88.7	0.2	0.23%
15	98.3	98.2	0.1	0.10%

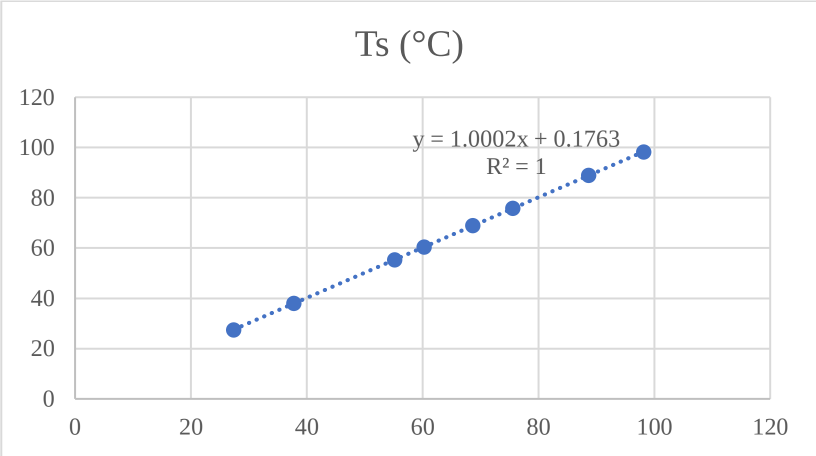

Figure C. 2. Curve Fitting for Thermocouple Calibration

From the result found on the above curve fitting the variation of the thermocouple is very low almost negligible. $R^2 = 1$ shows strong positive linear correlation. The slope is 1.02, which is very close to 1. That means for every degree increase in the thermocouple reading, the thermometer reading increases by almost the same amount. and the intercept is also less so the corrected temperature is most likely the same with the measured one.

Measurement of Water Quality Parameters (pH, EC, and TDS)

Figure C. 3. Combo pH, EC, and TDS Meter (low range)

Here the above temperature data gathered during the test made by heating the water to the boiling of water starting from ambient temperature.

The characteristics measurement of water, focusing on three essential parameters: pH, Electrical Conductivity (EC), and Total Dissolved Solids (TDS). These parameters are critical indicators of water quality, particularly in applications involving sterilization, laboratory use, or drinking water assessment. The pH measurement ranges from 0.00 to 14.00 with a resolution of 0.01 and an accuracy of ±0.05 pH at 25°C, supported by automatic temperature compensation and one or two-point calibration. The EC range extends from 0 to 3999 µS/cm, and the TDS measurement ranges from 0 to 2000 mg/L, both with a resolution of 1 unit and an accuracy of ±2% full scale. The device's automatic calibration and temperature compensation features ensure precise and reliable readings across varying environmental conditions.

Table C. 2. Summery for pH, EC, and TDS Meter Specifications

Category	Parameter	Value	Accuracy / Notes
pH	Range	0.00 to 14.00 pH	±0.05 pH (25°C/77°F)
	Resolution	0.01 pH	
	Temperature Compensation	Automatic	
EC	Range	0 to 3999 μS/cm	±2% F.S.
	Resolution	1 μS/cm	
TDS	Range	0 to 2000 mg/L (ppm)	±2% F.S.
	Resolution	1 mg/L (ppm)	

Appendix D

Python code for the solar potential assessment

```
import pandas as pd
import seaborn as sns
import numpy as np
%matplotlib inline
from PIL import Image
import math
import sympy as smp
from sympy import*
import scipy as sp
from scipy.integrate import odeint
from scipy.integrate import solve_ivp
import matplotlib.pyplot as plt
from IPython.display import FileLink
from IPython.display import display, Math

# read data csv data of sunshine hour of Kobo metehara

# month = pd.read_csv("Kobo_sunshine_hour.csv")

# month is the data frame for this study

n=month.Date
ϕ=8.9  # latitude of Kobo

ϕ_rad=np.radians(ϕ)

# Declination (δ)

month["δ "] = 23.45 * np.sin(np.radians(360 * (284 +
              month["Date"]) / 365))
```

```
# Sunset hour angle (ws)

month["ωs"] = np.degrees(np.arccos(-np.tan(np.radians(ϕ)) *
               np.tan(np.radians(month["δ"]))))
month["ω's"] = np.degrees(np.arccos(- np.tan(np.radians
               (month["δ"]- β))*np.tan(np.radians
               (month["δ"]))))
month["ωs_min"] = month[["ωs", "ω's"]].min(axis=1)

# Day_light Hours (N)
month["N"]=2*month['ωs']/15

# Ratio of (ns/N)
month["ns/N"]=month['ns']/month['N']

# Solar Constant (Isc=1367 W/m2)

# Modified solar constant I'sc(W/m²)

month["Isc"] = 1367 *(1 + 0.033 * np.cos(np.radians(360 * 17
                / 365)))

# Daily extraterrestrial radiation on a horizontal surface, Ho(MJ/M2/day)

# Calculate the day of the year

day_of_year = month['Date']

ωs=month['ωs']

ωs_rad = np.radians(ωs)
```

```
ωs_rad = np.radians(ωs)

day_angle = 360 * day_of_year / 365

# Calculate Ho for each row
month['Ho']= (24 * 3600 * 1367/ np.pi* (1 + 0.033 *
        np.cos(np.radians(day_angle))))/(np.cos(ϕ_rad) *
            np.cos(np.radians(month['δ']))*np.sin(ωs_rad)
        +np.pi* ωs/180*\np.sin(ϕ_rad) *np.sin\
            (np.radians(month['δ']))/10^6)

# Monthly Average Daily Global Radiation on a Horizontal Surface H(MJ/m2day)

month["a"]=-0.11+0.235*math.cos(ϕ_rad)+0.323*(month["ns/N"])

month["b"]=1.449-0.533*math.cos(ϕ_rad)-0.694*(month["ns/N"])

month["H"]= (month["a"] + month["b"] * month["ns/N"])*
             month["Ho"]


# Monthly Average Daily Diffuse Radiation on a Horizontal Surface Hd(MJ/m2day)

month["Hd"]=(0.931-0.814*month['ns/N'])*month['H']

# Monthly Average Daily Beam Radiation on a Horizontal Surface Hb(MJ/m2day))

month["Hb"]=month['H']-month['Hd']

# clearness index k

month["index(k)"]=month['H']/month['Ho']
```

```
# clearness index k

month["index(k)"]=month['H']/month['Ho']

# Monthly Mean Hourly Global (I), beam (Ib)and Diffuse Radiation (Id) for Each Month

hr_jan = pd.read_csv("hourr.csv")

ωs_jan = month["ωs"].iloc[0]

# Compute ω for all hours & Convert directly to radians

hr_jan["ω"] =np.radians(15 * (hr_jan['Hour'] - 12)

# Compute 'a' and 'b' based on the sunset hour angle

ω_s_radians=np.radians(ωs_jan-60)
hr_jan["a"] = 0.409 + 0.5016 * np.sin(ω_s_radians)
hr_jan["b"] = 0.6609 - 0.4767 * np.sin(ω_s_radians)

# Convert ω to radians for vectorized operation

ωs_jan_rad = np.radians(ωs_jan)

# Calculate the value using vectorized operations
value = month['H'].iloc[0] * (np.pi / 24) *(hr_jan['a']+
        hr_jan['b'] *  np.cos(hr_jan["ω"])) *
        (np.cos(hr_jan["ω"])-np.cos(ωs_jan_rad))/
        (np.sin(ωs_jan_rad) - (np.pi * ωs_jan / 180)*
         np.cos(ωs_jan_rad))
```

```python
# Set 'I' to 0 where value < 0, otherwise set 'I' to the computed value

hr_jan['I'] = np.where(value < 0, 0.0, value)

# Compute Id using vectorized operations
numerator = month['Hd'].iloc[0] * (np.pi / 24)*
            (np.cos(hr_jan["ω"])-np.cos(ωs_jan_rad))
Denominator = np.sin(ωs_jan_rad)-(np.pi*
                    ωs_jan / 180) * np.cos(ωs_jan_rad)

hr_jan['Id'] = np.maximum(numerator / denominator, 0.0)
# Ensures non-negative values

# Calculate Ib as I - Id for all rows
hr_jan['Ib'] = hr_jan['I'] - hr_jan['Id']

# Jan
# Monthly Average Hourly Diffuse Radiation on a Horizontal Surface Id

sunsethour_angles_jan = np.linspace(ωs_jan, ωs_jan, num=24)

# Instantaneous Solar Radiation
# Vectorized operations Instantaneous Solar Radiation

hr_jan['Is'] = hr_jan['I'] * 277

hr_jan['Isd'] = hr_jan['Id'] * 277

hr_jan['Isb'] = hr_jan['Ib'] * 277

# Tilted
ϕ = np.radians(ϕ)  # latitude in degrees (for example, 8 degrees)
```

```python
# Tilted
ϕ = np.radians(ϕ)  # latitude in degrees (for example, 8 degrees)

delta = month["δ"].iloc[0]  # iloc[0] for January δ is declination in degrees

δ = np.radians(delta)

β = np.radians(β)  # Tilt angle in radians

# Vectorized calculations for incident angle (inc), zenith angle (zen), and relative extraterrestrial radiation (Rb)

hr_jan['cosθ'] = np.cos(ϕ - β) * np.cos(δ) * np.cos(
              hr_jan['ω']) +np.sin(ϕ - β) * np.sin(δ)

hr_jan['cosθz'] = np.sin(β) * np.sin(β) + np.cos(ϕ) *
               np.cos(β)*np.cos(hr_jan['ω'])

hr_jan['Rb'] = hr_jan['cosθ'] / hr_jan['cosθz']


# Correct formula for 'It' using the existing 'Rb' column

hr_jan['It'] =(hr_jan['Isb'] * hr_jan['Rb']) +
             (hr_jan['Isd'] * ((1 +np.cos(β))/ 2))+(
             (hr_jan['Isb']+ hr_jan['Isd']) * 0.4*
             ((1 - np.cos(β)) / 2)

hr_jan['Ibt']=hr_jan['Rb']*hr_jan['Isb']
```